POLITECNICO DI TORINO

Corso di Laurea Magistrale
in Automotive Engineering

Tesi di Laurea Magistrale

Weldability of a cold forming AA5754 using laser, capacitor discharge and resistance technologies

Relatore:

Prof. Giovanni Maizza

Candidato:

Dario Piromalli

Marzo 2022

Index

0 Introduction

The aluminum alloys are being increasingly exploited as a light-weight material in the transportation industry in order to improve the fuel efficiency and reduce the greenhouse gas emission.

In particular 5754 aluminum alloy, which has properties of moderately high strength, good corrosion resistance, good weldability and formability is also used in other industries.

Welding is a highly important step in manufacturing processes, whether joining small components or large structures, particularly in the automotive industry.

In this thesis efforts were made to characterize lap joint welds carried out using laser, capacitive discharge and resistance technologies in order to appreciate the differences in the welded joints and to assess the benefits of each of these technologies.

Firstly, the metallographic characterization was implemented to understand the morphological change during welding. Then the micro and macro instrumented indentation tests were carried out to measure the mechanical properties of the welding joint; the indentation test is an effective analysis to characterize the mechanical properties in a specific region of the joint thereby permitting a correlation with conventional tensile test properties.

Capacitive discharge welding may be of particular interest when spot welding is required on alloys which dissipate heat rapidly, as the one we used, and which may therefore be critical for traditional resistance welding. Laser technology is undoubtedly the most expensive in terms of operation and initial investment, while resistance welding has been optimized in terms of cost but has obvious limitations on particular alloys.

Capacitive discharge technology is therefore more interesting for large-scale applications than laser technology, and potentially more effective than resistance welding for specific alloys.

CDW has been recognized to be a rapid solidification process (RSP), thus implying significant benefits in terms of metallurgy and manufactory. Although it has long been in existence, this process has not been widely used mainly due to the lack of in-depth studies of the process parameters and their correlation with different materials.

Some advantages of this process include a narrow HAZ, online quality monitoring, short welding times, and high cooling rates, these aspects also permit the joining of dissimilar metals. These features can be of great interest for the automotive industry, because of the automation and the production volume.

The steady growth of the automotive industry and the continuous increasing of fossil fuel consumption is becoming the largest sources of greenhouse gas emission. Thus, the strategies to improve fuel efficiency and reduce greenhouse gas emission are being continuously exploring by the transportation industry, the largest consumer of fossil fuel. These strategies include weight reduction, improving conventional engine efficiency, developing new and more energy efficient powertrains, such as electric and hybrid systems, and the use of low CO2 fuels, such as biofuels.

On average, for every 10% weight reduction the specific fuel consumption could reduce by 3-7%. As a result, lightweight materials are increasingly being developed and incorporated into automotive and aerospace structures.

Due to their low density, about one third of that of steel, and their good strength and stiffness to weight ratio, Aluminum alloys have great potential for weight reduction. They also possess excellent corrosion resistance, good impact strength, high thermal and electrical conductivity, good formability and machinability, and mass production capabilities at a reasonable price.

In addition, they have excellent recyclability which allows the industry to recycle scrap with about 5% of the energy required to produce new aluminum alloys. Therefore, these alloys are attractive in a variety of product forms (sheet, casting and extrusion) to many industries. Some applications of aluminum in vehicles include body panels, power units, fasteners, chassis, brake housings, air deflector parts and seat rails. In the future, it could also be a effective alternative to steel in other applications.

There are approximately 5000 spot welds in a single vehicle. The quality, structural performance, lifespan, safety design, strength, stiffness, and integrity of a vehicle depend not only on the mechanical properties of the sheets but also on the quality of spot welds.

1 Resistance Welding

1.1 Resistance Welding Process

Resistance welding refers to electrothermal processes of welding using an electric current to melt metal sheets placed between the electrodes. Resistance welding is widely used in the automotive industry for structural lightweight applications because it is characterized by low costs, the possibility to weld together simultaneously different materials and elevated speed production (Dulal Chandra Saha, 2011).

In resistance welding, the heating is based on Joule's principle: the heat Q produced by a current i circulating in an electric circuit expressed as

$$Q = i^2Rt$$

where R is the electrical resistance of the circuit and t is the welding time. In this process, the heating rate is more important than the heating itself because it influences temperatures and the microstructure of the work pieces (Zhang Hongyan, 2011). There are three approaches for resistance welding bonds. In the solid state bond, different materials are joined together using very high welding forces and energy in a very short time. The joint shows good tensile and shear strength but a little peel strength. In the fusion bond, instead, materials are heated to the melting point using high energies and, then, they cool creating a weld nugget, characterized by really good tensile, shear and peel strength. In the reflow braze bond, instead, heating happens at low temperatures, producing a definite bond interface with minimum grain growth. The resulting bond is characterized by a very good tensile strength but the shear and peel strength are poor (Aluminum Automotive Manual, 2015).

Different materials can be used for resistance welding, such as steel, copper and nickel alloy, aluminum and aluminum alloy (2c2m Studio di progettazione, s.d.). Aluminum welding is more difficult than steel one. Aluminum has a bigger thermal and electric conductivity so a higher electric current should be applied for heating.

There are many factors influencing resistance welding. First of all, the heating process is strictly influenced by the electric resistance. The total resistance of the sheet stack-up depends on the contact resistance at the interface between the sheet and the electrodes, R_1 and R_5, on the bulk resistance, R_2 and R_4, and on the sheet faying interface, R_3, as shown in Figure 1.1.

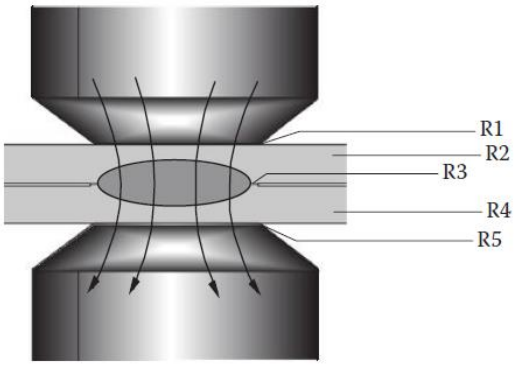

Figure 1.1 *Electric Resistance in a sheet stack-up (Zhang Hongyan, 2011)*

Electric resistance depends on the material resistivity, that changes with temperature, as shown in Figure 1.2.

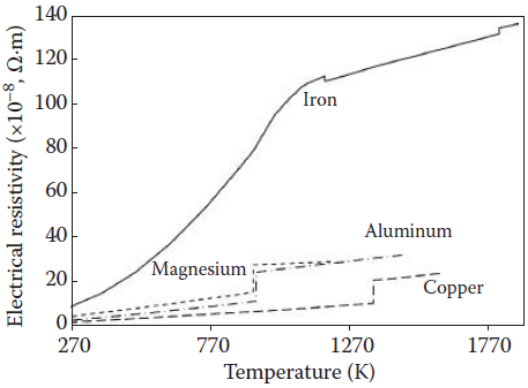

Figure 1.2 *Bulk resistance vs. temperature for Fe, Mg, Al, and Cu (Zhang Hongyan, 2011)*.

Aluminum has a very low electric resistivity, similar to copper; but pure aluminum is difficult to weld, so aluminum alloys are used.

While the bulk resistance varies only with temperature, the contact resistances are influenced by both temperature and pressure and by the surface irregularities at the sheet-electrode interface. Also the presence of oil, dirt, oxide or coatings for corrosion protection on the surface interface may affect the contact resistances.

As a consequence, the total resistance varies during the heating process and the changes reflect how the different resistances vary during welding. Figure 1.3 shows how the total resistance changes during welding for aluminum and uncoated steel.

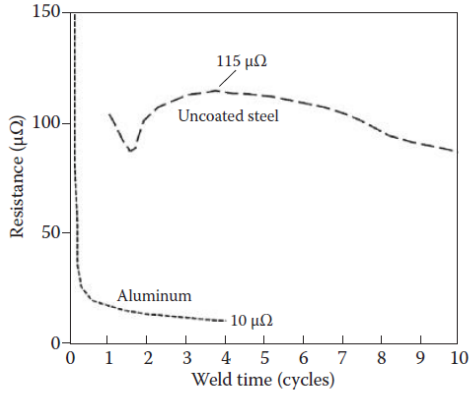

Figure 1.3 *Total resistance variation during welding (Zhang Hongyan, 2011)*

For aluminum, the resistance shows a rapid decrease at the beginning of the process, requiring a higher electrodes force.

The electric current is one of the most important parameters affecting resistance welding process. The values of the electric current employed during the heating process can vary based on materials, thickness, shape of the patches to join, shape and dimensions of the electrodes and so on. Moreover, the electrodes are connected to the secondary side of a transformer and the electric current circulating in the electrodes can be direct or alternate and it can be shaped according to the characteristics of the welding process. Figure 1.4 illustrates different profiles of the electric current.

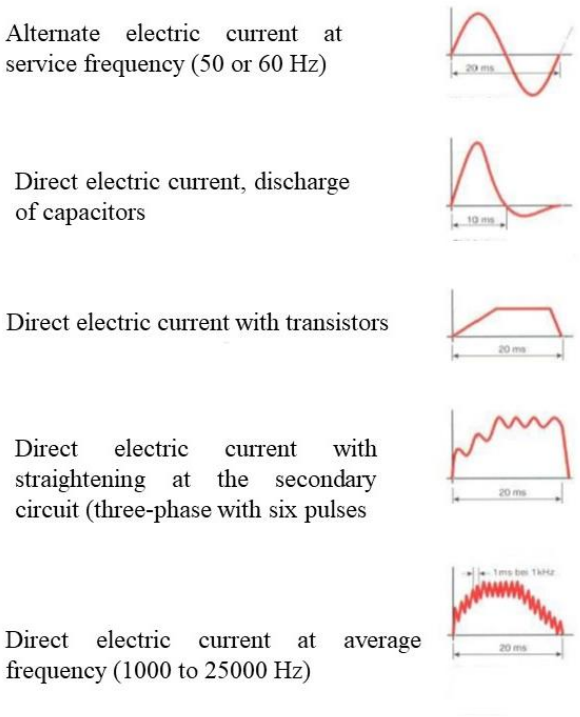

Figure 1.4 *Different profiles of the electric current (metasald, s.d.)*

The values of the electric currents usually employed in resistance welding vary between 2 kA and 100 kA, while the voltage applied at the second side of the transformer vary between 0,25 V and 25 V. Moreover, energy losses can occur in the transformer due to the high values of the electric currents, so very short conductors are used. The voltage applied at the second side of the transformer should be monitored because, if it is very high, the electrodes or the sheets could burn.

Another important parameter of resistance welding is the contact pressure on the sheets. The welding process occurs in three phases: juxtaposition, welding and cooling. During juxtaposition, the materials are elastically or plastically deformed to increase the contact surface. During welding, instead, the contact resistances and the plastic shell should be controlled and finally, during cooling, the applied pressure has to fix the joined parts, improving the mechanical characteristics, to avoid the formation of a retreat hole. Figure 1.5 displays how pressure and the electric current change during these three phases.

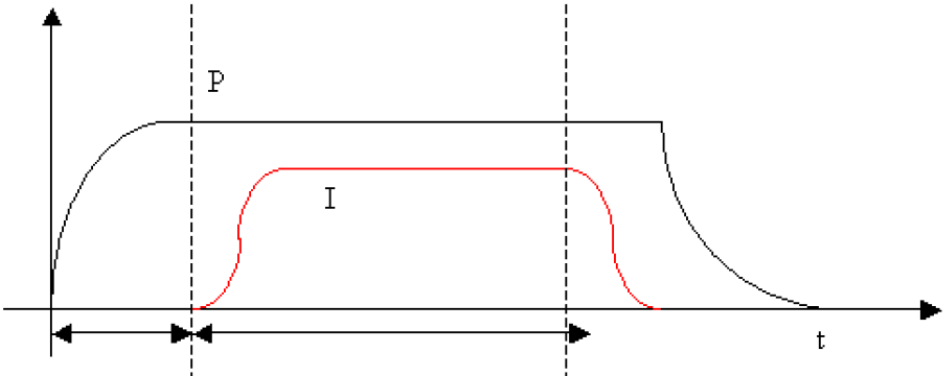

Figure 1.5 *Evolution of pressure and electric current during resistance welding (metasald, s.d.)*

Welding time is another important parameter in resistance welding. It should be shorter for very good thermal conductors. Maintenance time also affects the process because the crystalline structure is better if cooling happens slowly. For this reason, the electrodes are kept closed for some seconds after welding.

Welding can be jeopardized by the formation of cracks, which cause discontinuities in the welded structure, changing mechanical properties. These discontinuities are associated to the welding machine, the welding set up or the electrodes degradation. Figure 1.6 illustrates the grain structure at the center of a nugget obtained using resistance spot welding of 5754 Aluminum alloy (Dulal Chandra Saha, 2011).

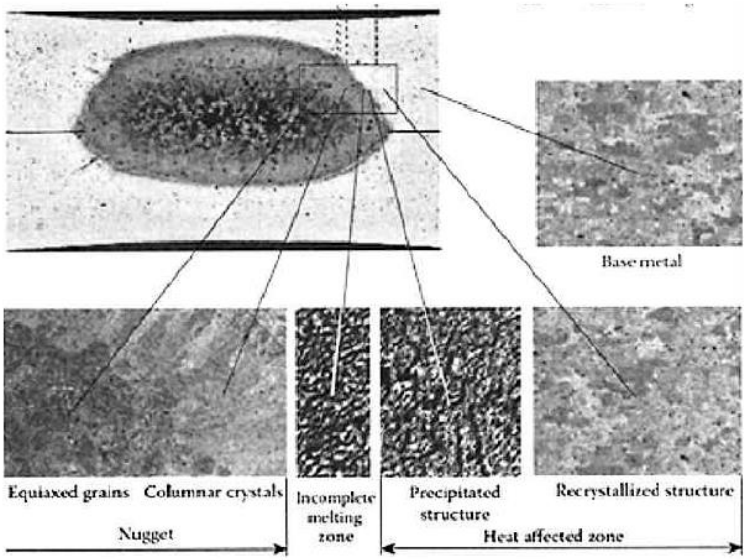

Figure 1.6 *Grain structure at the center of a nugget obtained using resistance spot welding of 5754 Aluminum alloy (Dulal Chandra Saha, 2011)*

1.2 Resistance welding technologies

There are different types of resistance welding:

Resistance spot welding

Resistance spot welding is used above all in automotive industries thanks to its low costs, elevated productivity and high performance and automation.

In Resistance spot welding, a very high electric current flows through electrodes to the weld area. The process is very fast, even if welding times depend on the material type and thickness, and on the dimensions and force of the electrodes. Two copper electrodes exert a pressure on two overlapped pieces to held them together and they concentrate the electric current in a little spot, as shown in Figure 1.7.

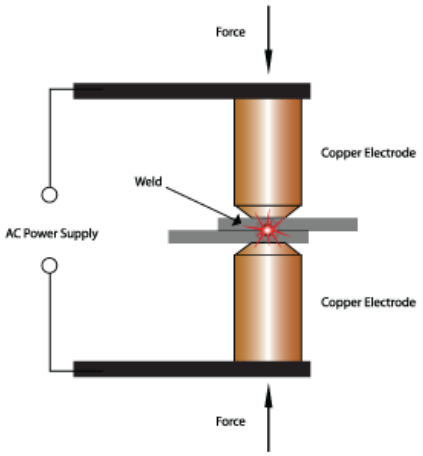

Figure 1.7 *Resistance Spot Welding Process*

The process takes place in three steps. First of all, the electrodes apply a pressure on the metals. Since the metals surface is rough, some peaks connect, the oxide layers break and some metal – to – metal bridges take place. When the electric current starts to flow in these metal bridges, heating generates melting, other peaks will make contact, creating new metal bridges. The process ends when all the surface is melted. The intensity of the electric current and the resistance between the electrodes determine the energy causing heating. Finally, the electrodes are kept together during cooling for a fraction of a second.

The welding process is strictly influenced by the shape of the tip of the electrodes, and their shape and size depend on the application. For aluminum resistance spot welding, for example, eccentric tips are used to reach corners and small spaces, while radius style electrodes are employed for applications at very high temperatures, instead, when pressure increases, a truncated tip is suitable.

Moreover, for aluminum resistance welding, the electrodes force usually varies between 0.2 kN and 8 kN, while the electric current is up to 40 kA. To ensure a regular surface of the interfaces of the joint, for aluminum sheet with thickness ranging between 0.8 mm and 0.4 mm, the face diameter of the electrode should measure 5.0-10.0 mm. Also the life time of the electrodes influences the welding process, so an additional cleaning step of the electrodes is added, favoring less aggressive maintenance procedures and a dressing cutter only if the tip is compromised. Besides, MFDC (medium frequency direct current) power supply are mostly used, even if also alternative power supplies are sometimes used. In resistance welding, the joint should be accessible from both sides and the flanges must be wide enough to ensure a flat portion greater than the weld nugget diameter.

Figure 1.8 illustrates typical flange for resistance welding.

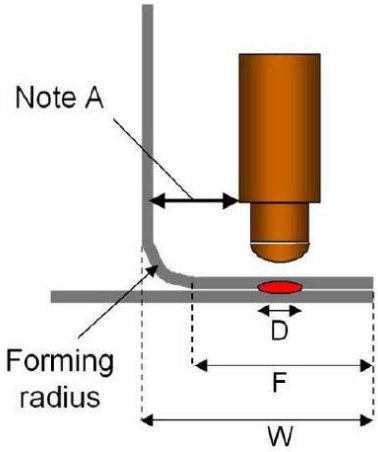

Figure 1.8 *Typical flange for resistance welding*

F, the weld flat dimension, is some millimeters greater than D, the weld nugget diameter, including tolerance for spot position. W, instead, is the overall flange width. The electrode tip can't touch the corner radii or the up part of the component, so the distance Note A must be preserved between the component and the electrode. Furthermore, the total resistance is affected by the forces acting on the surface. For this reason, it is necessary to minimize the force creating the intimate contact between the parts, i.e., the closing force, showed in Figure 1.9.

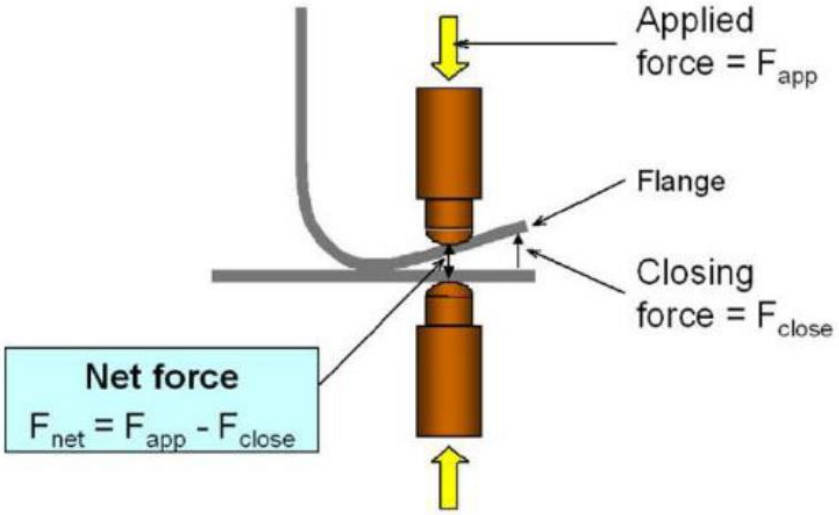

Figure 1.9 *Closing force*

Moreover, to avoid the crack formation and the sliding at the surface and to preserve the weld strength, the electrodes must be perpendicular to the sheet surfaces, as illustrated in Figure 1.10.

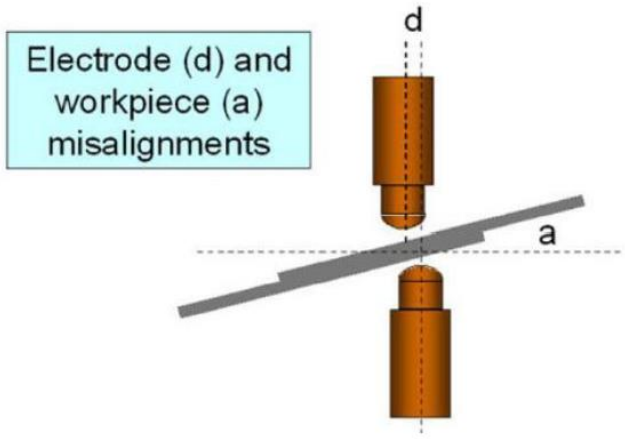

Figure 1.10 *Electrodes alignment*

Weld lobe diagram shows the acceptable values for welding parameters. Keeping the electrode force constant, the weld time is plot as function of the secondary current (Figure 1.11). The area marked by the lobe indicates safe values, the upper boundary indicates expulsion conditions, while the lower boundary indicates the conditions to create a weld piece of minimum dimensions.

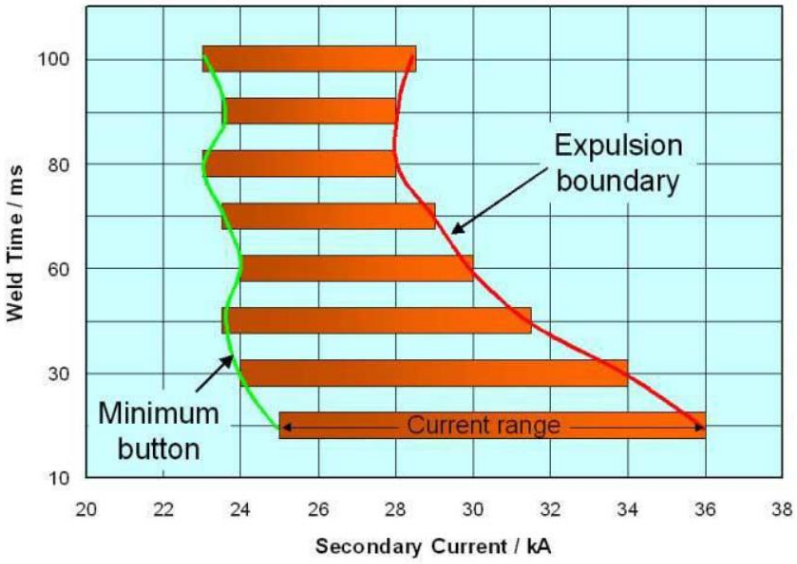

Figure 1.11 *Weld Lobe*

Too small or too big nuggets, cold welds, cracks and porosity are examples of the non-conformities occurring in resistance welding.
Aluminum resistance spot welding has many difficulties because the joint could result weak, very high electric current and pressure are necessary to melt the sheets, the electrode life is short, voluminous transformers are employed and there is more expulsion during welding (Yanjun Wang, 2019).
To avoid the formation of brittle interfaces during resistance spot welding, a new process has been recently introduced, the resistance spot welding with cover plate (Dulal Chandra Saha, 2011). In this process, a cover plate is placed between the electrode and the aluminum sheet, as shown in Figure 1.12.

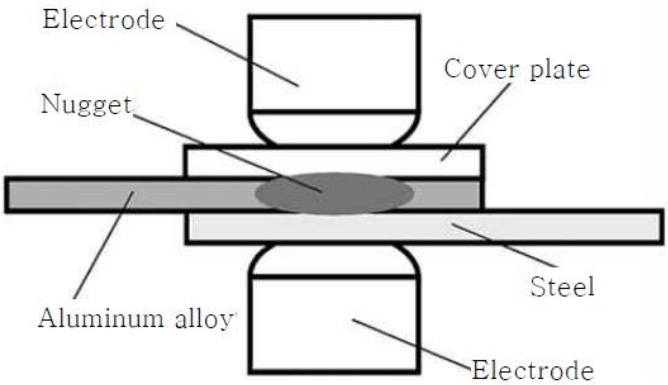

Figure 1.12 *Resistance Spot Welding with Cover plate (Dulal Chandra Saha, 2011)*

This plate allows to use very high temperatures because it has electrical conductivity lower than aluminum.
Moreover, a new technique has been also proposed to melt aluminum and steel, employing Aluminum-Zinc eutectic reaction, to eliminate the oxide film at the interface. When the eutectic reaction happens at the interface, the oxide and Zinc layer is removed and a diffusion reaction permits the creation of a uniform interface layer, as shown in Figure 1.13.

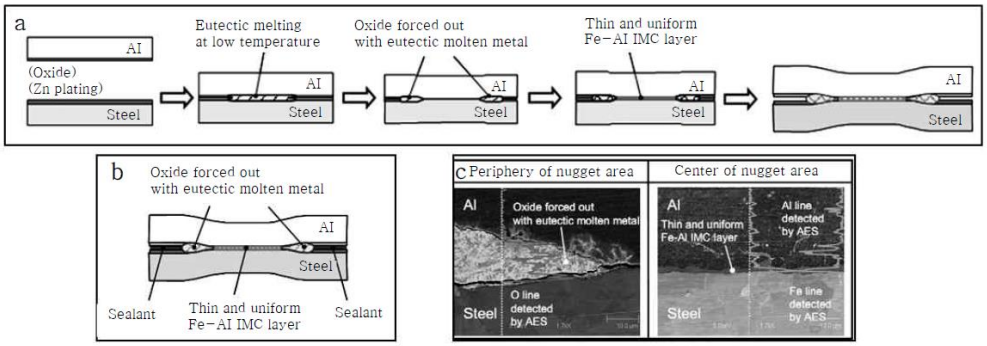

Figure 1.13 *Resistance spot welding between aluminum and steel using Aluminum-Zinc eutectic reaction (Dulal Chandra Saha, 2011)*

To improve resistance spot welding, researchers also employ screws or self-piercing rivets.
Figure 1.14, instead, illustrates Delta Spot welding.

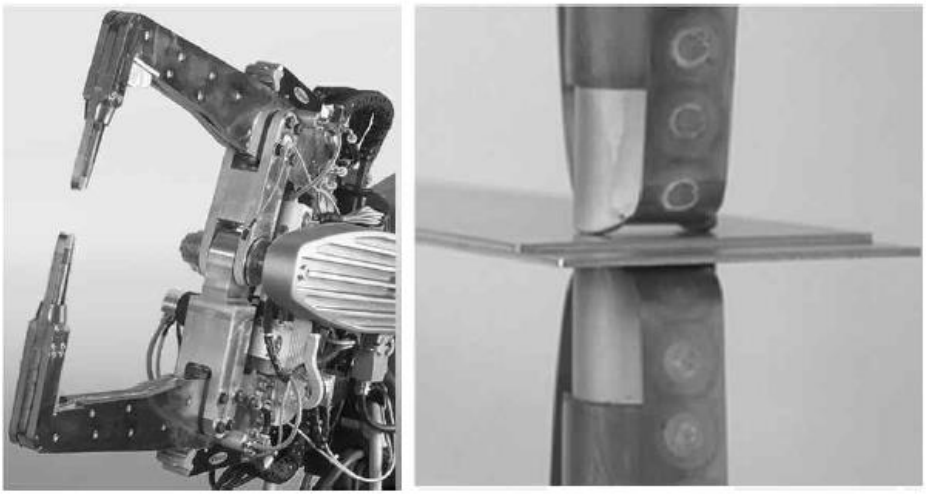

Figure 1.14 *Delta Spot Aluminum welding (Dulal Chandra Saha, 2011)*

Surface condition is another parameter affecting resistance spot welding, For this reason, to protect electrodes, a process tape can be used to prevent the deposit of aluminum, zinc or organic debris. Process tape lengthens the electrodes life and reduces the electric current circulating in the sheets.

Projection welding

In Projection welding, raised sections called projection localize the welding because embossed, cold headed and machined projections point heat generation on restricted areas. This process is used for heavier sections and to weld nuts, bars, crossed wires and screw machine parts. The welding electrodes focus current flow and heating on the point of contact. The welding sequence is illustrated in Figure 1.15.

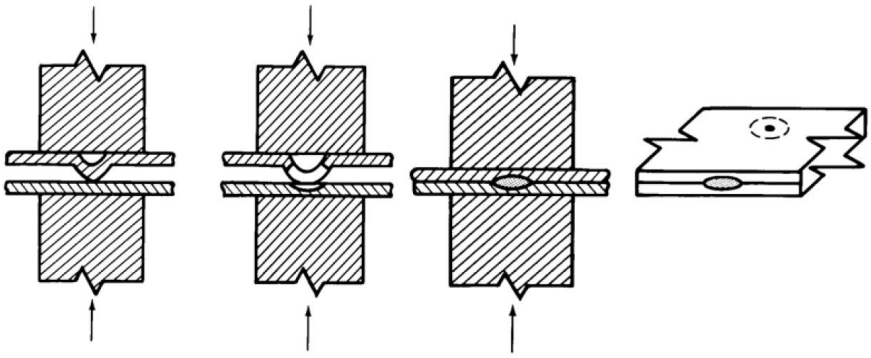

Figure 1.15 *Welding sequence for projection welding*

Projection welding is very useful for challenging material combinations or to join pieces with complex shapes. It is not suitable for aluminum because special projections geometries are necessary and aluminum alloys are not strong enough to survive to this welding process.

Resistance element welding

Resistance element welding takes advantage of both thermal and mechanical principles to bond an auxiliary joining element with the bottom plate. First of all, the cover sheet is perforated and the weld rivet is introduced inside it. One electrode is placed onto the rivet, while the other one on the bottom sheet. When pressure and electric current are applied, a weld nugget is created by heating in the contact zone (Figure 1.16). Finally, the electrode force deforms the weld rivet axially and the surface pressure between the cover sheet and the river head determines a force connection, while a frictional connection establishes between the cover sheet and both the river shaft and the rivet head.

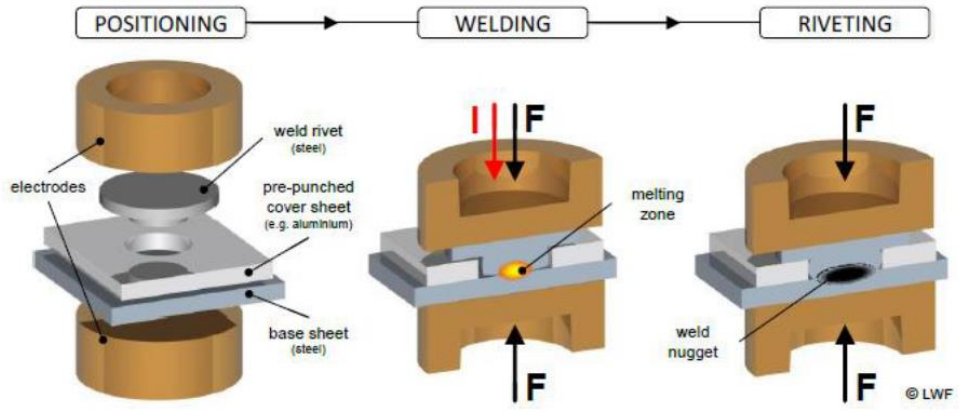

Figure 1.16 *Resistance element welding sequence*

Resistance butt welding (flash welding)

In Resistance flash welding, the pieces to melt are linked to the secondary circuit of a transformer. One piece can move because it is connected to a movable platen, while the other one is fixed. First, there is a gap between the pieces to be joined. Then, the movable platen starts moving slowly and, when the two pieces touch, the flashing period begins: a very high current circulates until all surfaces are heated enough to ensure plasticity to the joint. Finally, during the upset period, the surfaces are squeezed applying a great force.

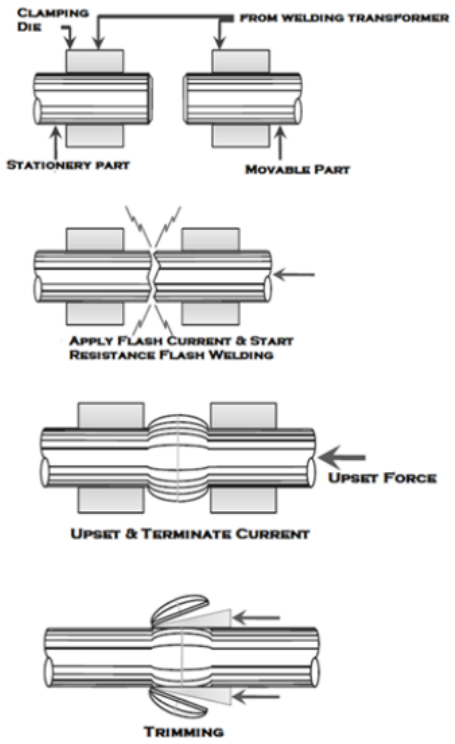

Figure 1.17 *Flash welding process*

Resistance stud welding

Resistance stud welding is used for aluminum dent removal equipment. Studs used in resistance welding have a small tip on the base to ensure welding time control. When currents flow in the tips, a timed arc is produced to melt the diameter of the stud and the corresponding area on the piece. The process ends when the stud enters in the molten metal.

Resistance seam welding

In Resistance seam welding, the working pieces pass through two copper wheels or under a single wheel acting on a stationary backing piece. A pulsed welding current is applied to heat the surfaces. The semi-molten surfaces are then compressed to ensure bonding after cooling. In this process, thermal loading is smaller than in resistance spot welding because the electrodes rotate and so the current flows in different parts of the electrodes. Resistance seam welding is influenced by sheet configuration, welding wheel configuration and power supply.

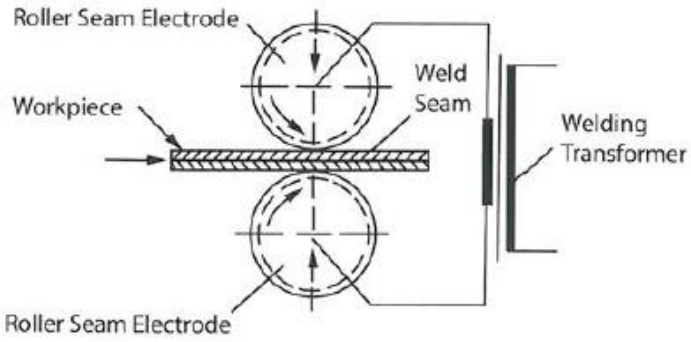

Figure 1.18 *Resistance seam welding process*

High frequency welding

High frequency welding is used above all to produce tubes or pipes. Some rolls transform the aluminum strip into a cylindrical shape and, then, squeeze rolls bring together the faying edges for welding. High frequency welding can be of two types: induction welding or contact welding, illustrated in Figure 1.19.

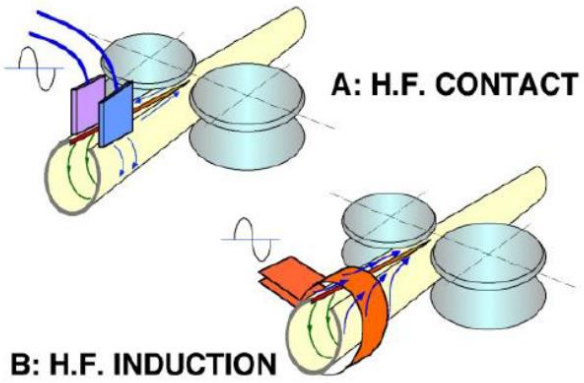

Figure 1.19 *High frequency welding*

1.3 Aluminum Alloys Resistance Welding

Aluminum alloys are mainly used in automotive industries. To reduce air pollution and to optimize fuel consumption, it is important to reduce weight, for this reason aluminum and magnesium alloys are employed in automotive applications to replace or flank steel. Aluminum offers many advantages because it is very resistant to corrosion, it doesn't change color during heating, it is a non-magnetic material and aluminum alloys show better mechanical properties than steel (for the same weight).
However, Resistance spot welding can't be directly applied to aluminum. Aluminum welding, in fact, is a delicate phase because the formation of brittle intermetallic compounds can occur determining weak joints. The increase of the surface resistance at the interface between the electrode and the metallic sheet really causes a raise in the ohmic heating, determining the electrodes overheating.
Moreover, there are several problems in aluminum welding. First of all, aluminum alloys have a very high thermal and electrical conductivity so elevated electric currents are necessary with a short welding time, also pressure and electric current should remain uniform during the process. Researchers demonstrated that a larger contact area between the electrode and the aluminum sheet can determine a smaller current density, determining a reduced weld nugget (Yanjun Wang, 2019).
Another problem is the electrode life: high currents and pressures can determine the electrode erosion, which could cause undersized welds. For this reason, surface treatments are used for the electrodes to prevent their undermining.
Another element influencing welding process is the aluminum tendency to react with the oxygen in the atmosphere determining the formation of a surface oxide. The oxide film has a very high resistivity and it can threaten the welding process, requiring higher contact pressure. The oxide layer should be destroyed uniformly to guarantee the formation of the nugget. In aluminum welding, in fact, the weld current and the electrode force are, respectively, about three times and two times with respect to steel welding. To improve electrode life, researchers suggest to clean the surface with chemical agents to reduce the oxide film thickness (Dulal Chandra Saha, 2011).
Moreover, weld defects and the expulsion could be considerably reduced modifying electrode shapes (Mazur W, 2016). Wang et al. (Yanjun Wang, 2019) tested a new type of electrode, the New Ton Ring (NTR) electrode on AA 5182-O Aluminum Alloy. NTR electrode shape is compared to other electrodes in the following figure.

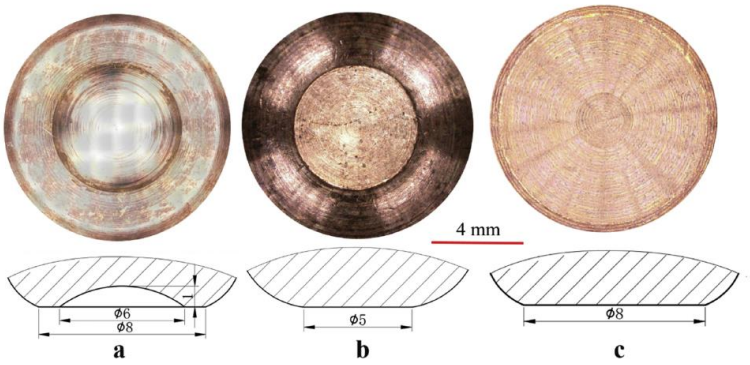

Figure 1.20 *Outer appearance of electrode (a), NTR electrode (b) and FT electrode (c) (Yanjun Wang, 2019)*

NTR electrode reduces drastically the weld porosity and the mechanical properties of the joint are considerably improved. In addition, the nucleation growth proceeds from the edge of the electrode to the center and this nucleation mechanism significantly improves the weld nugget growth (Yanjun Wang, 2019).
Aluminum alloys must have suitable mechanical properties that are strictly influenced by the industrial processes used for their production. While aluminum is a homogenous material, aluminum alloys are not homogenous, and the mechanical properties depend on their chemical composition and the treatments employed. The most important properties affecting the design processes are the ultimate tensile strength, the 0.2% proof strength and other mechanical properties such as the Poisson's value and the Young's modulus, determined through a standardized procedure prescribed by ISO 6892 – 1. (Tihomir Doksanovic, 2017).
Figure 1.21 shows typical stress-strain curve for a metal material, with a pronounced yield stress and without a pronounced yield stress.

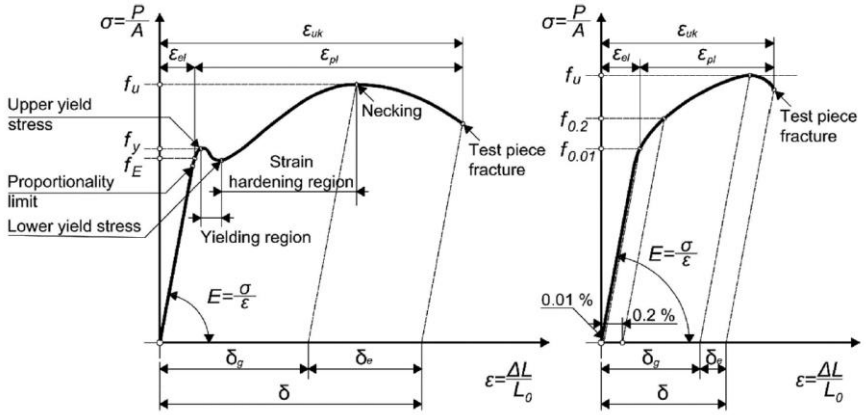

Figure 1.21 *Typical stress-strain curve for a metal material, with a pronounced yield stress and without a pronounced yield stress (Tihomir Doksanovic, 2017)*

1.4 AA5754 Aluminum Alloy

AA5754 Aluminum Alloy is widely used in automotive applications. It has a good formability and for this reason it is employed as structural internal panel. Table 1.1 contains mechanical properties and chemical composition of AA5754 Aluminum Alloy.

MECHANICAL PROPERTIES				
Young's Modulus (GPa)	Tensile strength (MPa)		Elongation	Hardness (H_V)
70	240		22%	63.5
NOMINAL COMPOSITION(BALANCE Al) wt%				
Si	Fe	Cu	Mn	Mg
0-0.40	0-0.40	0-0.10	0-0.50	2.60-3.60

Table 1.1 *Mechanical properties and chemical composition of AA5754 Aluminum Alloy (L. Han)*

Han et al. investigated the surface effects for AA5754 Aluminum alloy sheets. For 5xxx series, in fact, the surface should be cleaned and pretreated to ensure cohesion and durability (L. Han).
Table 1.2 illustrates the surface conditions tested on AA5754 Aluminum Alloy.

Variant	Cleaning	Lubricant
1	Full cleaning	Wax lubricant
2	Reduced cleaning	Wax lubricant
3	Full cleaning	None (removed)

Table 1.2 *Surface conditions tested on AA5754 Aluminum Alloy (L. Han)*

When the surface is full cleaned (Variant 1), the weld growth curve is shown in Figure 1.22.

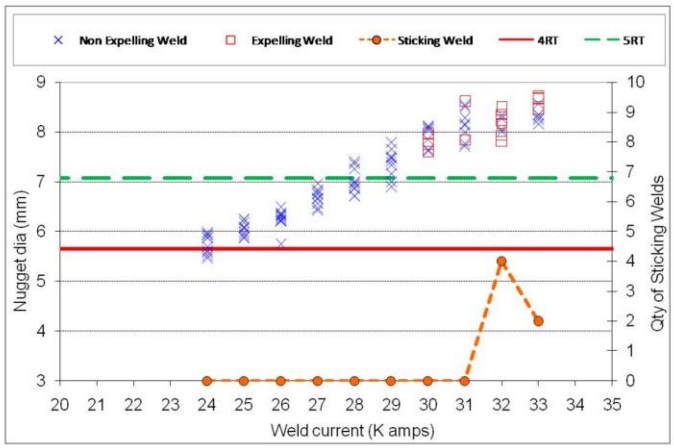

Figure 1.22 *Weld growth curve when the surface is full cleaned (Variant 1) (L. Han)*

When the surface is reduced cleaned (Variant 2), the weld growth curve is shown in Figure 1.23.

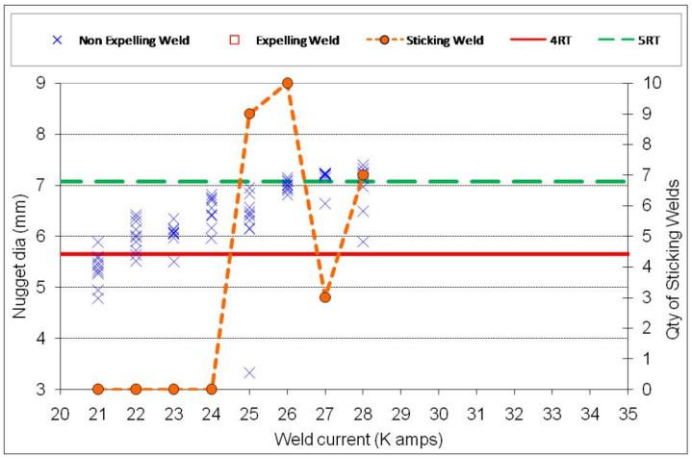

Figure 1.23 *Weld growth curve when the surface is reduced cleaned (Variant 2) (L. Han)*

Figure 1.22 and 1.23 highlight the effect of cleaning on the welding process. When the surface is full cleaned, there is a wider process window and a smaller probability of sticking. Moreover, when the surface is reduced cleaned, electrodes show a considerable damage, as displayed in Figure 1.24, reporting the electrodes indentations for both testing conditions (L. Han).

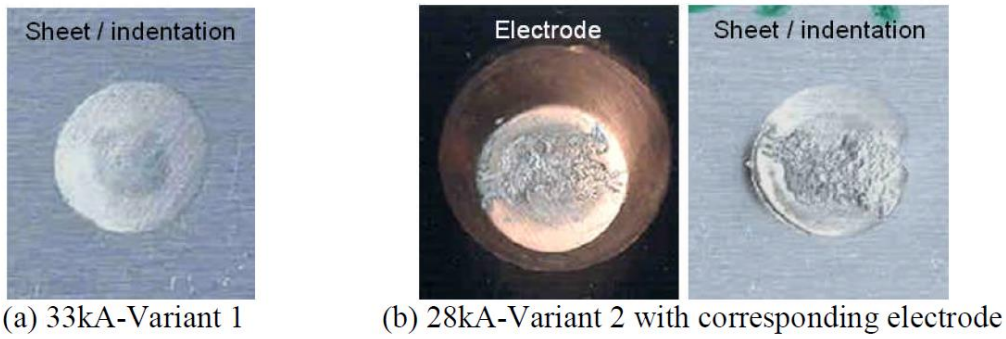

Figure 1.24 *Electrodes indentations for both testing conditions (L. Han)*

Figure 1.25, instead, shows micro sections of the spot welds. Variant 1 testing conditions, determine good shape and penetration, while, for Variant 2 testing conditions, there is an overpenetration of the weld nugget because the melting process has happened near the anode contact surface (L. Han).

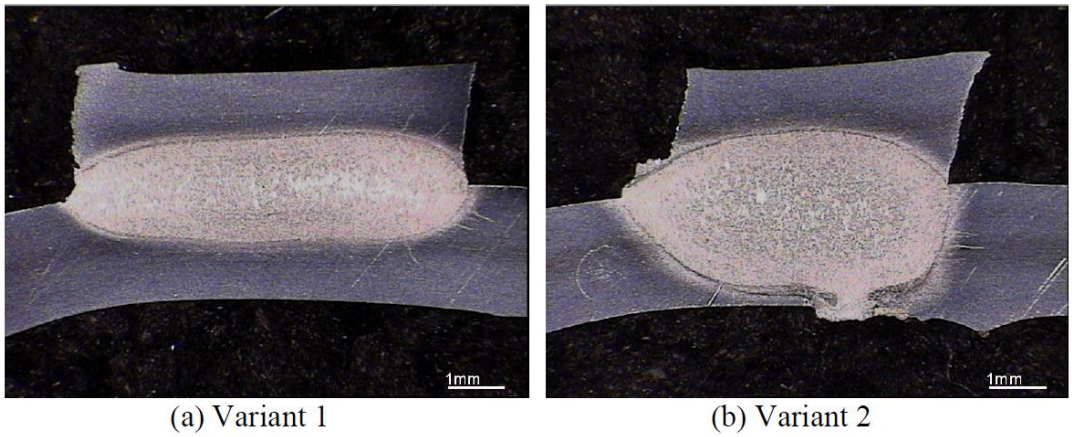

Figure 1.25 *Micro sections of the spot welds for Variant 1 and 2 testing conditions (L. Han)*

Finally, the effect of a solid wax lubricant has been investigated, showing an improvement of the contact resistance when the lubricant is used, as illustrated in Figure 1.26 (L. Han).

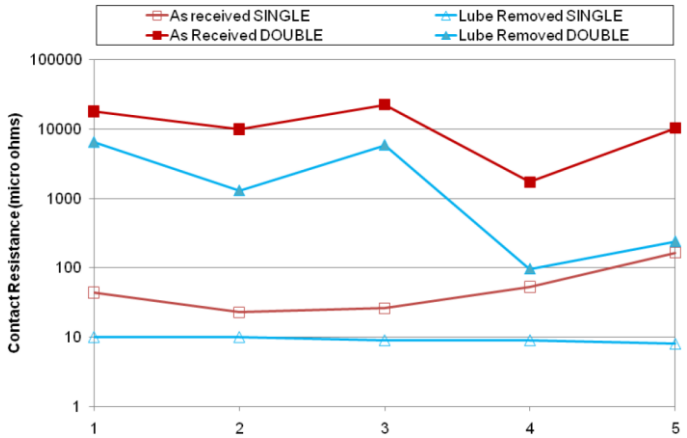

Figure 1.26 *Contact Resistance measurements for AA5754 Aluminum Alloy for Variant 1 and 3 Testing Conditions* **(L. Han)**

The growth curve of Figure 1.27 has been, instead, obtained after wax removal before welding (L. Han).

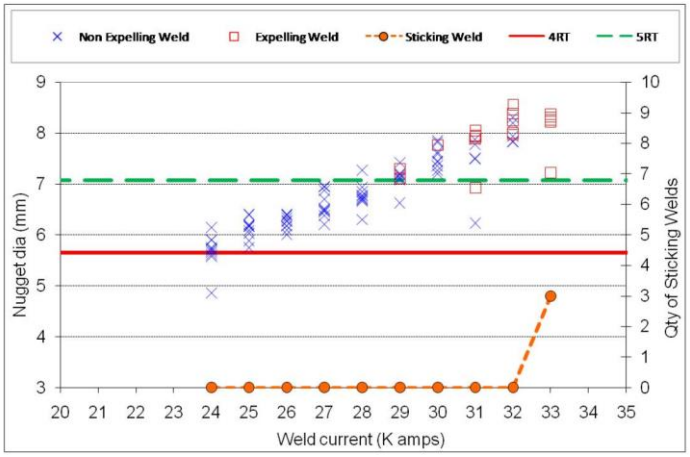

Figure 1.27 *Weld growth curve for AA5754 Aluminum Alloy for Variant 3 Testing Conditions (L. Han)*

The experimental results underline the importance of the removal of the disrupted surface layer before surface treatments. Full cleaning reduces sticking and prevents electrodes deterioration. The use of a wax lubricant reduces the contact resistance. However, employing a low current pre-pulse can reduce the risk of expulsion (L. Han).
Long et al. (X. Long, 2005), instead, proposed a Finite Element Model to predict the residual stress field in a 5754 Aluminum Alloy. They simulated all the resistance spot welding process with a thermo-electrical-mechanical coupled model using ANSYS commercial software, following the flow chart illustrated in Figure 1.28.

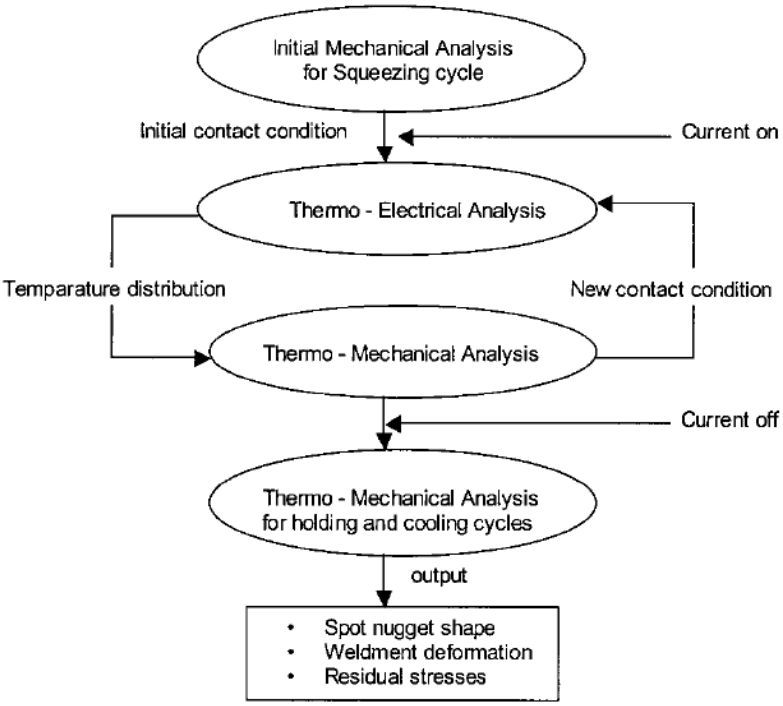

Figure 1.28 *Flow Chart describing the FEM Analysis steps (X. Long, 2005)*

They obtained the stress distributions shown in Figure 1.29.

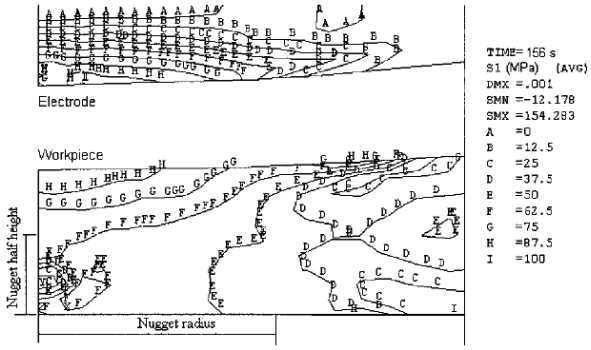

Principal residual stress σ_1 in aluminium spot welded joint

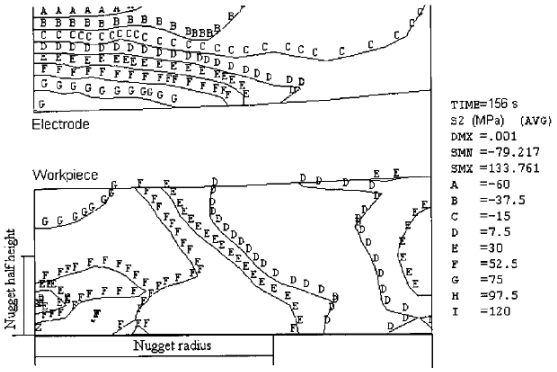

Principal residual stress σ_2 in aluminium spot welded joint

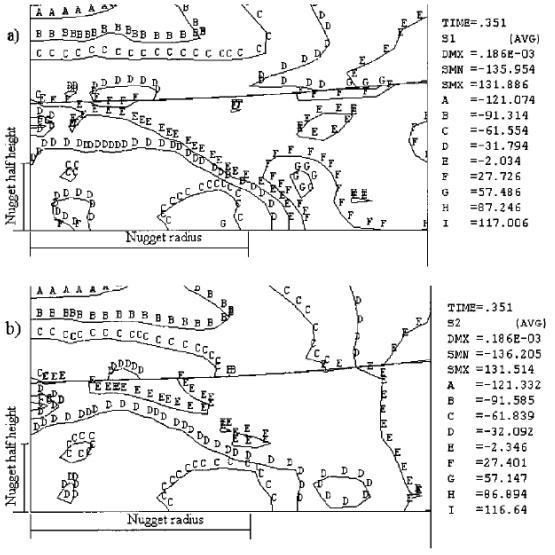

Internal stress *a* principal stress σ_1 and *b* principal stress σ_2 distribution in aluminium spot welded joint at end of holding cycle

Figure 1.29 *Stress distributions in the spot weld*

The FEM model, then, could help understanding the deformation mechanism and the developed stresses during welding process. This evaluation could become a determining factor in the design of more reliable and durable thin aluminum sheets.

A very important problem occurring during Resistance spot welding for AA5754 Aluminum alloy is the crack formation. Zhang et al. (H. Zhang, 2002) conducted several tests to understand crack formation mechanism and the effect of constraining. They used different types of electrodes, as shown in Figure 1.30: a crown-shaped tip (A), a dome shaped tip (B) and a truncated cone (C). The AA5754 Aluminum alloy samples have different dimensions to understand if sizes affect crack formation.

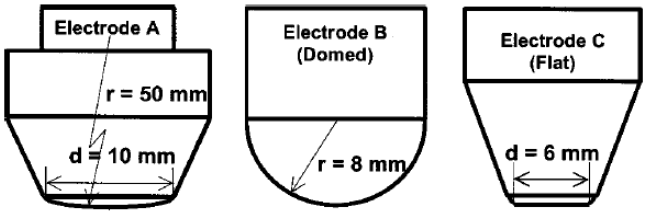

Figure 1.30 *Electrodes used to test crack formation (H. Zhang, 2002)*

Researchers found that crack formation occurs mainly when electrode B is employed and cracks have a preferential direction, the longitudinal one, as shown in Figure 1.31.

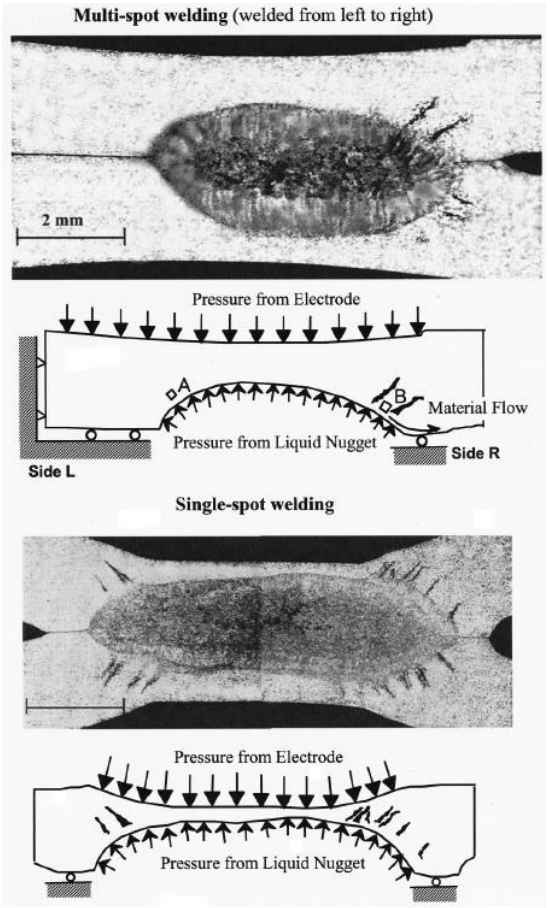

Figure 1.31 *Longitudinal cross section for single and multi-spot welding (H. Zhang, 2002)*

Tests results show that crack formation occurs on the unwelded edge. Figure 1.32, instead, depicts the effects of specimen sizes and electrode types on crack formation.

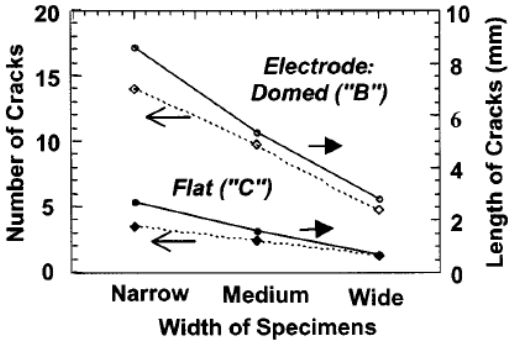

Figure 1.32 *Effects of specimen sizes and electrode types on crack formation (H. Zhang, 2002)*

When specimen sizes increase, the crack number drastically reduces. Moreover, the cracks occur above all when Electrode type B is employed.
Also constraining conditions influence crack formation in fact the number of cracks tends to zero with constraining form neighboring welds. For this reason, constraining is a determining factor in cracks reduction.
Zhang et al. (H. Zhang, 2002) also performed a thermal mechanical analysis of crack formation and they found that thermal stresses develop on the unconstrained side in multi spot welds and on both sides in single spot welds. The probability of crack formation increases in the region adjacent to the nugget, where there is the coexistence of solid and liquid phases.
These analyses are very important because they identify the factors influencing crack formation, that could be monitored during resistance welding process, as shown in Table 1.3.

Variable	Influence on Cracking
Electrode type	Domed (+); Flat (–)
Increase in specimen width	(–)
Constraining by washer	(–)
Constraining by neighboring welds	(–)
Using insulator with washers	(0)

Note: (+) — increasing cracking tendency
(–) — decreasing cracking tendency
(0) — no clear influence on cracking

Table 1.3 *Factors influencing crack formation (H. Zhang, 2002)*

Kang et al. (J. Kang, 2015) investigated, instead, the fatigue behavior of an AA5754 Aluminum alloy sheet and an Aural2 sheet, using the General Motors proprietary RSW electrode.
A controlled fatigue test was executed to determine the maximum tensile load and the specimens were analyzed using X-ray computed tomography (XCT).
Figure 1.33 shows the macrostructure and microhardness of AA5754 Aluminum alloy sheet and Aural2 sheets with and without adhesive.

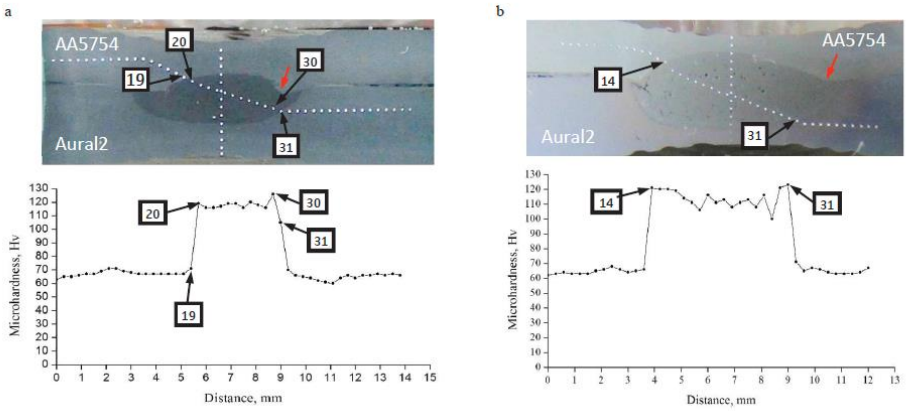

Figure 1.33 *Macrostructure and microhardness of AA5754 Aluminum alloy sheet and Aural2 sheets with and without adhesive (J. Kang, 2015)*

The use of adhesive increases the nugget size and promotes penetration. Moreover, the tensile shear stress is higher and the fatigue life is longer when the adhesive is added, as shown in Figure 1.34.

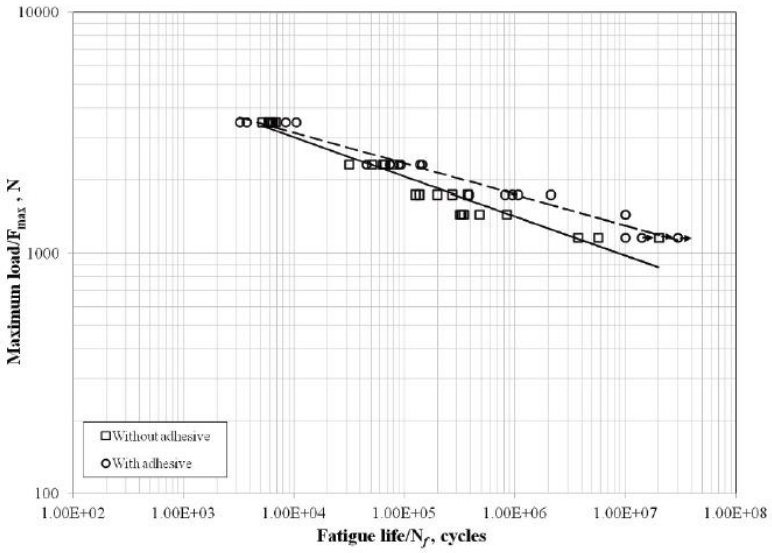

Figure 1.34 *Fatigue test results (J. Kang, 2015)*

The nugget sizes increase with the use of adhesive, but the maximum shear stress is the same with and without adhesive.
Finally, Hu et al. (S. HU, 2020) compared the resistance spot weldability form AA5754 and AA6022 Aluminum to steel. They used a Multi-ring Domed electrode to join the two aluminum sheets with an interstitial free low carbon steel. This technique is one research trend in the automotive sector to reduce vehicles weight. Figure 1.35 shows a schematic representation of the test.

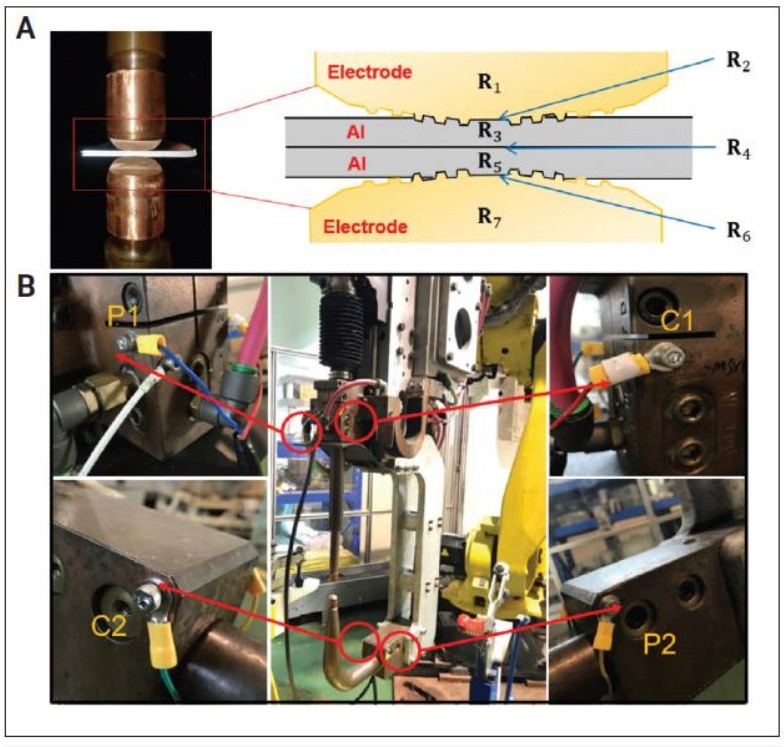

Figure 1.35 *Schematic representation of the test: C1 and C2 are the current probes, while P1 and P2 the voltage probes (S. HU, 2020)*

Tests result show that the formation of the brittle intermetallic compounds (IMCs) is reduced in AA5754 sheet thanks to the Mg content, which favors the growth of the Fe_2Al_5 phase.
AA5754 develops also a greater contact resistance, and the aluminum nuggets are smaller due to the internal expulsion.
Oxide film defects reduces the load carrying capability in AA5754 sheet, but this effect is not present when the surface is cleaned. So, cleaning step results determining in the development of Al-steel Resistance welding processes.

Observations

Resistance welding has some disadvantages:

- It is a very slow process
- It doesn't adapt to fast changes in technological processes
- The heating process is very expensive because it requires a big amount of energy

For this reason, other welding processes have been recently introduced, such as friction stir welding and laser welding. Laser welding is a very fast and flexible process, which allows an accurate control on the technological parameters. It is characterized by a high machining speed and a high automation, but laser welding requires a binding cost of investment (Anna Maloveczky, 2018).
However, resistance spot welding is still the most used process in automotive industry because it results low-cost, highly automatized and easy to control.

2 Laser Welding

2.1 Laser Welding Process

Laser Welding Process uses Laser technology to create a so called *Keyhole*, that is to say that melting happens all around a hole filled with vapor (Forsman, 2000).

Laser welding is faster than traditional welding processes and it requires only 10% of heat input to cause welding in an aluminum sample with a thickness of 2 mm.

Different types of laser can be used in laser welding, but only CO_2, Excimers, ND:YAG and diode lasers have enough power to ensure melting of the material used in industrial processes.

Laser welding was first applied to steel and stainless steel, but the interest in aluminum for automotive applications has extended the use of laser welding to aluminum sheets and aluminum alloys.

However, laser welding is employed above all in big automotive industries because it is too expensive for small companies.

Compared to other melting techniques, laser welding has a better performance in terms of melting, repair and maintenance thanks to its high welding speed, low heat input, highly focused energy, deep penetration, possibility of automation and so on.

Aluminum laser welding requires a higher beam intensity than steel. The laser power P, in fact, can be expressed as

$$\frac{P}{d} \propto \frac{T_b \lambda}{A_0}$$

where d represents the beam diameter at the surface, λ is the thermal conductivity of the material, A_0 is the absorptivity of laser light when light incises normally on the surface and T_b is the boiling temperature for the material we are considering.

Aluminum and steel have similar boiling temperature, but aluminum has lower absorptivity and higher thermal conductivity, so it requires more power to produce the same sample welding.

Thanks to research developments, CO and ND:YAG lasers have been successfully employed for aluminum laser welding but the actual challenges are focused on improving strength and quality of welding.

The main problem of laser welding is the formation of a plasma against the laser ray beam, due to the reflection properties of the melted materials.

Laser Welding Modes of Operation

There are different modes of operation for laser welding (Ebindustries, s.d.). In Pulsed Laser welding, the beam works between on and off values at very high frequency. Each pulse determines a welded region and then another pulse is applied. The pulse series determines a continuous bead, but high frequency is important to reduce defects in the melting samples. This is the best technique for aluminum welding. Figure 2.1 shows a comparison between continuous and pulsed laser welding (Williams, s.d.).

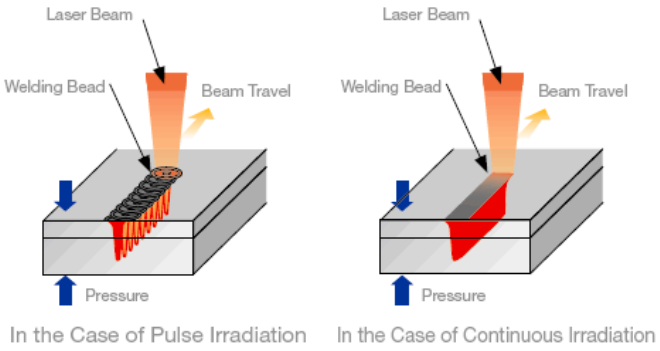

Figure 2.1 *Comparison between continuous and pulsed laser welding* (*Williams*, s.d.)

In continuous laser welding (Ebindustries, s.d.), instead, a steady beam of laser light is applied to the sample to be welded and this technique is very useful to produce deep penetration welds. Continuous waves travel at a speed of about 25/100 inches per minute. This kind of laser welding is applied, above all, on crack sensitive aluminum alloys.

Laser assisted friction stir welding consists in the use of a filler to prevent crack formation. The filler is usually a more weldable alloy and this technique is suitable for heat sensitive components, such as electronics components.

Figure 2.2 shows a scheme of laser assisted friction stir welding process (Daftardar, 2009).

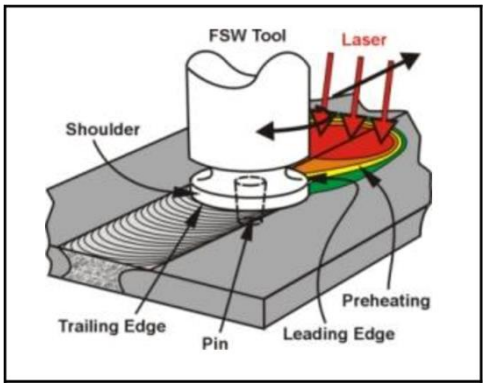

Figure 2.2 *Scheme of laser assisted friction stir welding process (Daftardar, 2009)*

2.2 Aluminum Laser Welding

Aluminum is the most important material in automotive applications because:

- it is abundant in earth crust
- it has a very low density, so aluminum vehicles have a reduced weight and a resulting reduced fuel consumption
- it forms a very hard oxides that protects the material from corrosion
- it has a very high thermal conductivity (209 W/mK)
- it has a low melting point (660.3 °C)

The laser power is strictly influenced by absorptivity. Aluminum is highly reflective, as shown in Figure 2.3.

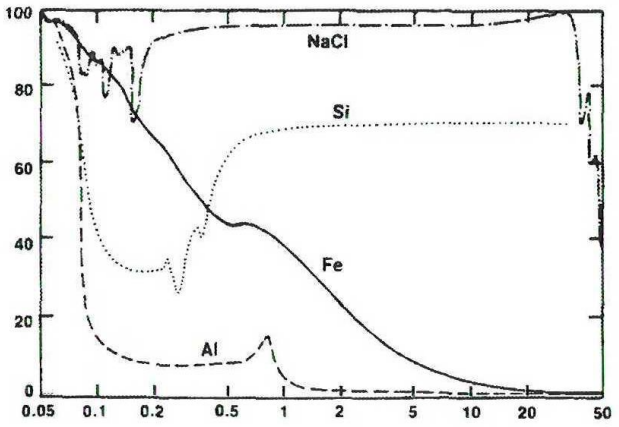

Figure 2.3 *Dependence of absorptivity from wavelength for different materials (Forsman, 2000)*

Figure 2.4 shows, instead, that aluminum absorptivity increases with thickness in aluminum alloys.

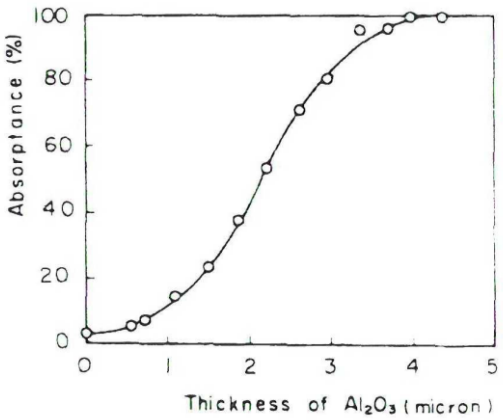

Figure 2.4 *Dependence of absorptivity of a CO light as function of Al2O3Thickness (Forsman, 2000)*

Moreover, aluminum has a melting point lower than steel (660°C), determining a wider weld sample, as depicted in Figure 2.5.

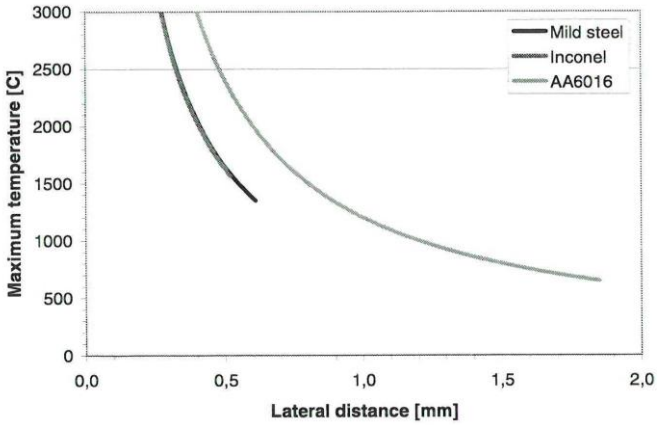

Figure 2.5 *Maximum temperatures with respect to lateral distance for different materials (Forsman, 2000)*

Aluminum melts have a low viscosity, that reduces the risk of irregular keyhole movements and of melt sagging. During melting process, heat is concentrated on a very small area because heat flow can travel and reach other areas, causing the melting of non-desired samples or deformation. For this reason, melting process should be controlled accurately and automated methods, such as Laser and Electron Beam should be preferred because they allow rate and power regulation and the exact positioning of the sample.

Nd:YAG laser is usually used for aluminum laser welding because CO_2 laser is not suitable due to aluminum optical absorptivity.
Recently, high power Yb glass fibers lasers have been introduced because they allow deep penetration with a continuous wave in highly reflective materials, such as aluminum alloys. Moreover, when these lasers operate in a keyhole mode, there is the formation of a weld seam with high aspect ratio but there is a major probability of defects formation (Garavaglia M., 2020).
During melting, there could be the formation of an oxide layer on the working surface and the sample could be contaminated or it could result porous. Chemical or mechanical processes can be applied on samples surfaces to remove the oxide film, that could affect the surface reflectivity.
Aluminum samples also require pre-welding processes to eliminate lubricants and hydrocarbon contamination, which could influence melting process.
Laser welding is also very useful with crack sensitive materials, because employing filler materials can prevent crack formation.

Joint preparation, fixturing and types.

Moreover, joints need to be prepared before melting because aluminum is a soft material and contamination could occur. Grinding process, machining methods, compressed shop air should be avoided to protect samples and the use of stainless-steel wire brushes is recommended.
Additionally, joints need good weld fixturing to ensure the correct positioning of the laser beam.

There are three joint types (Ebindustries, s.d.):
1) Butt joint
2) Lap joint
3) Fillet joint

Figure 2.6, 2.7 and 2.8 show different joint types.
Referring to Figure 2.6, in a butt joint, there are two thermoplastic materials, A, with variable scattering and B, absorbing the transmitted light at the interface. WHAZ represents the width of heat affected zone, while WB is the width of material B. WL is, instead, the width of laser beam at joint and WLB the width of laser beam at face of part A. Finally, MA and MB are respectively the depths of heat affected zone in part A and B (ResearchGate, s.d.).

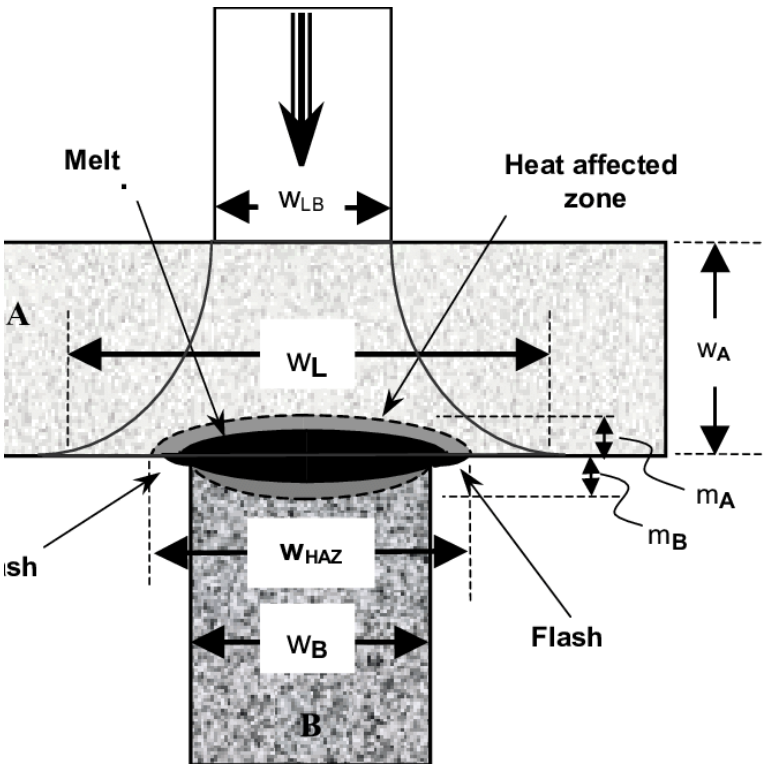

Figure 2.6 *Butt joint scheme (ResearchGate, s.d.)*

Figure 2.7 shows instead an example of lap joint.

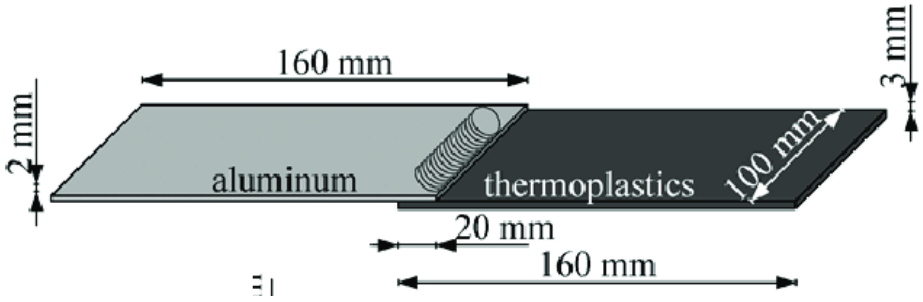

Figure 2.7 *Lap Joint scheme (ResearchGate, s.d.)*

Finally, Figure 2.8 shows an example of fillet joint in various orientations. Images from (a) to (d) illustrate the transverse section of the fillet joint perpendicular to the welding direction, while images from (e) to (g) illustrate the central longitudinal section of the fillet joint parallel to the welding direction.

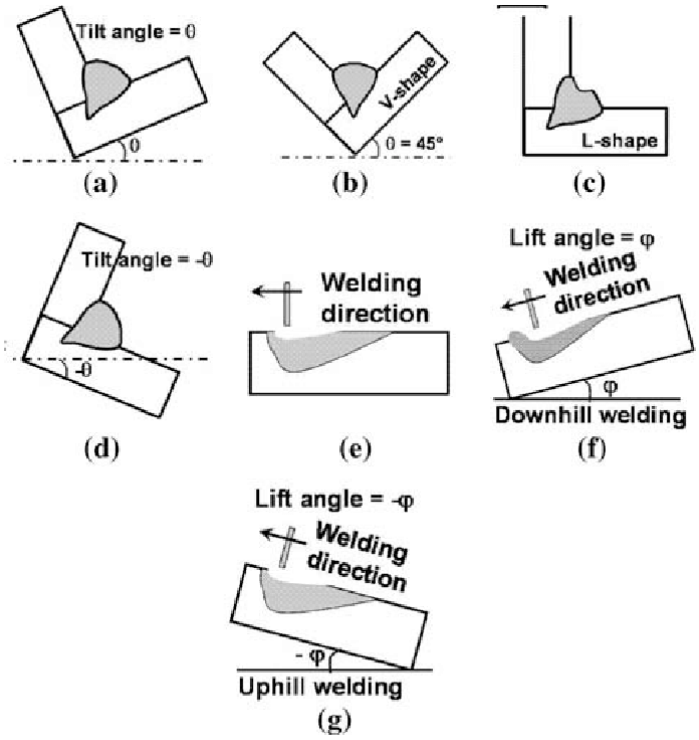

Figure 2.8 *Fillet Joint Scheme. (a) Fillet joint with tilt angle θ, (b) symmetric V-shaped joint, (c) L-shaped joint, (d) fillet joint with tilt angle - θ, (e) welding in flat position, (f) downhill welding with lift angle φ (g) uphill welding with lift angle - φ (ResearchGate, s.d.)*

To improve aluminum welding, cover gases are often used, but they must be chosen according to the laser employed, because the wrong cover gas can produce the plasma generation or changes in the mechanical properties of the material. Argon is usually used for Nd:YAG lasers, helium reduces the plasma formation but it requires very high flow rates, argon and helium mixtures are applied in the most part of aluminum welding processes, while argon and oxygen mixtures ensure high efficiency and weld quality. Argon and Hydrogen mixtures are mostly used in steel welding while nitrogen and CO_2 mixtures are also often employed but they can determine the oxide formation.
However, cracks, pores, edge defects can occur during melting so different aluminum alloys have been tested to reduce imperfections formation.

2.3 AA5754 Aluminum Alloy

Aluminum alloys are used to improve melted samples quality and strength. 5xxx aluminum alloys become sensitive when temperature reaches 65°C and crack formation can be reduced using a supplemental welding material, which also increases the strength of the alloy. Moreover, gas covering, mainly Argon or Helium, may improve the weld quality.
AA5754 alloy is employed in most automotive and naval applications for its low weight, medium-high mechanical properties, high resistance to corrosion, low cost and high recyclability (Leo P., 2016).
Kose investigated microstructure and mechanical properties of AA5754 aluminum alloy joints, obtained with pulsed Nd:YAG micro scale laser welding technique (Kose, 2016). There was no evidence of pore formation in the welded joints, as shown in Figure 2.9 and 2.10.

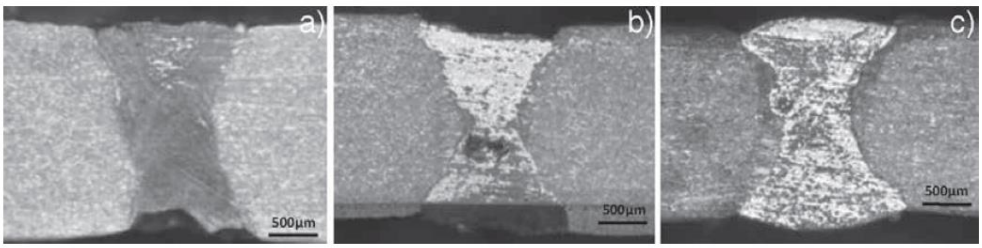

Figure 2.9 *Weld seam profiles (Kose, 2016)*

Welded joints obtained with pulsed current exhibit a finer grain microstructure than welded joints obtained with continuous current. Medium heat inputs let to the formation of a coaxial grain microstructure that prevents crack formation. Nd:YAG laser, in fact, doesn't require a high power density, so, there is the development of a fine coaxial grain microstructure in the melt samples, that prevents element losses and cracks development.

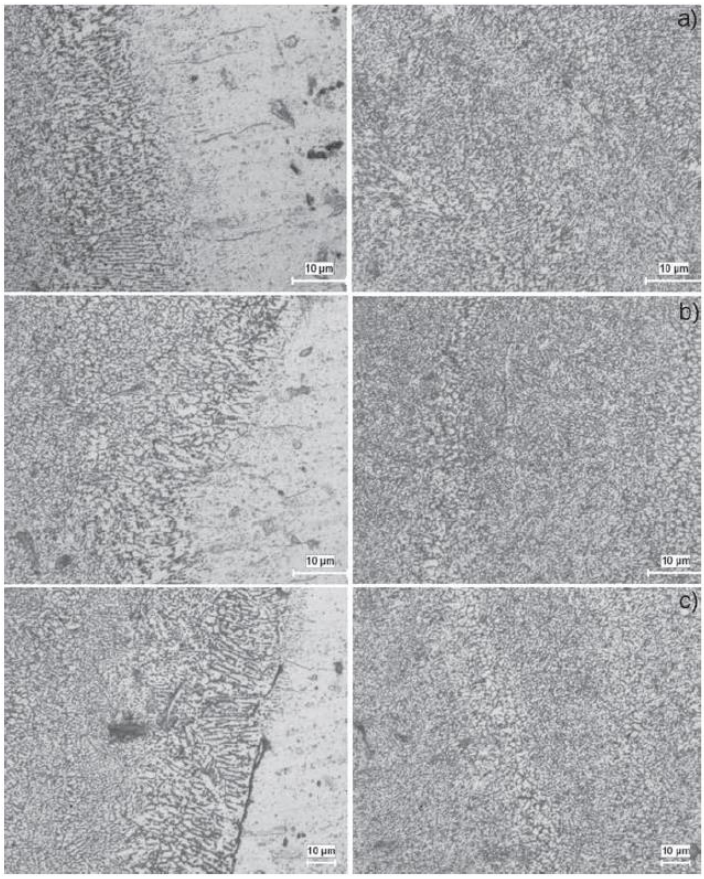

Figure 2.10 *Weld samples microstructure (Kose, 2016)*

Tensile test showed that melt samples have greater tensile and yield strength than the base metal and joint strengths can be improved using siliceous supplemental welding wires. Bending tests showed, instead, that joints have little formability. All the tests showed that joints obtained with pulsed Nd:YAG micro scale laser welding technique are suitable for the most part of industrial applications.
Aluminum Alloys Laser welding is very important for fillet and lap-joints configurations. Double lap-joints are very important in automotive applications because there is a reduction in the number of joints, but gap formation can occur (Garavaglia M., 2020). Keyhole Laser welding mode allows a deep penetration process which facilitates the joining of the different parts, reducing gap formation but autogenous laser beams ensure a bigger accessibility to the welding zone. Moreover, the full penetration in laser welding is suitable for the complete connection of all layers. Garavaglia et al. (Garavaglia M., 2020) analyzed the laser welding of A5754 Alloy in a double lap-joint configuration and they used a laser source with integrated photodiodes to monitor the reflected laser light coming from the emission process. Figure 2.11 illustrates the schematic representation of the measured weld seam characteristics, while Figure 2.12 shows the tests performed on the samples. Autogenous laser welding has been used for a three sheets sample.

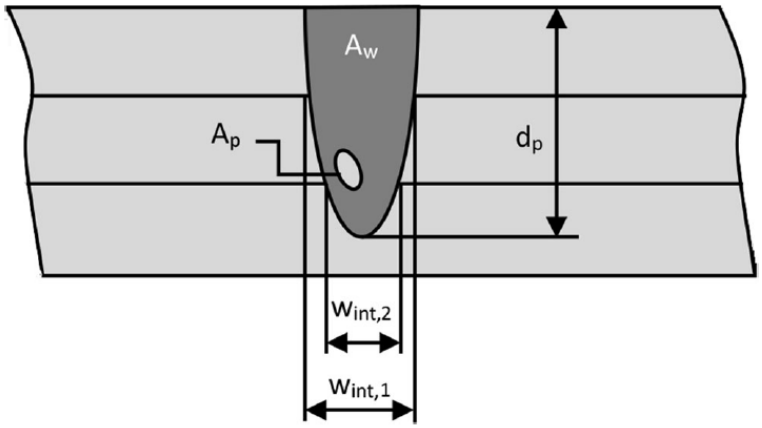

Figure 2.11 *Schematic representation of the measured weld seam characteristics (Garavaglia M., 2020)*

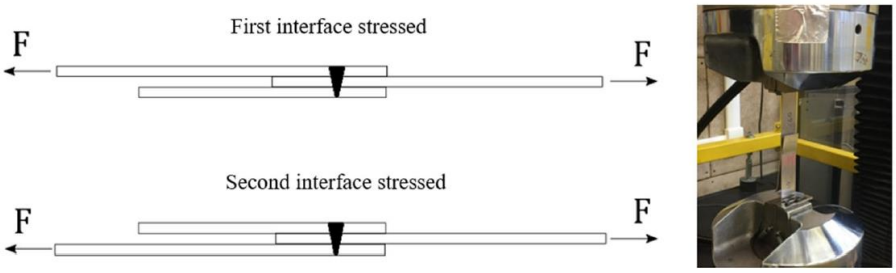

Figure 2.12 *Tests performed on the samples (Garavaglia M., 2020)*

Table 2.1 reports the testing values.

Fixed parameters	Values
Power	3000 W
Variable parameters	**Values**
Welding speed, v	2.2, 5.2, 8.2, 11.2, 14.2 m/min
Focal position, f	0, − 2, − 4 mm

Table 2.1 *Testing values (Garavaglia M., 2020)*

Figure 2.13 shows the keyhole induced porosity for various weld speeds, *v*, and focal positions, *f*, while Figure 2.14 illustrates mechanical strengths at the interfaces of the samples for different values of the process parameters.

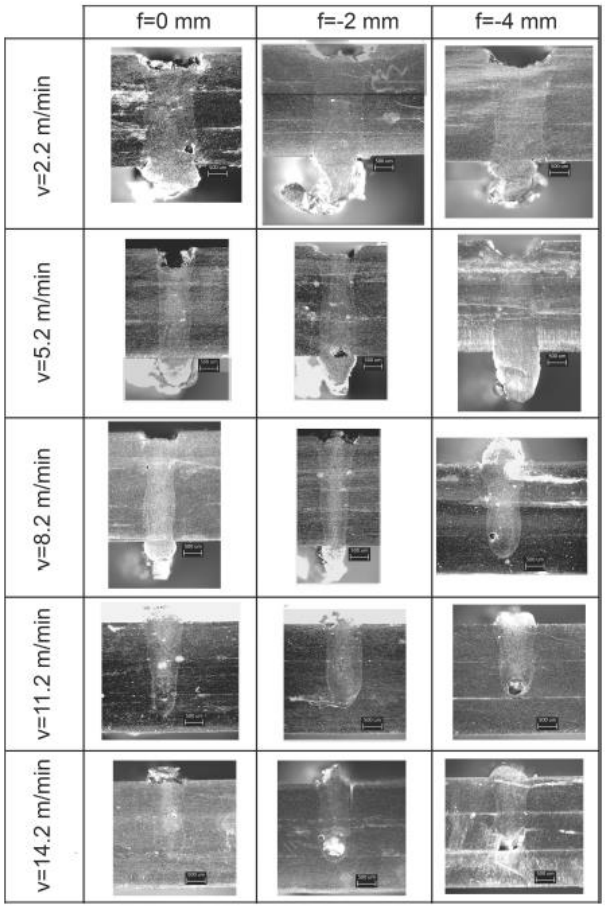

Figure 2.13 *Keyhole induced porosity for different process parameters (Garavaglia M., 2020)*

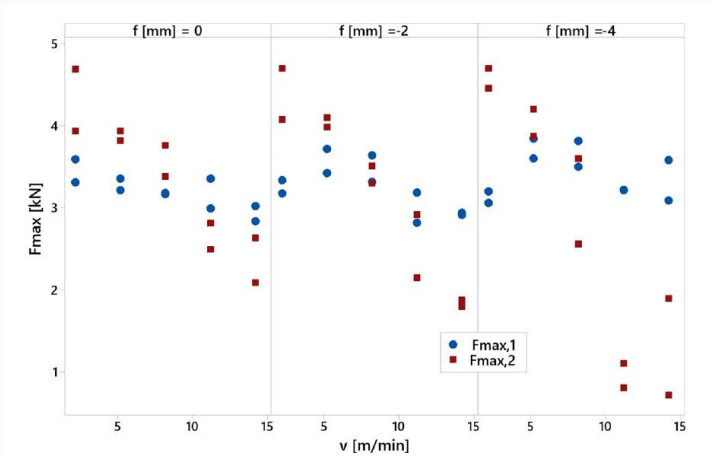

Figure 2.14 *Mechanical strengths at the interfaces of the samples for different values of the process parameters (Garavaglia M., 2020)*

The second interface strength is deeply affected by the welding speed while the first interface is less influenced by the variation of the process parameters.
The back reflected light signal intensity is a useful predictor of the efficacy of the process, in fact a lower signal intensity is associated with a more stable weld, where full penetration happens. The back reflected light signal intensity is also associated to the second interface strength.

2.4 Laser welding application in dissimilar joints

AA5754 is used with Titanium alloys to create dissimilar joints for applications where dissimilar properties are required simultaneously. These joints are realized with laser welding because this technique allows to focus high energy beams on restricted areas, also reducing imperfections formation. Most part of hybrid structures is composed by the combination of aluminum and titanium and the primary problem is the formation of brittle intermetallic zones.

AA5754 and Ti -6Al-4V joints

Leo et al. (Leo P., 2016) analyzed mechanical properties of AA5754 and Ti -6Al-4V joints. They use the laser system Ytterbium Laser System (wavelength 1070.6 nm) to melt the two alloys' pieces, covered with Argon and Helium protection. The laser beam was focused on Titanium side, as shown in Figure 2.15 and they used different beam powers and melting speeds.

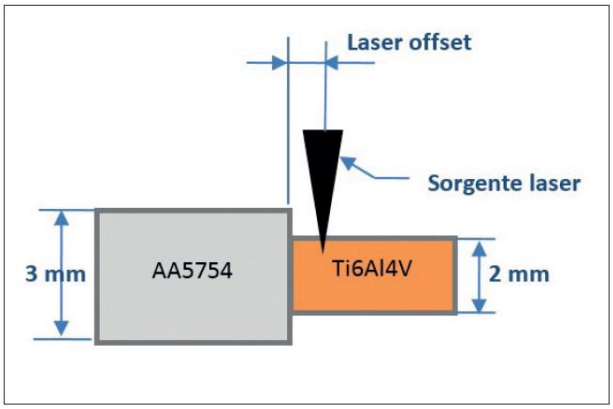

Figure 2.15 *Working layout for AA5754 and Ti -6Al-4V joints (Leo P., 2016)*

Experimental plan is shown in Table 2.2 (Leo P., 2016)**.**

Samples	Power (W)	Melting Speed (mm/min)	Line Energy (J/mm)	Laser Offset (mm)
S_1	1200	1000	72.0	1
S_2	1200	2000	36.0	1
S_3	1500	3000	30.0	1
S_4	1500	3000	30.0	0.75

Table 2.2 *Experimental plan (Leo P., 2016)*

Analyzing the optical macrographs of the joints cross sections, the authors noticed that all samples exhibited a complete keyhole penetration, as illustrated in Figure 2.16.

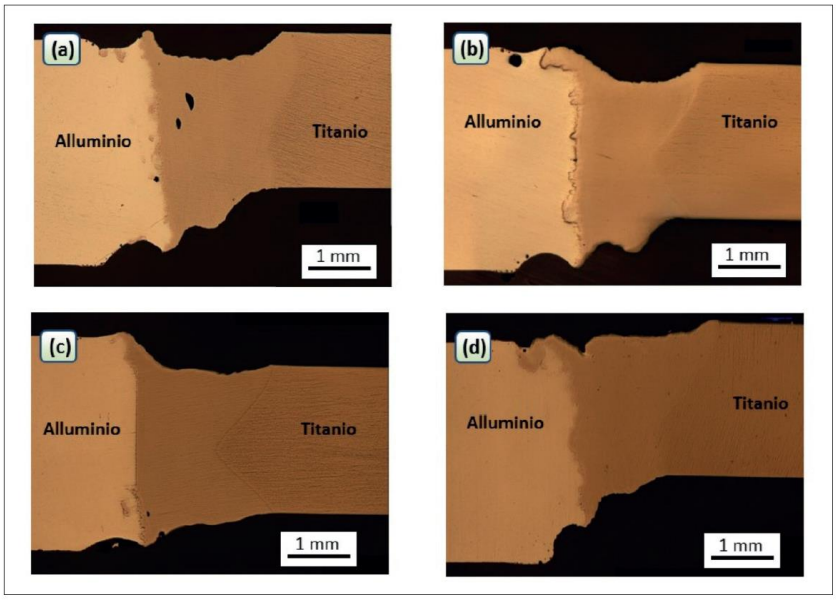

Figure 2.16 *Optical macrographs of the joints cross sections (Leo P., 2016)*

Aluminum-titanium laser joining is usually made with the brazing approach, while keyhole approach associated with butt joint is more difficult to be applied because there may be the mixing of aluminum and titanium. However, keyhole mode reduces the preparation times of the samples, and the process needs less parameters to be controlled. Tomaschchuk et al. (Tomashchuk I., 2014) analyzed the weldability of AA5754 alloy to titanium alloy Ti6A14V using YB:YAG laser (up to 6kW and spot diameter of 600μm) working in a keyhole mode at high speeds (up to 12 m/min), in terms of mechanical properties and macrostructure of the joints. The butt configuration was employed, as illustrated in Figure 2.17.

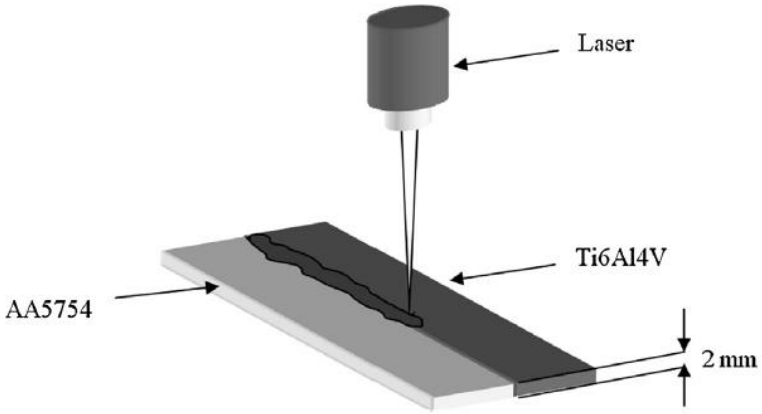

Figure 2.17 *Butt Welding Configuration (Tomashchuk I., 2014)*

The samples were analyzed with a scanning electron microscope and x-ray diffraction was used to study phase composition. The samples exhibited two mixing zones, one rich of aluminum and the other one rich of titanium, separated by a well-defined interface, composed by aluminum and titanium lamellae (Figure 2.18). Aluminum and titanium have very different fusion temperatures so there isn't the mixing between these two materials. Beam position affects the shape of the capillary. 0.2 mm offset causes the shift of the capillary in only one material, while centered beam position determines a shared capillary between the two materials.

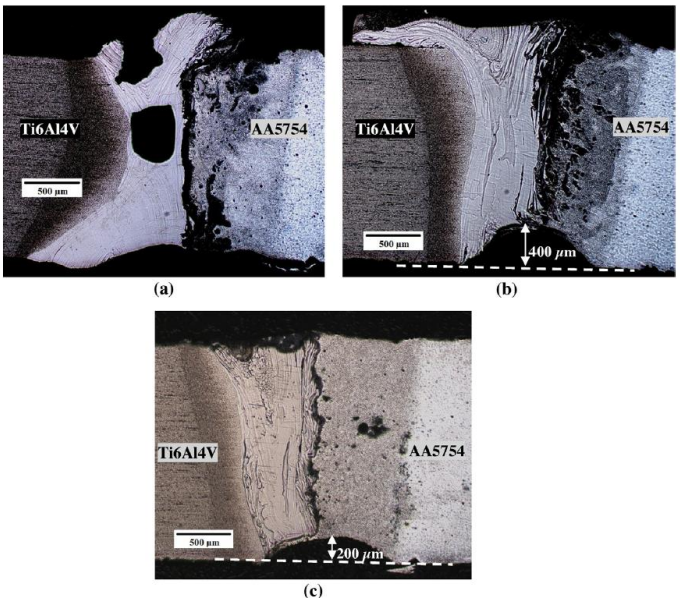

Figure 2.18 *AA5754 - Ti6A14V joints obtained with different positions of laser beam: (a) 0.2 mm beam shift to Ti6A14V, (b) centered beam, (c) 0.2 mm beam shift to AA5754 (Tomashchuk I., 2014)*

Mechanical properties tests showed that tensile behavior is similar for all samples even if tensile force reaches its maximum value when the beam offset is shifted to aluminum side and linear high energy is used (Figure 2.19).

When the laser beam is shifted to aluminum side there is the formation of a thin interface, and the tensile strength is maximal. On the contrary, when the laser beam is shifted to titanium side there is the formation of a thick interface with a great risk of cracks and voids formation. Finally, when the laser beam is centered, there is a formation of a thick interface, and the tensile strength drastically reduces.

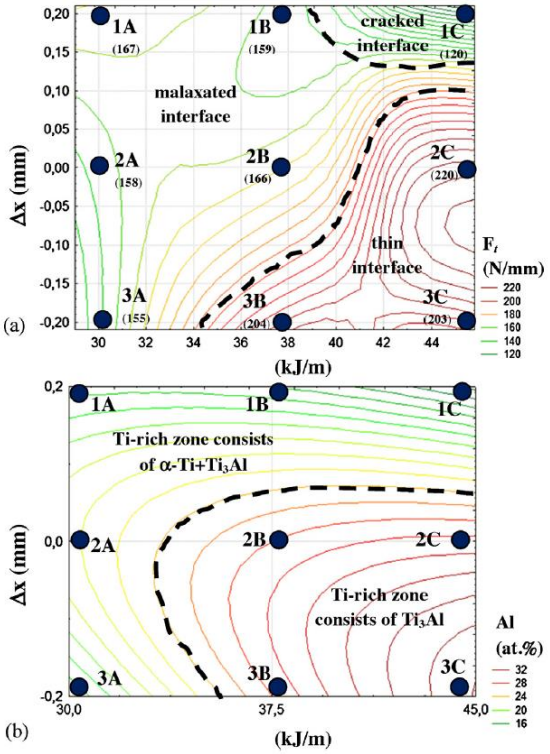

Figure 2.19 *Linear Tensile Force (N/mm) of the welds (Tomashchuk I., 2014)*

Figure 2.20 shows, instead, how hardness varies in the different zones of the samples. High tensile forces correspond to limited brittle zones.

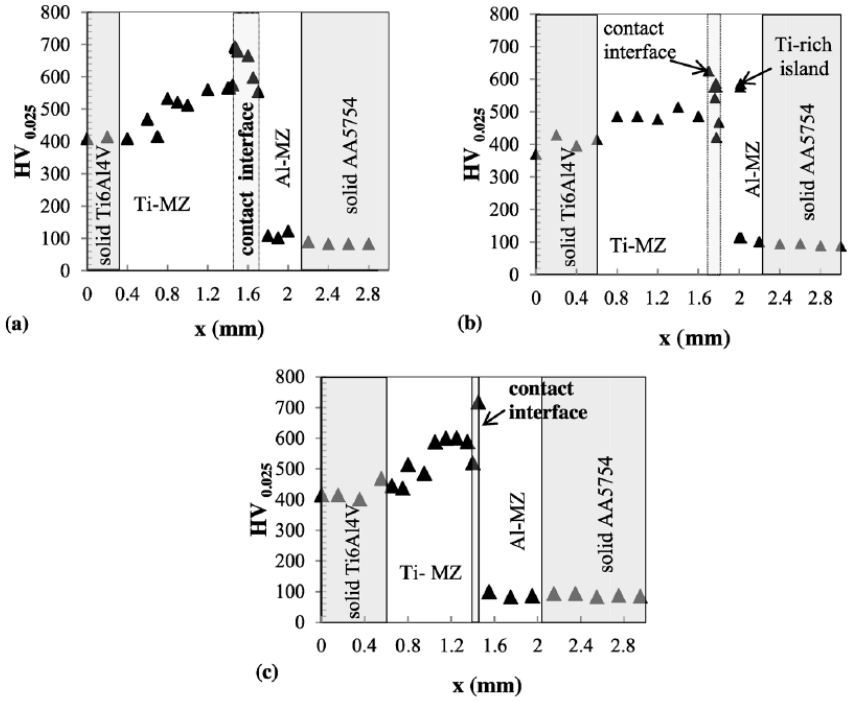

Figure 2.20 *Microhardness across the samples with crack contact interface (a), mixed interface (b) and thin interface (c) (Tomashchuk I., 2014)*

Tomaschchuk et al. (Tomashchuk I., 2014) also analyzed how contact interface affects the tensile strength of the welds (Figure 2.21). Cracks probably starts at the thin interface and then propagate in the aluminum region. Aluminum is more ductile than brittles, determining a higher tensile strength of the welding.

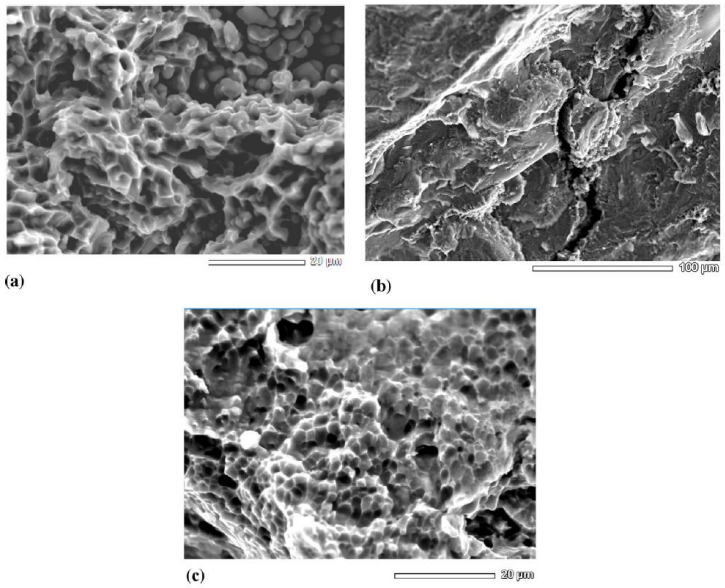

Figure 2.21 *SEM images of fracture surfaces: aluminum zone (a), titanium zone (b). aluminum-titanium zone (c) (Tomashchuk I., 2014)*

So, for thick interfaces fracture involves only intermetallic layers, while thin interface fracture affects both aluminum zone and intermetallic layers.

AA5754 and T40 joints

Peyre et al. (Peyre P., 2014) investigated the application of laser welding to AA5754 and T40 joints in conduction regime, that is to say without considering keyhole formation, with low scanning speed, to allow liquid aluminum-solid titanium inter-diffusion. They also analyzed the effect of a A40430filler wire. The experimental joining conditions are shown in Figure 2.22.

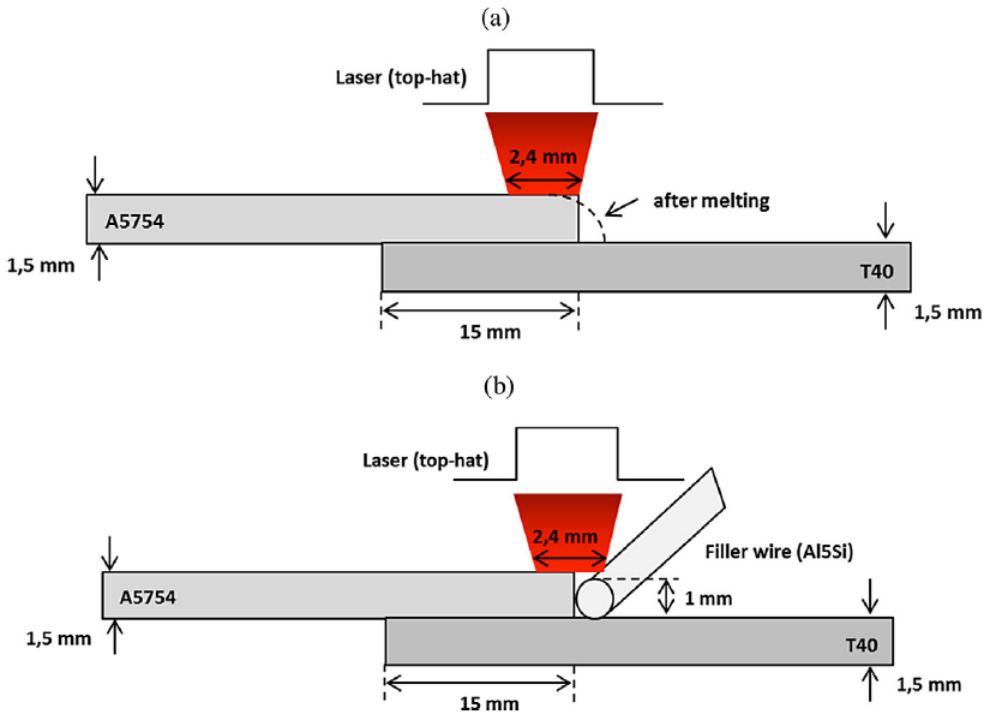

Figure 2.22 *Experimental joining conditions without (a) and with (a) a filler wire (Peyre P., 2014)*

A vertical clamping was applied to limit deformations and surface treatments were applied on both aluminum and titanium to improve welding. Moreover, a black paint was sprayed on aluminum surface to increase absorptivity.

Mechanical properties were tested using a LASAT bond analysis technique: a uniaxial tensile stress is applied on the Al-Ti interface through a shock wave and evaluating the crossing between incident and reflected waves. This dynamic test was also carried through a finite element analysis with Abaqus 6.9.

The tests were carried out varying the scanning speed and the power levels. All the samples showed good mechanical properties even if ripples occurred near aluminum side and they were probably due to a limited aluminum melt-pool flow, as shown in Figure 2.23.

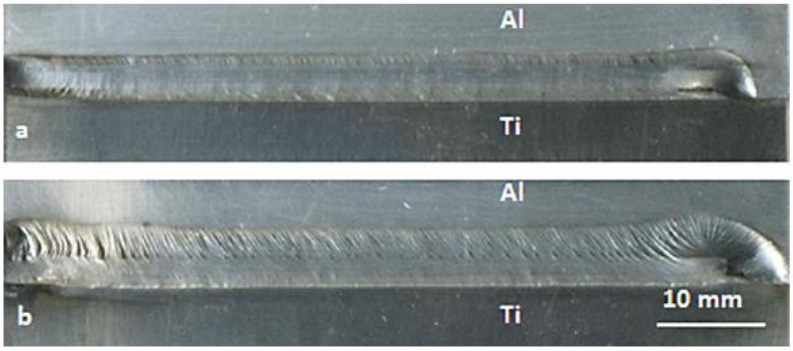

Figure 2.23 *Top view of Al/Ti joints (Peyre P., 2014)*

Figure 2.24 illustrates, instead, tests result on Ti/Al joints related to Power values and scanning speed.

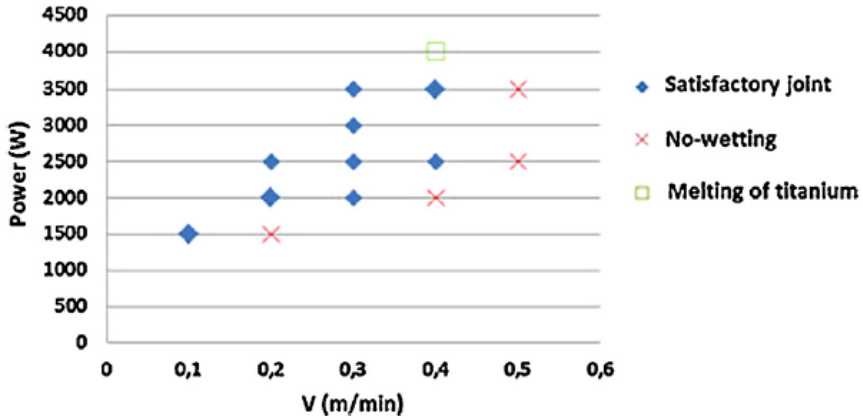

Figure 2.24 *Tests results on Ti/Al joints related to Power values and scanning speed (Peyre P., 2014)*

Mechanical tests estimated a joint resistance of 120 MPa, with a similar behavior with and without a filler wire (Figure 2.25).

Failures happened above all near discontinuities and cracks created in aluminum, but they propagate in a limited area near the interface.

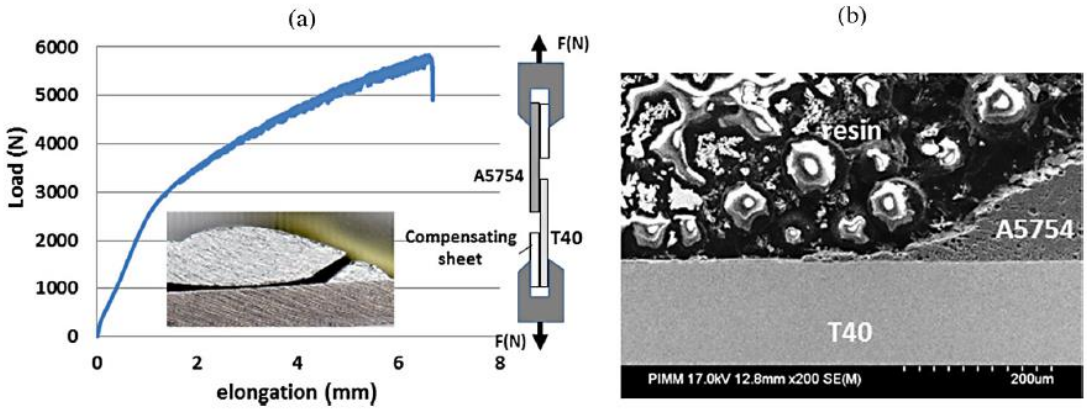

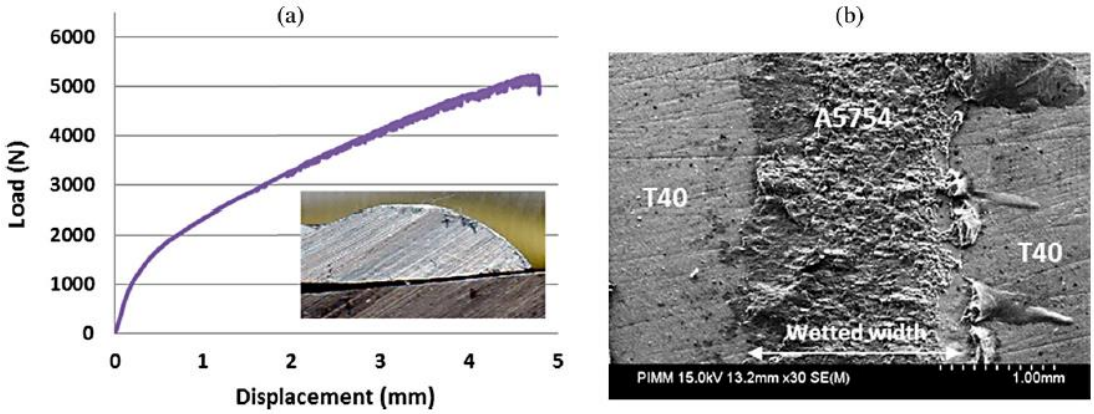

Figure 2.25 *Tensile curves obtained without a with a filled wire respectively (Peyre P., 2014)*

LASAT bond tests finally showed a good interface resistance, of about 0.68 GPa but it wasn't possible an accurate identification of cracks.

Behulova et al. (Behulova M., 2017) analyzed temperature fields for laser welding of 5754 Aluminum Alloy and Titanium Grade 2 through a numerical simulation with the finite element software Ansys. Numerical results were employed to set the welding parameters. Table 2.3 shows chemical compositions of the sheets materials.

TABLE 1: Chemical composition of titanium Grade 2.

Element	Fe	C	O	H	N	Ti
wt.%	0.3	0.1	0.25	0.015	0.03	Balance

TABLE 2: Chemical composition of AW 5754 aluminium alloy.

Element	Mg	Mn	Fe	Si	Al
wt.%	2.6 to 3.2	0.5	0.4	0.4	Balance

Table 2.3 *Chemical composition of 5754 Aluminum Alloy and Titanium Grade 2 (Behulova M., 2017)*

Numerical simulation was implemented through the solution of a coupled thermal-fluid and stress-strain problems, also considering phase transformations. The authors also evaluated stresses acting during welding and residual stresses after cooling, to predict crack formation. Data obtained with numerical simulation were, then, used perform tests on the sheets. Figure 2.26 illustrates temperature fields in the welds when laser power is set to 850 W and the laser offset to 250 μm.

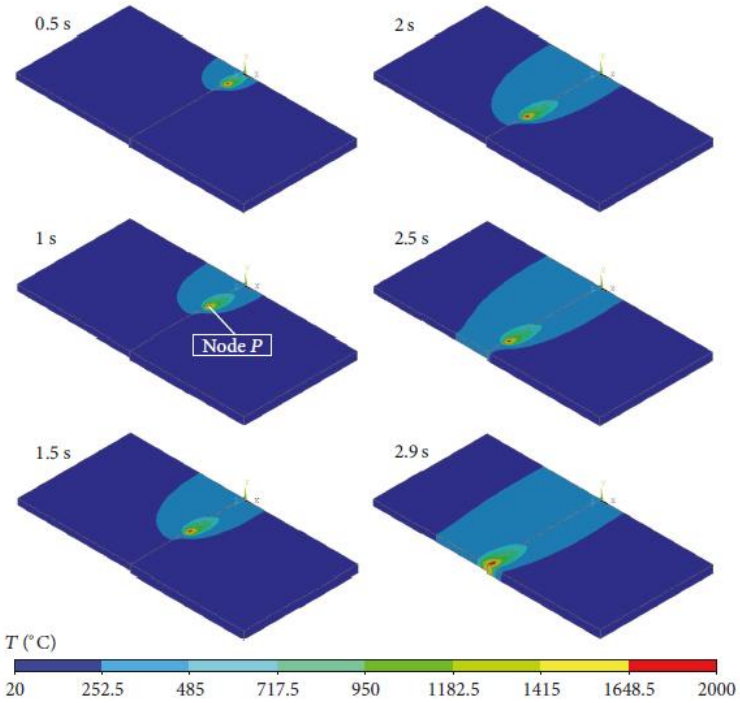

Figure 2.26 *Temperature fields in the welds when laser power is set to 850 W and the lase offset to 250 µm (Behulova M., 2017)*

Figure 2.27 shows instead the temperature time history for a node placed on Titanium side, while Figure 2.28 depicts how temperature is influenced by the distance from the weld center for different laser powers (a) and laser offsets (b).

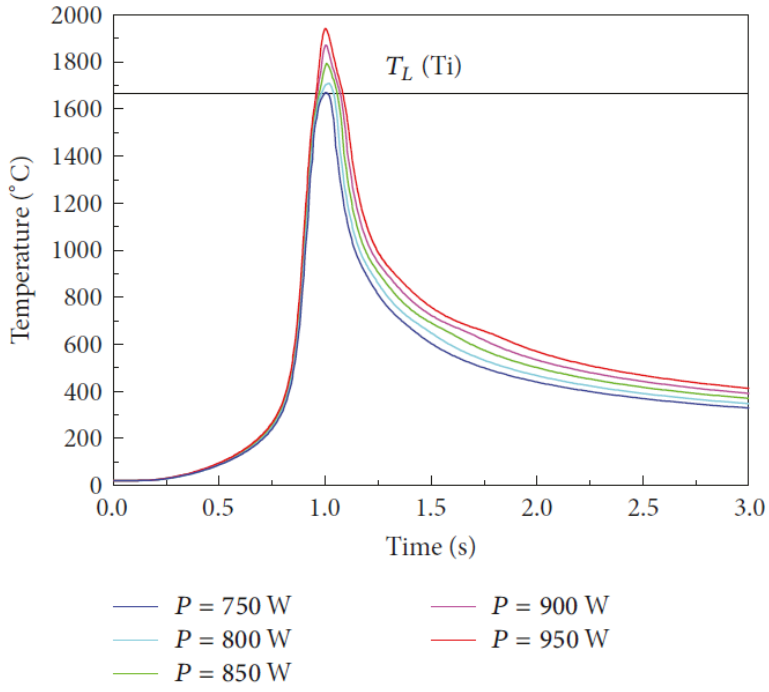

Figure 2.27 *Temperature time history for a node placed on Titanium side (Behulova M., 2017)*

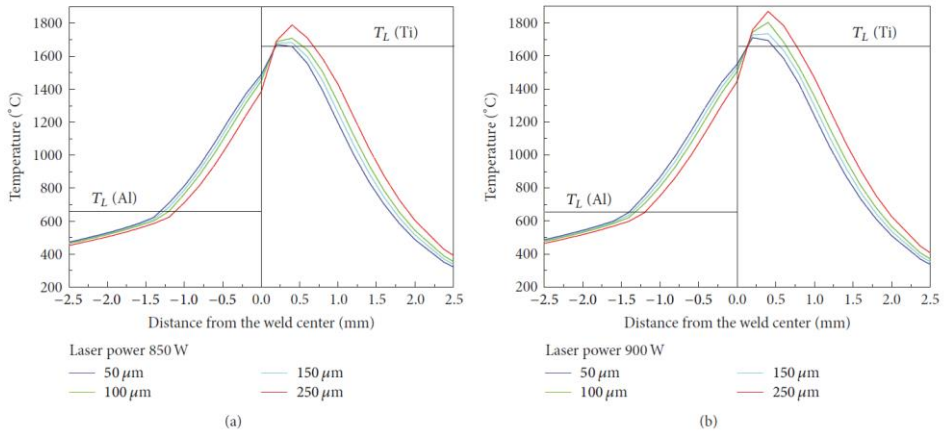

Figure 2.28 *Influence of the distance from the weld center for different laser powers (a) and laser offsets (b) on temperatures (Behulova M., 2017)*

Maximum weld pool temperature increases when laser power is higher and also the interface temperature has the same behavior. Moreover, smaller laser offsets are not suitable for useful thermal conditions. Numerical results suggest that the best conditions for the production of butt weld joint of Titanium and AA5754 Aluminum Alloy are (Behulova M., 2017):

- Laser Power ranging between 800W and 900W
- Laser beam offset ranging between 150μm and 250 μm

Figure 2.29 shows macrostructure and microstructure of the joint and of Titanium and aluminum interfaces.

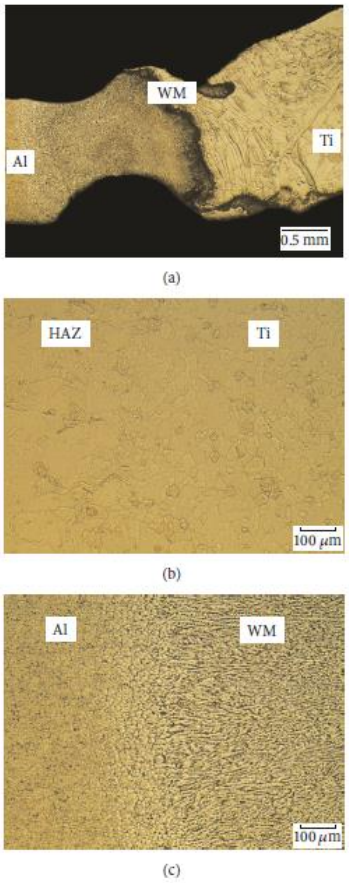

Figure 2.29 *Macrostructure and microstructure of: joint, Titanium interface and aluminum interface (Behulova M., 2017)*

Laser and Scanning electron microscopy, X-ray diffraction, microhardness and tensile stress tests were conducted on the weld samples. The authors found brittle intermetallic compounds at the interface of the weld sheets and their formation reduces when laser beam offset increases at the titanium side. Moreover, microhardness is higher in the weld metal than in the base metals. Tensile strength reaches its maximum value when laser power is set to 800 W and the laser beam offset to 250μm. Tensile strength also increases when heat input decreases and when the laser beam offset is higher at titanium side. Finally, Figure 2.30 illustrates how tensile strength varies with laser power and laser offset (Behulova M., 2017).

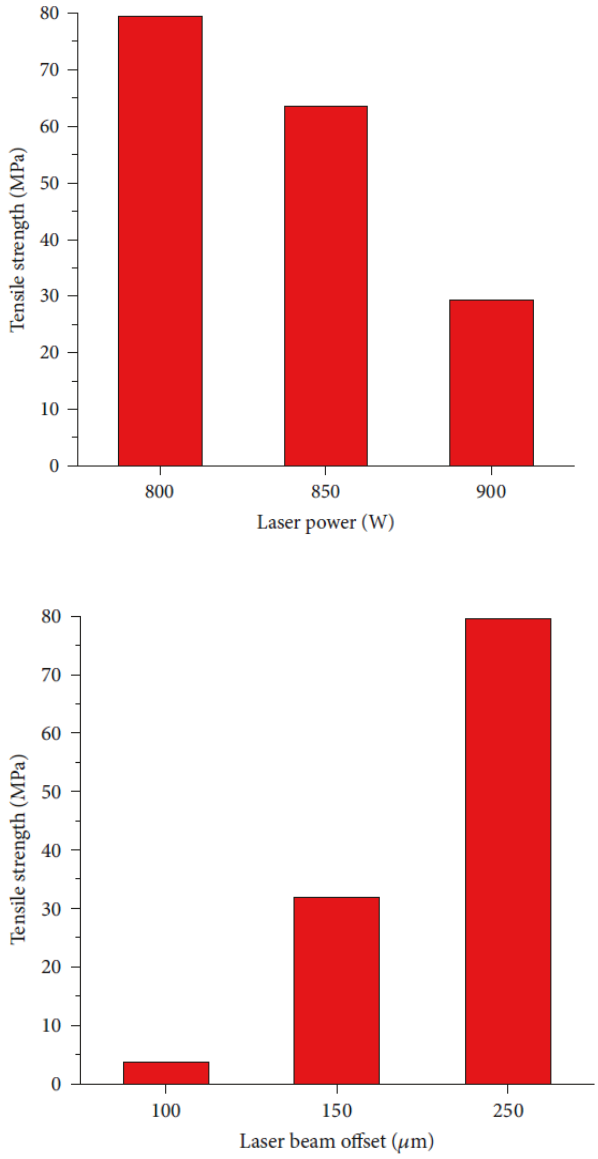

Figure 2.30 *Dependence of tensile strength with laser power and laser offset (Behulova M., 2017)*

3 Capacitor Discharge Welding

3.1 Capacitor Discharge Process

Capacitor discharge (CDW) is a welding technique that employs large capacitors banks to store energy and quick release it, as shown in Figure 3.1 (Power Stream, 2006).

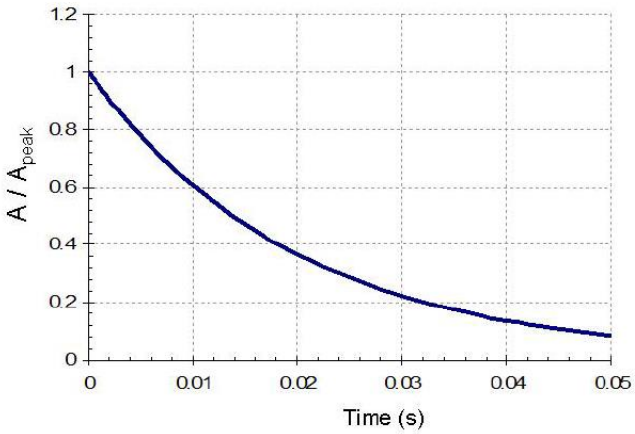

Figure 3.1 *Capacitor Discharge curve (Power Stream, 2006)*

CDW process can be divided into four steps, Figure 3.2. During the first step, a press force is applied to ensure the workpiece positioning, then, during the second step, capacitor discharge begins and mechanical load and heating lead to the fusion and the softening of the material. The third step is the sink-in phase, while, during the fourth step, cooling determines the formation of the metallurgic joint, above all due to conduction.

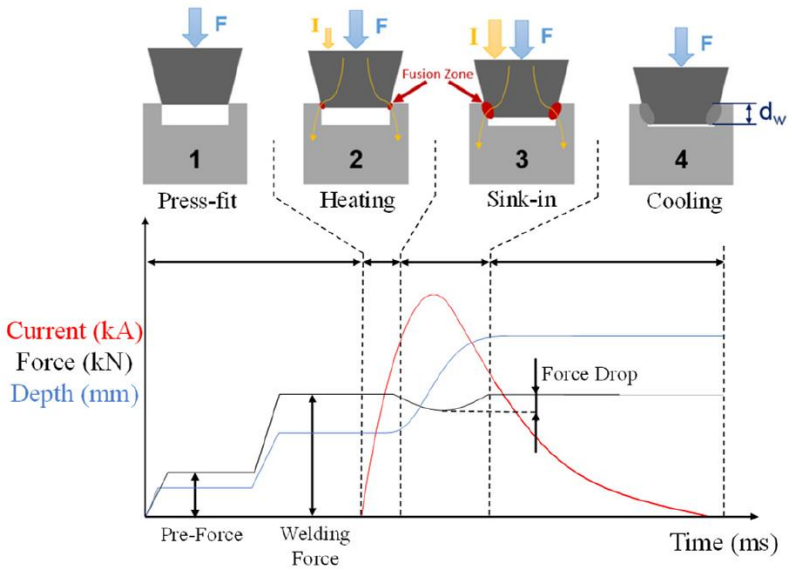

Figure 3.2 *CDW process steps (Meiners M., 2020)*

There are different possibilities to joint materials, as shown in Figure 3.3. Melting can occur without previous heating, with the application of a very high pressure (area I), or combining the effects of pressure and heating (Area II) or heating materials at a temperature higher than melting point (area III).

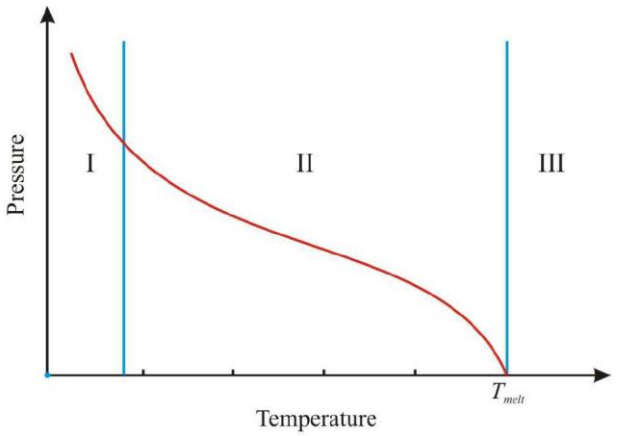

Figure 3.3 *Pressure-Heating diagram for welding (Dziho M.E.)*

Capacitor discharge welding belongs to the area II because the process uses both pressure and heating. First, an electric arc is created, determining the parent material heating, then a pressure is applied to join the melted components. Moreover, pressure values are crucial for melting process, because a low pressure can cause unconnected areas, while too high pressures can affect geometrical and mechanical properties of the joints.

There are two types of discharge welding: contact mode welding and electrical resistance welding. Contact mode is widely used in civil engineering applications, such as dowels melting.

The energy stored in the capacitor is expressed as

$$E = \frac{1}{2}CV^2$$

Where E represents the energy, C is the capacitance of the capacitor, while V is the electric voltage. According to this relation, a small difference in voltage is associated to a big difference in welding energy. So, capacitor discharge process requires less energy than resistance welding.

Figure 3.4 shows, instead, typical values of the peak currents occurring during contact mode welding.

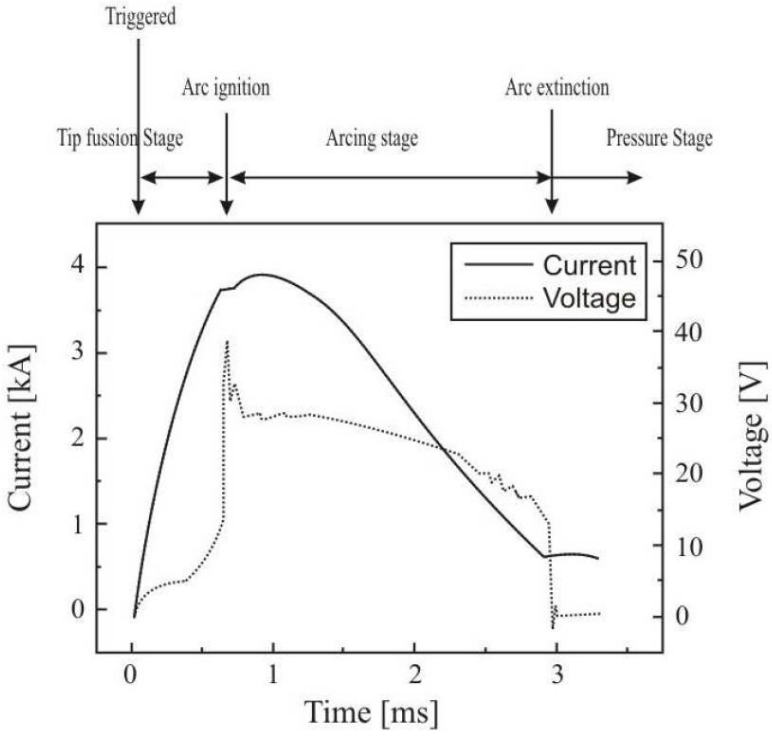

Figure 3.4 *Typical electric current and voltage occurring during capacitor discharge welding (Dziho M.E.)*

Figure 3.4 shows that welding happens in a very short time and the process can be divided into three phases:

1) Melting of ignition tip
2) Arcing
3) Phase of pressing

In the first phase, ignition tip is heated, and melting begins. Then, there is the arc generation and, finally, pressure completes the welding.

Since the discharge process is very quick, this welding technique is suitable for very electrical and thermal conductive materials, such as aluminum and copper. During melting, a very high current is applied on the pieces and there is energy dissipation in the form of heat due to the electric resistance of the materials involved. On the microscale, contact points affect welding because there are only few contact points at the beginning but then, metal bridges melt determining the formation of other metal bridges. Later, all the bridges fuse, the contact resistance becomes zero and the weld formation is determined by the material bulk resistance. Figure 3.5 illustrates microscale surface roughness.

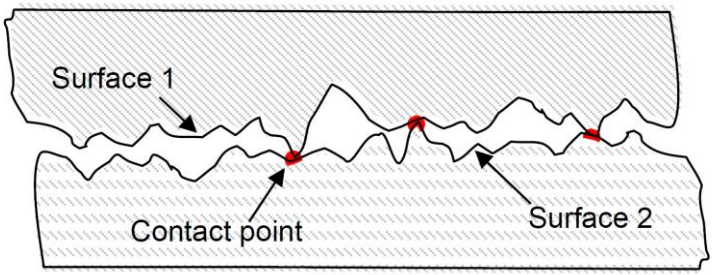

Figure 3.5 *Microscale surface roughness (Power Stream, 2006)*

Contact resistance is very important in this process because high resistance is associated to hotter welds, while a reduced contact resistance, obtained with more metal bridges, determines cooler weld. Moreover, when electrodes apply a lower pressure, metal contact reduces, and the resistance increases.

Capacitor discharge has recently been introduced for welding applications because it has many advantages with respect to traditional resistance welding. Because this technology is based on the energy stored by a large capacitor bank, welding process is short and concentrated, in fact it usually lasts 12 milliseconds against the 100 milliseconds of a traditional resistance welding machine (Davis, 2018). This time difference could become significant in a lot of industrial applications.

The advantages of capacitor discharge are (Davis, 2018):

1) The capacitor recharge is very quick
2) Weld nugget formation occurs only in the first few milliseconds
3) Limited surface deformations and spatter
4) Economic welding equipment
5) Fast energy release using large peak currents
6) Reduced draw on a power distribution network
7) Longer electrodes life, thanks to the reduced time of energy application
8) Reduced overheating of the welding pieces

Figure 3.6 shows the comparison among the current waveforms for capacitor discharge (CD), line frequency (AC), high frequency inverter (HF) power supplies. As it can be noticed, in capacitor discharge the electric current is applied in a time interval that is significantly smaller than the other ones.

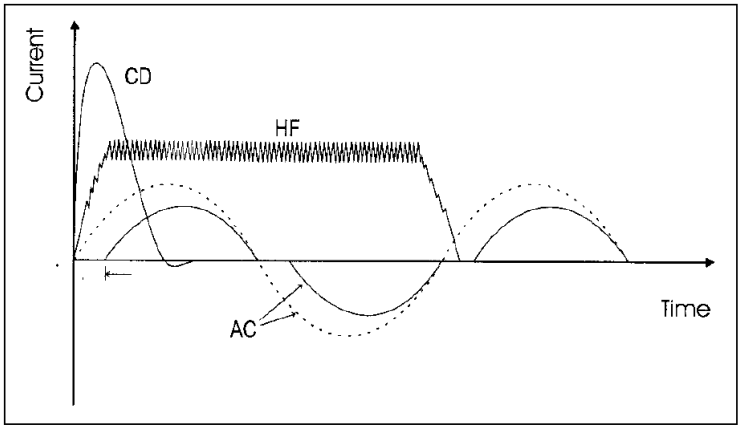

Figure 3.6 *Schematic of current waveforms for CD, AC and HF power supplies (Zhou Y., 2001)*

Differently from other resistance welding processes, joints don't present nugget formation (at least in projection welding) and different hypotheses have been proposed to explain CDW joints formation. Ketzel et al. (Ketzel M., 2019) supposed that high energy density causes vaporization in the welding zone, activating the surfaces and inducing the joint formation under the application of the pressure forces.

Capacitor discharge is widely used for the production of automatic transmission components. However, automotive industry requires stronger and lighter components that are very difficult to melt, and capacitor discharge technology seems to overcome welding problems, ensuring stronger weld strengths necessary for automotive applications.

However, even if capacitor discharge has a very big potential thanks to its low thermal stresses, quick times and automation possibility, it requires the control of the crucial parameters affecting the process to understand how to automate the process and new application areas. For this reason, Meiners et al. (Meiners M., 2020) implemented new in situ measurements to analyze the electric current distribution and the parameters governing the process. With respect to the other resistance welding processes, in capacitor discharge welding, it is not possible to set electric current and welding time manually. The only parameters to be controlled are the pressure applied and the welding energy (voltage). The authors used a round steel lid and Figure 3.7 shows the positioning of the measurement system. This system provides a qualitative measure of the distribution of the electric current flow in the components.

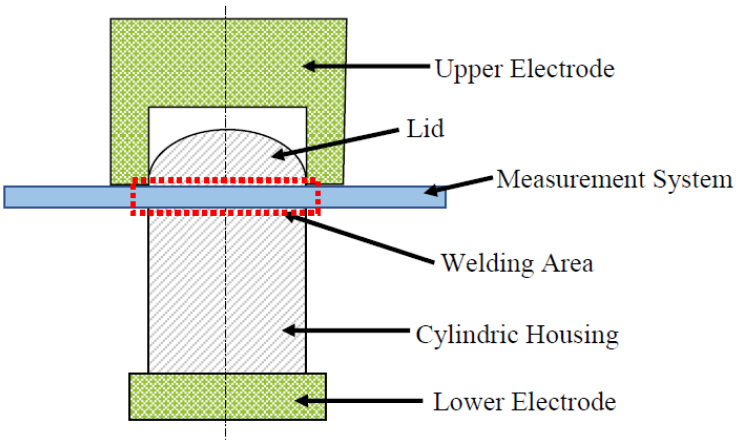

Figure 3.7 *CDW process schematization and measurement system (Meiners M., 2020)*

The measurement system employed magnetic flux sensors and each sensor triplet was positioned radially. The middle sensor had to detect the magnetic field at the measurement area (Figure 3.8).

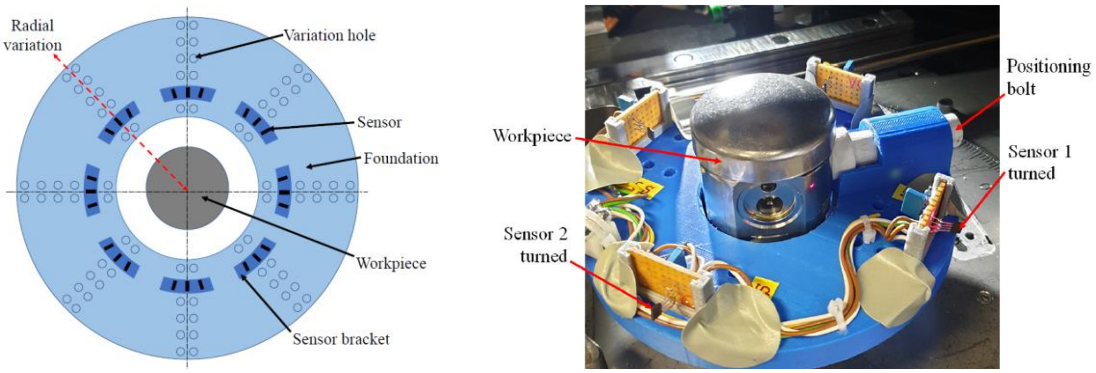

Figure 3.8 *Schematization and prototype of the measurement system (Meiners M., 2020)*

The sensor measured the magnetic flux density after 6 ms from the beginning of the CDW process. Figure 3.9 illustrates experimental results.

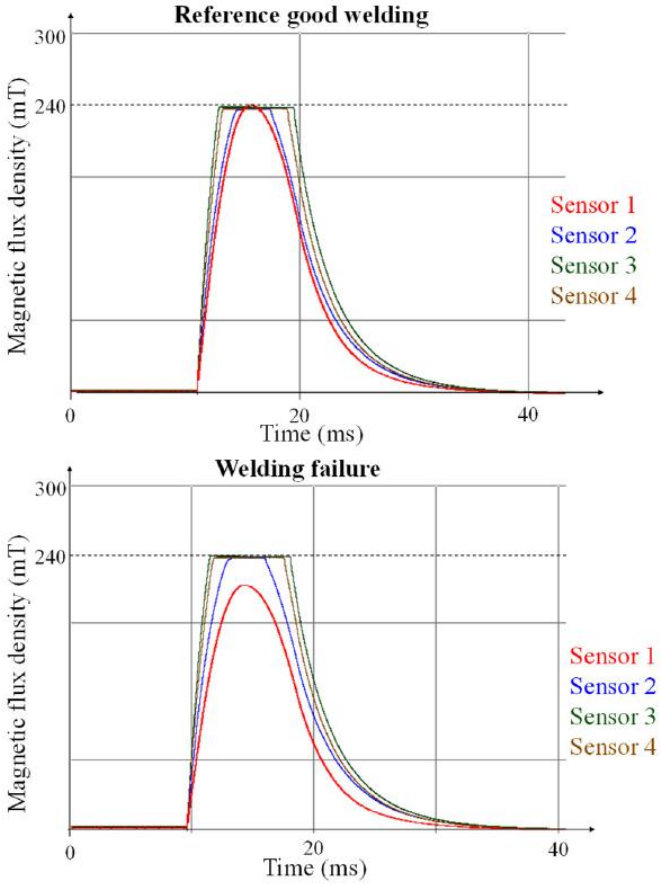

Figure 3.9 *Experimental results (Meiners M., 2020)*

Tests results demonstrated that the measurement system can detect failures occurring during welding. Moreover, it gives information about the process quality, and it gives the possibility to better understand what happens in situ. The measurement system could be also improved to be applied to other resistance welding processes.

3.2 Capacitor Discharge Technology

For capacitor discharge welding, different kind of electrodes configuration can be used:

1) In direct welding, the electric currents flow directly from the electrodes to the work pieces
2) In a step electrode configuration, instead, only one side of the work piece is accessible and there the electric current is applied
3) In a series configuration, the electrodes are placed on one metal surface and the electric current flows through the two parts

Figure 3.10 shows the electrodes configurations.

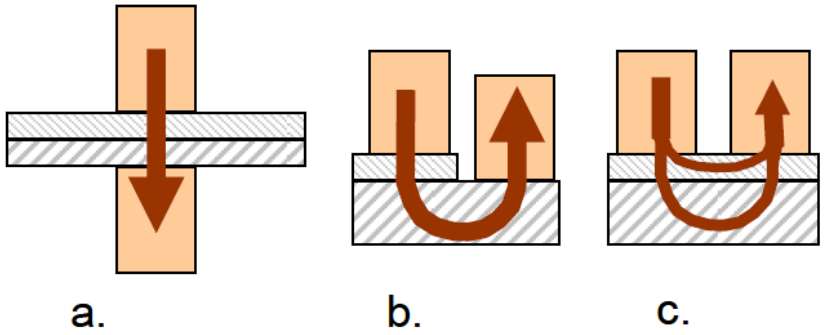

Figure 3.10 *Electrodes configurations: a) Direct welding, b) Step electrode configuration, c) Series configuration (Power Stream, 2006)*

Figure 3.11 illustrates the schematic representation of the electric circuit for capacitor discharge welding (Gould J. E., 2016).

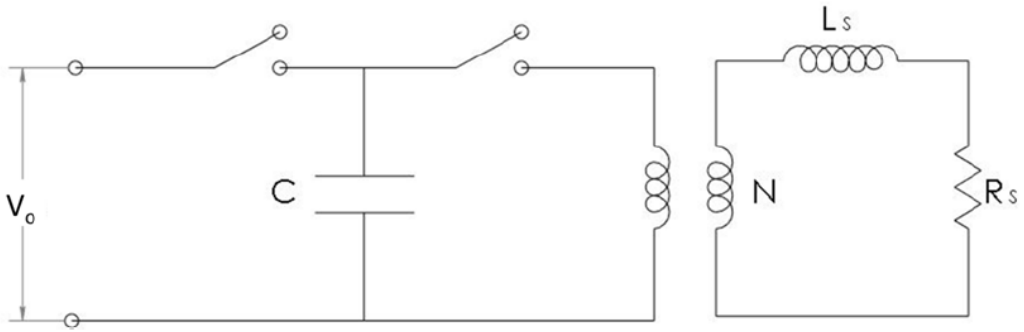

Figure 3.11 *Schematic representation of the electric circuit for capacitor discharge welding (Gould J. E., 2016)*

In the circuit, there are a primary capacitor, C, charged at the voltage V_o, a transformer, with ratio N, a load resistance R_s and a secondary inductance L_s.

The differential equation describing the circuit is:

$$L_S \frac{d^2q}{dt^2} + R_S \frac{dq}{dt} + \frac{1}{N^2 C} q = 0$$

Taking the second derivate respect to time, the equation becomes:

$$L_S \frac{d^2I}{dt^2} + R_S \frac{dI}{dt} + \frac{1}{N^2 C} I = 0$$

According to the different parameters values, the solution could be under, critically or over damped, as shown in Table 3.1. ω is the natural frequency of the system, evaluated as

$$\omega = \frac{1}{\sqrt{N^2 L_s C}}$$

Under-Damped Solution		Over-Damped Solution	
$I_s(t) = V\sqrt{\frac{C}{L_s}}e^{-\zeta\omega t}sin(\omega t)$	Eqn. 3	$I_s(t) = \left(\frac{V}{2NL_s}\right)\frac{e^{s_1 t} - e^{s_2 t}}{\left(\left(\frac{R_s}{2L_s}\right)^2 - \omega^2\right)^{1/2}}$	Eqn. 5
$\zeta = \frac{NR_s}{2}\sqrt{\frac{C}{L_s}}$	Eqn. 4	$s_1 = -\frac{R_s}{2L_s} + \sqrt{\frac{R_s{}^2}{4L_s{}^2} - \frac{1}{N^2 L_s C}}$	Eqn. 6
		$s_2 = -\frac{R_s}{2L_s} - \sqrt{\frac{R_s^2}{4L_s^2} - \frac{1}{N^2 L_s C}}$	Eqn. 7

Table 3.1 *Welding Electrical Response Solutions (Gould J. E., 2016)*

These equations are very useful to analyze the influence of the electric parameters of the current waveforms, as shown in Figure 3.12.

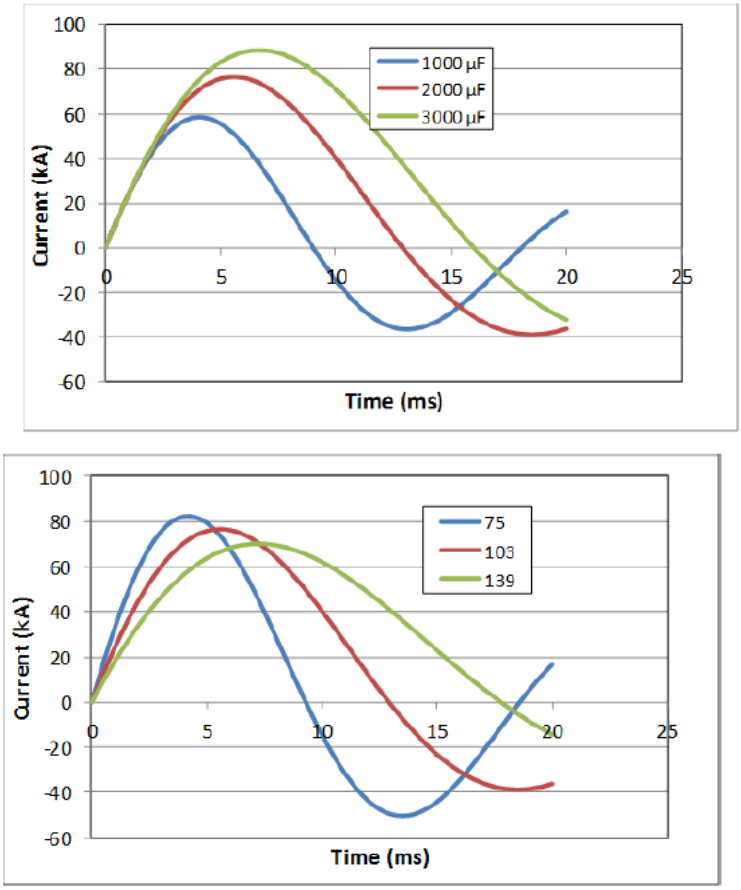

Figure 3.12 *Influence of Capacitance and winding ratio on current waveform for CDW (Gould J. E., 2016)*

3.3 Capacitor Discharge Applications

Resistance projection welding is an important welding process, but it is very difficult to apply to aluminium components for the high electric currents employed to generate heating of materials with very high resistivity. Capacitor discharge welding can, thus, be used thanks to the very short time of application of the electric current. To investigate inner processes occurring during welding, an indirect coupled FEM analysis can be performed with the software Ansys (Koal J., 2020).

Figure 3.13 shows typical values of electric current and welding time, used in the FEM simulation.

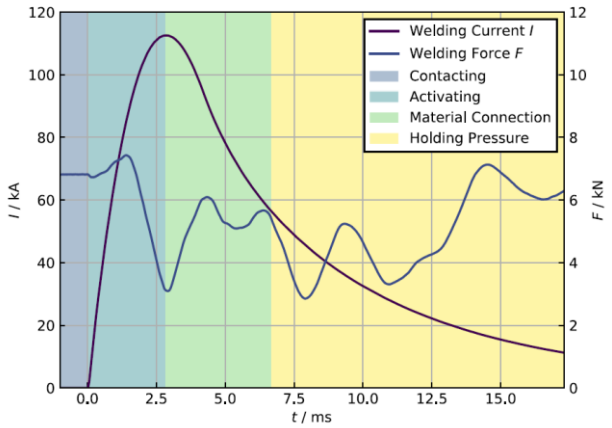

Figure 3.13 *Capacitor discharge process and input data used in the FEM simulation (Koal J., 2020)*

The welding time is set to 7.1 ms. Figure 3.13 shows the four typical phases of the welding process:

1) Contacting: the electrodes apply the welding force and plastic deformation starts in the contact area
2) Activating: electric current starts to flow, the oxide layers are eliminated with surfaces cleaning and the contact surfaces are activated
3) Material Connection: the activated surfaces are pressed together to create connection, the electric current starts to decrease and plastic deformation and softening of the projection begin
4) Holding Pressure: the electric current and the plastic deformation reduce and there is the cooling of the joining zone

The FEM model is illustrated in Figure 3.14.

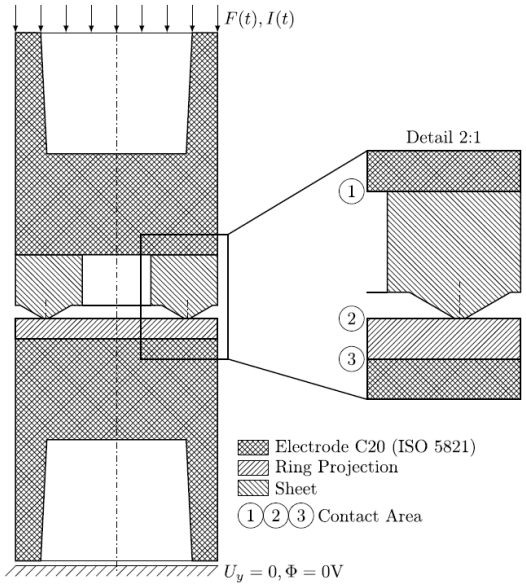

Figure 3.14 *FEM model with applied loads and boundary conditions (Koal J., 2020)*

In this model, the electrical contact resistance for aluminium spot welding is evaluated employing the contact theory as (Tuchtfeld M., 2019)

$$ECR(T,\sigma_{cont}) = 3\,d\left(\frac{\sigma_s(T)}{\sigma_{cont}}\right)^{\kappa}\cdot\left(\frac{\rho_1(T)\cdot\rho_2(T)}{2}\right)$$

To avoid distorted meshes, a nonlinear adaptive meshing and rezoning analysis was performed with the software ANSYS MECHANICAL. The authors used an indirect coupling simulation to minimize the computing effort and to allow rezoning in the structural physics and the dynamic simulation of the contact resistance. Figure 3.15 illustrates the experimental setup and the electrical voltage of the different areas.

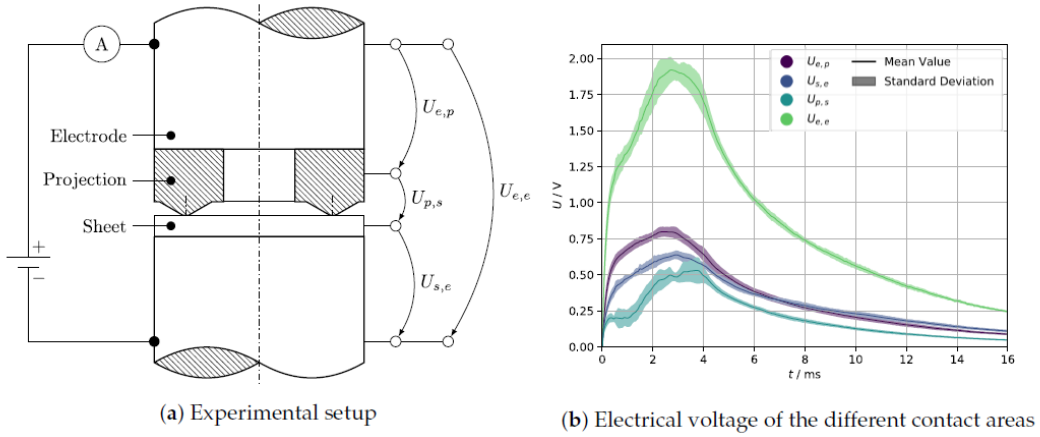

(a) Experimental setup

(b) Electrical voltage of the different contact areas

Figure 3.15 *Experimental setup and the electrical voltage of the different areas (Koal J., 2020)*

FEM analysis results show how the numerical parameters affect the whole simulation, as shown in Figure 3.16.

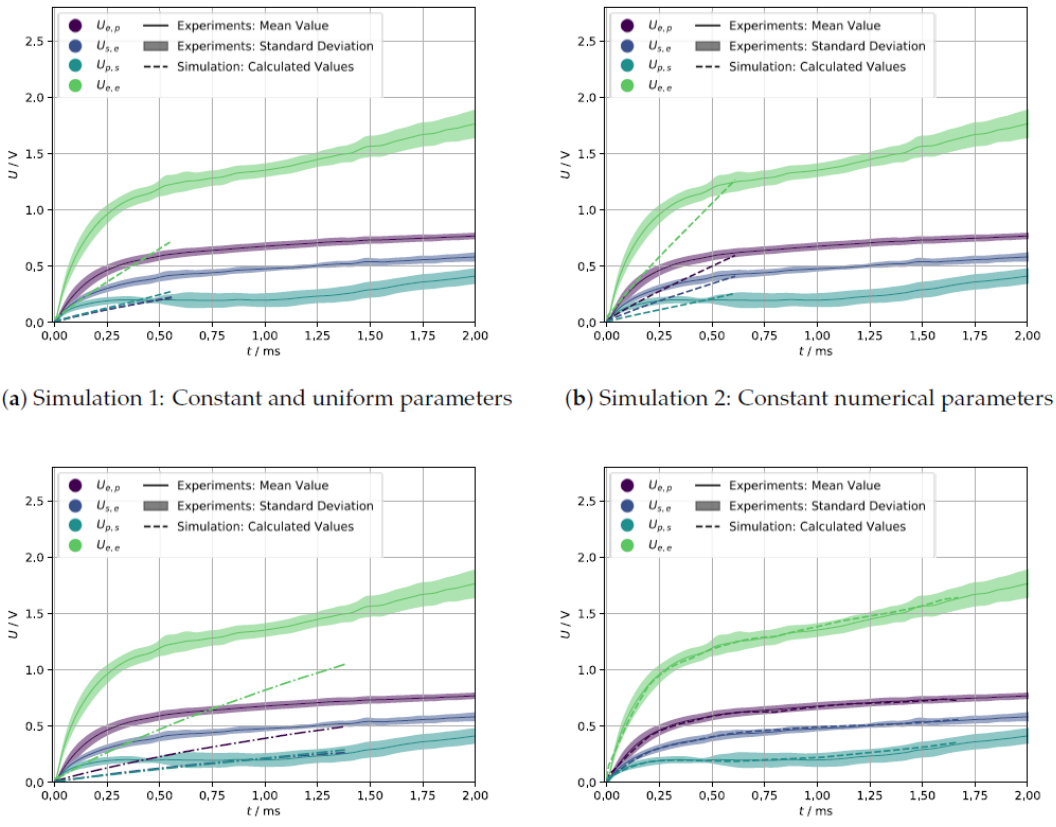

(a) Simulation 1: Constant and uniform parameters

(b) Simulation 2: Constant numerical parameters

Figure 3.16 *Numerical parameters affecting simulated electric voltage and comparison with the experimental results (Koal J., 2020)*

Thus, the FEM simulation can adapt to the model complexity and it could be used in further investigations to evaluate the model parameters.

Dziho et al. (Dziho M.E.) applied discharge welding to small diameter wires, analyzing the influence of contact force occurring during welding on joints properties. Traditional welding processes are not suitable for melting small diameter wires because it results very difficult to control melted materials. In fact, when melting begins, welding temperatures are reached only by the top part of the wire, while the other zones continue to melt. They applied capacitor discharge to Cr-Ni steel 19-9 small wires. Heat input was kept constant during experimental tests, while pressure varied. Tests results showed that when the pressure applied on wires was increased, joints strength also increased, as shown in Figure 3.17.

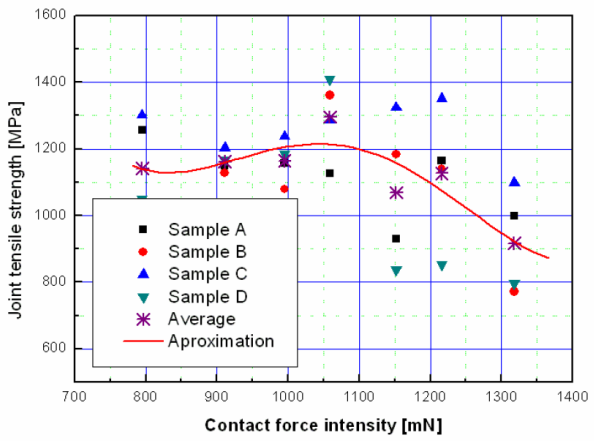

Figure 3.17 *Joints tensile strengths dependance on pressure intensity (Dziho M.E.)*

At low pressures, instead, joints exhibited unfilled gaps. The best mechanical properties and geometries were obtained with pressure values ranging between 1020 mN and 1080 mN.

Maizza et al. (Maizza G., 2020) investigated the correlation between the indentation properties and microstructure for a tungsten carbide-cobalt (WC-Co) composite rod and steel joints applying capacitor discharge welding (CDW). The combination of the electric current pulse and the uniaxial pressure in CDW is associated to a very high heating and a quick cooling, determining the formation of a thin layer, characterized by an ultrafine microstructure with high strength and toughness. Tests results showed that CDW process allows the creation of a net shaped joint with improved corrosion resistance and which preserves the micro-grain structure.

Kolarikova et al. (Kolarikova M., 2018), instead, used capacitor discharge to join aluminum thin sheets. Capacitor discharge, in fact, is very useful for melting modern materials because it allows the application of high electric currents for very short times, usually about 20 ms. They used the multi-capacitor source (MCS) system, which is very important to control the parameters that affect the process because the resistance and the inductance of the machine and the capacitance of the capacitor bank influence the electric current progression and, as a consequence, welding itself. Welding current course is strictly affected by the use of four capacitor in parallel. The control on the welding parameters ensures the joints quality.

The authors used aluminum alloy EN AW 6016T4 sheets with a thickness of 1.5 mm. Tests were performed employing three different capacitors, H, A and B. Three pulses were applied: the first one was used to remove oxides from the sheets surfaces and its energy was 0.496 kWs, while the other two were used to melt the joints. The time between the first and second pulse was set to 2 ms. Table 3.2 shows the parameters values.

Number of weld	Capacitor H		Capacitor A		Capacitor B	Total E [kWs]
	E [kWs]	t [ms]	E [kWs]	t [ms]	E [kWs]	
1	0.496	2	0.918	6	1.406	2.820
2	0.496	2	3.673	6	2.324	6.493
3	0.496	2	2.812	4.5	2.324	5.632
4	0.496	2	2.812	5.5	2.324	5.632
5	0.496	2	2.812	6.5	2.324	5.632
6	0.496	2	2.812	7,5	2.324	5.632
7	0.496	2	2.812	8.5	2.324	5.632

Table 3.2 *Welding parameters (Kolarikova M., 2018)*

The authors analyzed the weld nugget size and the presence of defects, such as cracks, porosity and inclusions.

Figure 3.18 illustrates pressure and power values for the three pulses.

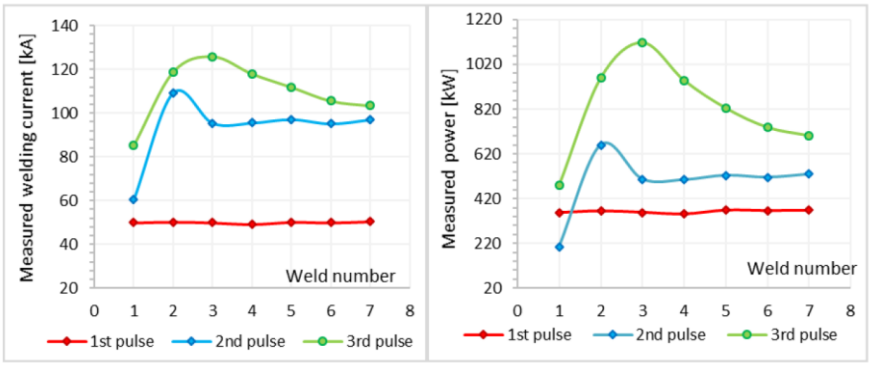

Figure 3.18 *Pressure and power values for the three pulses (Kolarikova M., 2018)*

Figure 3.19, instead, shows welding current, power values, resistivity, voltage and electrode displacement for all the joints.

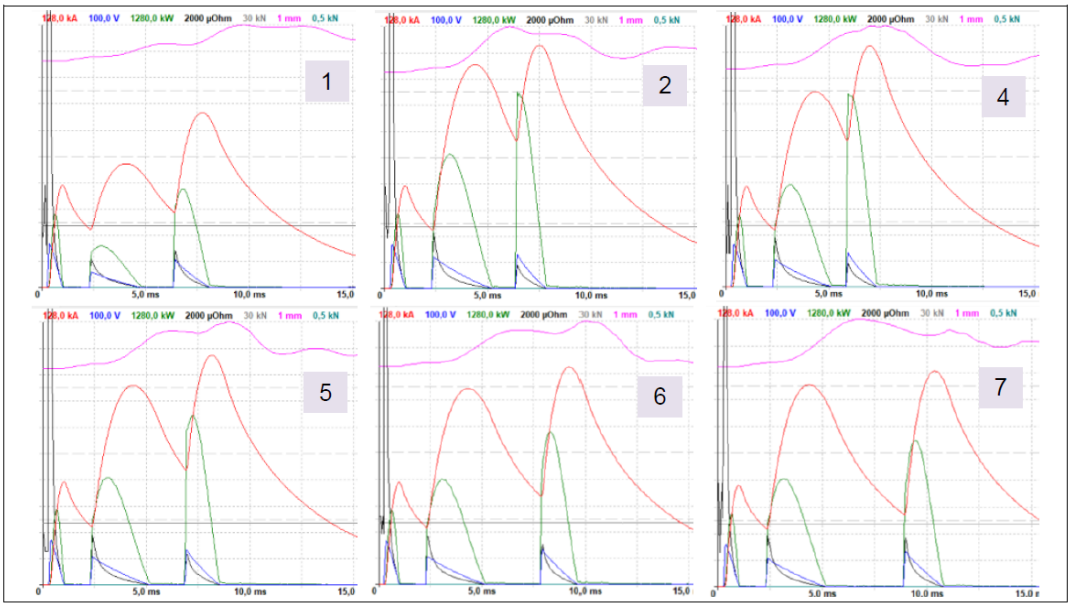

Figure 3.19 *Welding parameters (welding current – red line, power – green line, resistivity – black line, voltage – blue line, electrode displacement – purple line) (Kolarikova M., 2018)*

Figure 3.20 illustrates, instead, macro-sections of the spot welds.

In spot weld 1, energy is too low to ensure good welding, so pores appear in the nuggets; in spot weld 4, it is possible to notice a lot of cracks.

Welding parameters affect shape and size of the welds. When the time between the second and the third pulse increases (welds from 4 to 7), the number of pores and cracks decreases.

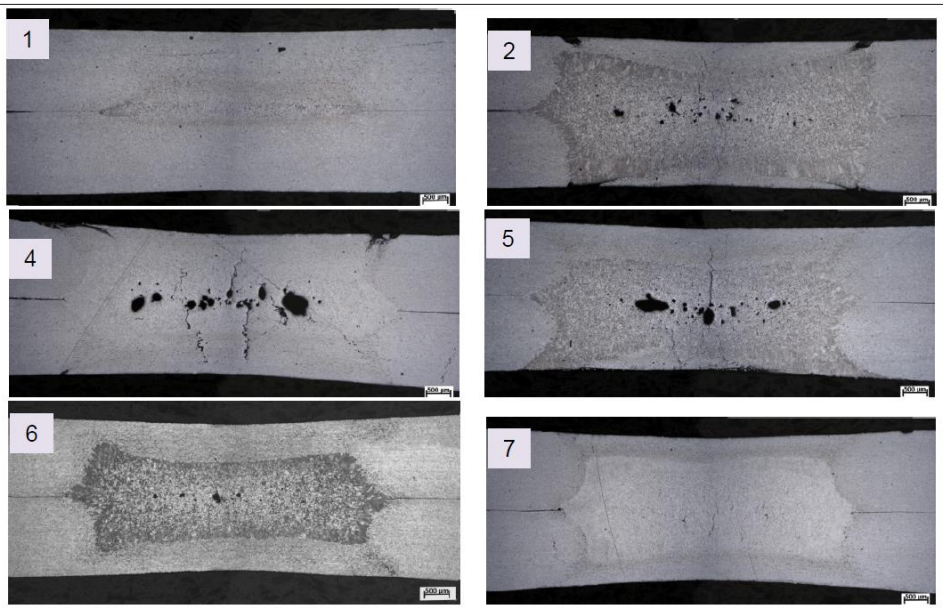

Figure 3.20 *Macro-sections of spot welds (Kolarikova M., 2018)*

Zhou et al. (Zhou Y., 2001), instead, investigated the use of capacitor discharge in small-scale resistance spot welding (SSRSW) applied in the fabrication of electrical and electronical components. The authors analyzed SSRSW of copper, aluminum and brass comparing capacitor discharge (CD) and high frequency inverter (HF). The schematic setup is reported in Figure 3.21.

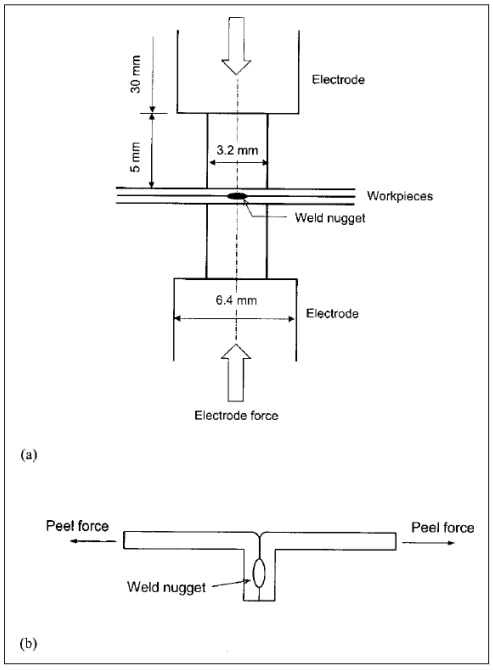

Figure 3.21 *Schematic setup for both resistance spot welding and peel test (Zhou Y., 2001)*

Excessive heat generation determined locally melted areas at the electrode-sheet interface. Surfaces were cleaned with methanol before melting.

Mechanical tests showed that failure could occur in three different modes:

1) Interface Failure
2) Weld failure
3) Button Pullout

Peel tests showed that, for brass, the same pulse energy could be applied for all kinds of electrodes and weld metal expulsion began with a pulse energy of about 70 J. Electrode sheet sticking is important for Class 14 Electrodes. Figure 3.22 shows peel force and nugget diameter versus pulse energy.

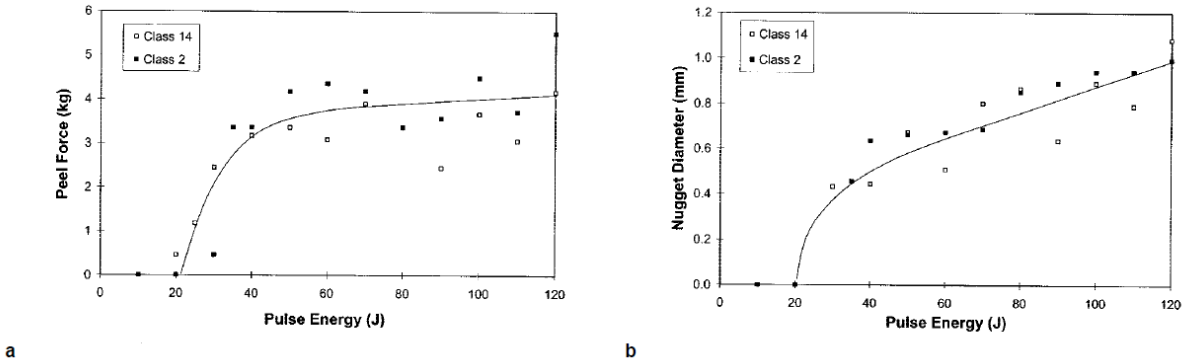

Figure 3.22 *Peel force and nugget diameter versus pulse energy in brass melting (Zhou Y., 2001)*

Figure 3.23, instead, shows peel force and nugget diameter versus pulse energy for aluminum melting.

SSRSW is not suitable for copper because the power supply required is too high for the very big copper thermal conductivity. With capacitor discharge, bonding didn't happen, also when the maximum settings were used.

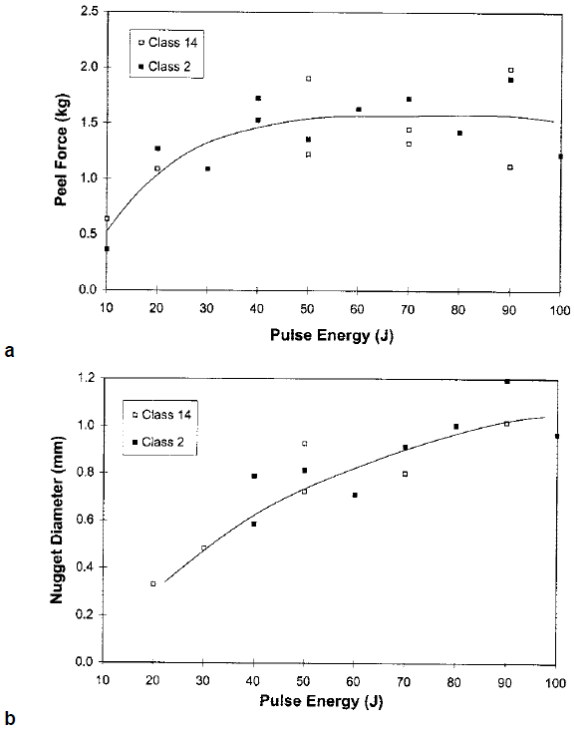

Figure 3.23 *Peel force and nugget diameter versus pulse energy in aluminum melting (Zhou Y., 2001)*

SSRSW is considerably affected by electrical resistivity and the resistance weldability of the materials is related to their resistivity. For this reason, aluminum is more weldable than brass, that is more weldable than copper. Moreover, the resistance weldability is also affected by other physical properties, such as melting point, heat of fusion, specific heat and so on.

Table 3.3 shows the comparison among AC, CD and HF in terms of power supply and welding current.

. Welding Current or Pulse Energy Required to Produce Weld Nuggets of 0.4 mm in Diameter

Electrodes Power Supply	Class 2 AC (kA)	Class 14 HF (kA)	CD (J)	AC (kA)	HF (kA)	CD (J)
Al	1.1	1.9	30	0.7	1.2	30
Brass	1.6	2.6	35	1.2	1.6	35
Cu	>2.2	—	>125	>2.8	>3.3	>125

Notes: Electrode force = 4.5 kg, Weld time = 8 cycles when using an AC power supply, Weld time = 20 ms when using a HF power supply, Pulse width = 2.0 ms when using a CD power supply. The results with an AC power supply were from Ref. 7.

Table IV. Comparison of Power Supplies Used for Micro-Resistance Welding

Power Supply	Equipment Cost	Work Capacity	Ease of Operation	Ease of Control	Maintenance
AC	Low	High	Mid	Low	Low
DC	High	Low	Mid	High	High
HF	High	Mid	Low	High	High
CD	Mid to Low	Low	High	Self Regulating	Low

Table 3.3 *Comparison among AC, CD and HF in terms of power supply and welding current (Zhou Y., 2001)*

Tests results showed that the energy supply is the same in CD for all the electrodes because the welding time is very brief.

Panella et al (Panella F.W., 2019), instead, applied the improved hybrid capacitor discharge welding to aluminum alloy 5754, and then analyzed the mechanical properties of the joints and the presence of defects. The contact conditions and the number of discharges at different power inputs are critical parameters of the process. The authors modified the ignition point geometry on the weld to induce a more uniform welding process of the samples. The researchers employed the innovative multipoint CDW technique (MCDW), which represents a hybrid process between projection welding and capacitor discharge welding. The aim of the study was to weld larger areas reducing porosity and the lack of fusion. The joints had a trapezoidal profile, as shown in Figure 3.24.

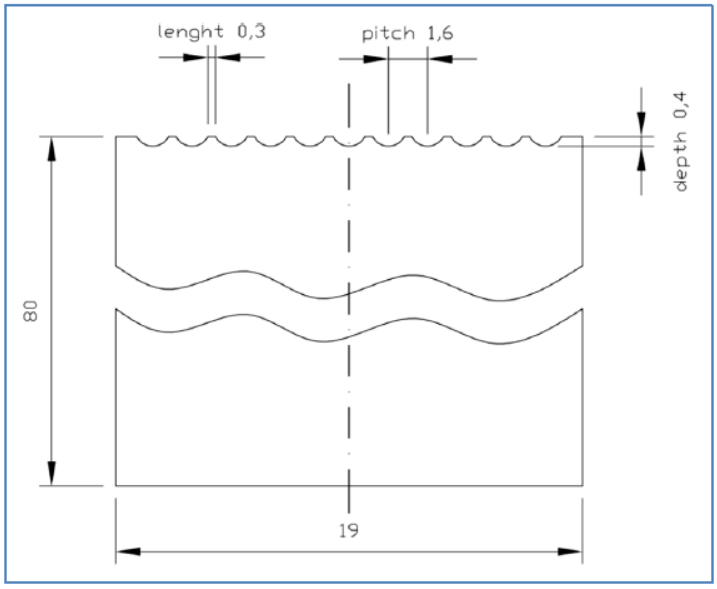

Figure 3.24 *Trapezoidal profile of the joints (Panella F.W., 2019)*

Figure 3.25 illustrates, instead, welding equipment.

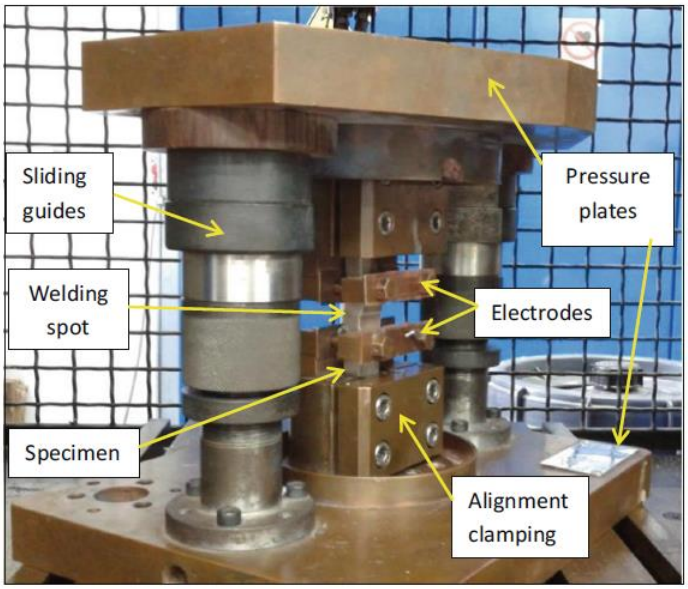

Figure 3.25 *Welding equipment (Panella F.W., 2019)*

The MCDW process is characterized by the application of a very high electric current to small igniters, placed on the areas to be joined. The igniters partially fuse with a plasma formation for Joule effect and the areas in the proximity of the joining surface melt, determining a complete welding, also thanks to the application of compression forces.

Moreover, in this process, cooling is very quick and the deformations are negligible. The MCDW process is applied to aluminum alloy 5754 butt-weld rectangular specimen, which were machined to obtain a trapezoidal contact profile. The tests were performed varying the input parameters, i.e., the applied compressive force F, the discharge electrical energy E_i, the maximum current peak I_p and the integrated current over time I_i, as shown in Table 3.4.

Specimen	F [daN]	E_1 [J]	E_2 [J]	E_3 [J]	E_4 [J]	E_5 [J]	I_p [kA]	I_i [C]
1	2500	2000	4000	6000	8000	10,000	n.d.	n.d.
2	3000	2500	5000	5000	18,000	5000	156	953
3	3000	2500	4000	4000	20,000	10,000	156	963
4	2500	2500	4000	6000	22,000	15,000	156	911
5	2000	2500	4000	6000	22,000	15,000	156	606
6	2000	2500	4000	8000	20,000	25,000	156	882
7	2000	3000	6000	10,000	25,000	35,000	156	571
8	2500	3000	6000	8000	12,000	25,000	156	984
9	2500	4000	8000	12,000	25,000	15,000	156	943
10	2500	4000	8000	15,000	25,000	25,000	156	1010
11	2500	4000	8000	15,000	30,000	15,000	156	917
12	3000	4000	8000	12,000	25,000	15,000	156	920
13	3000	4000	8000	12,000	30,000	15,000	156	920
14	2500	4000	8000	12,000	30,000	15,000	156	930
15	2500	2500	4000	8000	20,000	25,000	156	930
16	2000	2500	4000	8000	15,000	25,000	156	887
17	2500	2500	4000	8000	15,000	30,000	156	909

Table 3.4 *Input parameters (Panella F.W., 2019)*

Figure 3.26 shows the discharged current intensity on specimen 16 and 17, Tables 3.5 and 3.6 refer to the Uniaxial tension tests results and Fatigue tests results respectively.

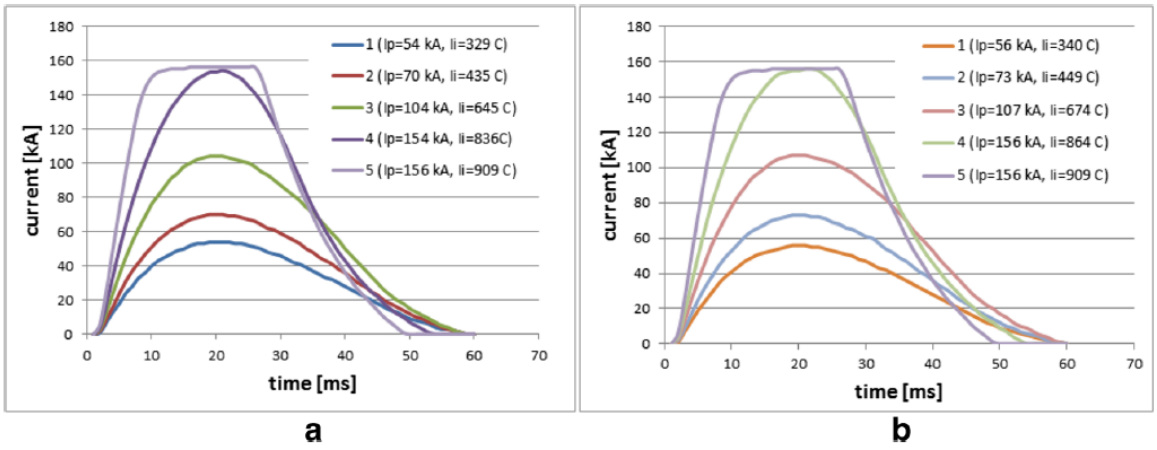

Figure 3.26 *Discharged current intensity on specimen 16 and 17 (Panella F.W., 2019)*

Specimen test number	Area$_I$ [mm^2]	Maximum load [kN]	Elongation [%]	UTS [MPa]
2	184.8	22.0	0.30	119
4	171.0	25.5	9.61	149
6	184.8	42.8	5.72	232
7	192.6	19.5	0.48	101
9	183.8	49.2	13.99	267
10	171.0	6.0	2.27	35
11	185.3	22.8	3.09	123
12	183.8	13.3	0.11	73
13	184.1	28.9	10.33	157
14	188.2	19.2	0.58	102
16	185.8	39.0	5.10	210
17	187.5	51.5	4.43	275
18	184.8	36.4	4.60	197
19	187.5	44.2	6.44	236

Table 3.5 *Uniaxial tension tests results (Panella F.W., 2019)*

N	σ_{max} [MPa]	σ_m [MPa]	σ_a [MPa]	F_m [N]	Fa [N]	Cycles
33	180	99	81	14,256	11,664	1869
32	130	71.5	58.5	10,296	8424	25,362
28	115	63.25	51.75	9108	7452	2806
27	110	60.5	49.5	8712	7128	1087
21	100	55	45	7920	6480	7782
30	90	49.5	40.5	7128	5832	1,000,000

Table 3.6 *Fatigue tests results (Panella F.W., 2019)*

Figure 3.27 shows, instead, the classification of the samples according to the severity of the defects. It is possible to consider three different classes: large defects (a), medium-size defects (b) and small defects (c).

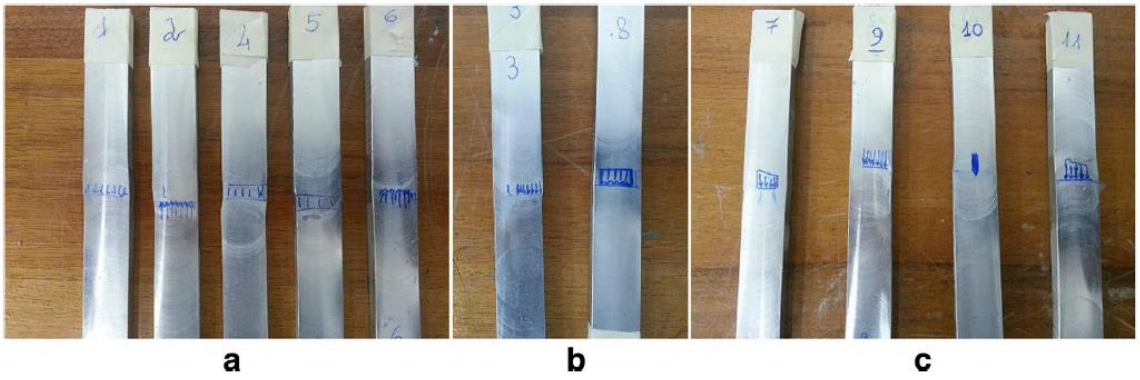

Figure 3.27 *Classification of the samples according to the severity of the defects (Panella F.W., 2019)*

Best results were achieved on the specimen 3, with reduced defects and a suitable weld shape. Fatigue tests showed very good results, thus MCDW represents an interesting technique for future applications.

Observations

Capacitor discharge welding allows welding of aluminum alloys, improving samples mechanical parameters and reducing defects. Moreover, the application of the electric current in a very short time reduces stress concentrations and crack formations and it gives the possibility to melt thin and complex pieces, with very important application in automotive industry.

However, even if CDW is so interesting for its low thermal stresses, quick times and automation possibility, it requires the control of the crucial parameters affecting the process to understand how to automate the process and new application areas.

4 Experimental Results

4.1 Sample preparation

The test specimens were cut to produce sections with flat and parallel faces, so that they could be polished and used in subsequent steps.

This procedure is essential to avoid optical distortions under the microscope and to obtain sensible results in the subsequent indentations.

The cut was carried out at low speed (0.025 mm/s) and with high water flow in order not to alter the structure of the nugget.

Figure 4.1 *Circular saw*

Figure 4.2 *Polishing machine*

After cutting the specimens, they were embedded in resin so that they could be polished and chemically attacked.

Mirror polishing was performed through a polishing machine (Figure 4.2) initially using different abrasive discs and then 6, 3, and 1 μm diamond suspensions.

The chemical attack was carried out with Keller and Weck reagents.

Figure 4.3 *Sample embedded in resin already polished*

Chemical composition of the reagents used:

Keller reagent
2,5 ml HNO3
1,5 ml HCl
1,0 ml HF
95 ml H2O

Weck reagent
4 g of KMnO4
1 g of NaOH
100 ml H2O

4.2 Process analysis

Figure 4.4 *Optical microscope*

The metallographic optical microscope is a device used to study the structure of metals and metal alloys; it provides information about the size and shape of grains, the distribution of phases and the possible presence of inclusions, porosity and cracks. Optical microscope observation is carried out by illuminating the samples by reflection; previously they must be prepared by polishing and chemical attack. The main limitations of the optical microscope are the limited resolution power (less than 0.2 microns) and depth of field, which means that it is impossible to focus on details located on different planes. The optical microscope (figure 4.4) was used in this thesis to study the microstructure of the aluminum alloy at low magnifications (from 25x to 1000x).

4.3 Resistance Welding

sample 1, 1st half, first polishing

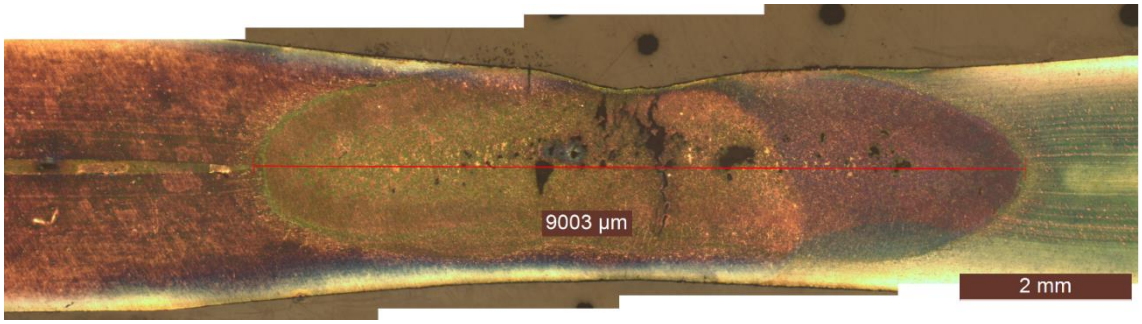

Figure 4.5 *25x Weck 20s*

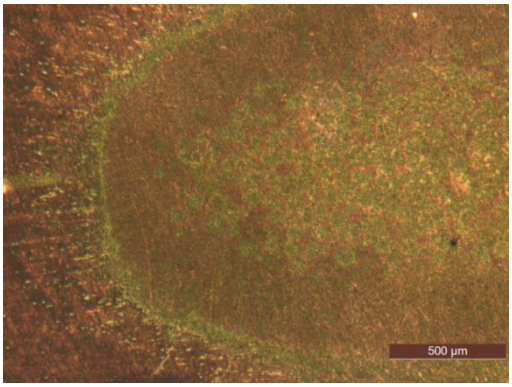

Figure 4.6 *50x Weck 20s*

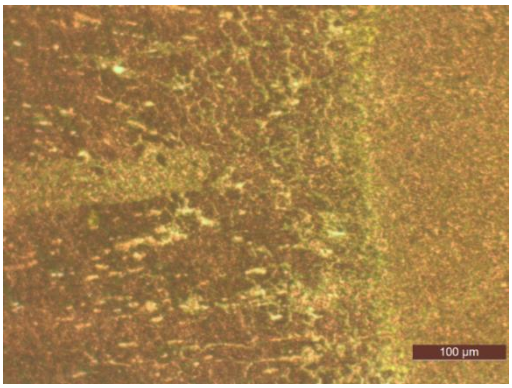

Figure 4.7 *200x Weck 20s*

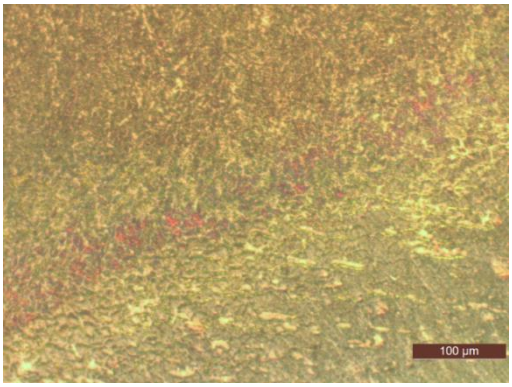

Figure 4.8 *200x Weck 20s*

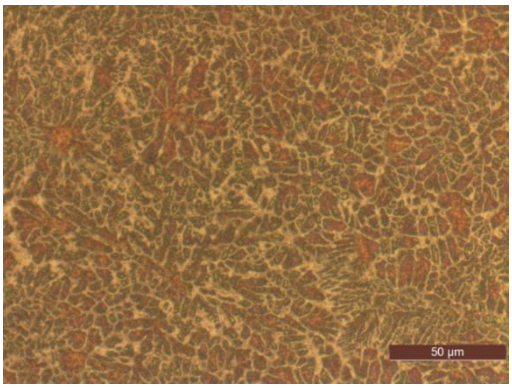

Figure 4.9 *500x Weck 20s right from the porosity*

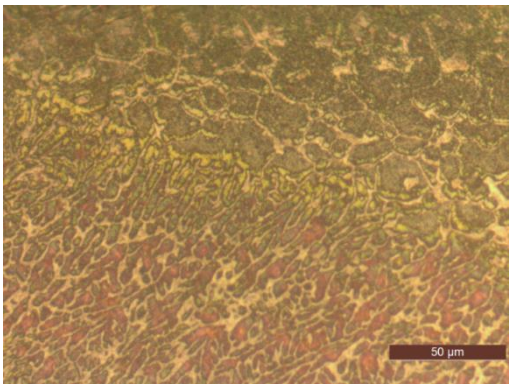

Figure 4.10 *500x Weck 20s*

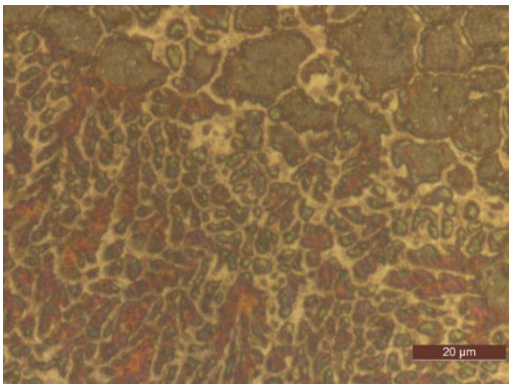

Figure 4.11 *1000x Weck 20s*

As for the capacitive discharge welding, we can find larger rosettes approaching the nugget, which will disappear in the transition zone.

The temperature tends to be higher in the area around the nugget in the case of resistance welding, so the grains are more enlarged, but you can also see sub grains that are recrystallizing in those areas.

Towards the base material the structure is coarser.

We can see areas surrounded by the white phase that have a granular structure inside them, indicating that they are recrystallizing.

The first grains form near the white zone, because the temperature there tends to be higher, the granular areas are denser and therefore dissipate heat better, while the areas at the interface tend to generate nuclei.

This second half of the resistance welded specimen is certainly less affected by porosity, in general the microstructure of the resistance welded specimen is less rich in detail, you can see the molten nugget and the transition zone that is practically unaffected.

Resistance welding is the most widely used industrial welding method because it has benefits if it is sufficiently standardized, first and foremost the lower cost of use compared with other technologies and a more optimized process. These considerations are valid as long as we are dealing with easily weldable alloys, such as most steel alloys.

In the case of an aluminum alloy, being a material that dissipates electrical current and heat very easily, the problem becomes obtaining a reliable weld from the point of view of mechanical resistance.

We were also able to achieve a good weld with resistance technology, but for later tests we would certainly have chosen a larger bending radius and a lower applied force.

Characteristic parameters used:

Electrode diameter	16 mm
Electrode curvature radius	50 mm
Force	5500 N
Current	45000 A
Duration	100 ms

The duration of 100 ms is given by 5 periods of 20 ms.

The desired, and obtained, nugget diameter is 9 mm.

We used 1000 Hz medium-frequency technology, an evolution of the now obsolete 50 Hz resistance welding.

This technology allows the welding current to be delivered in a continuous and constant manner, thus enabling the fusion zone to be heated more evenly.

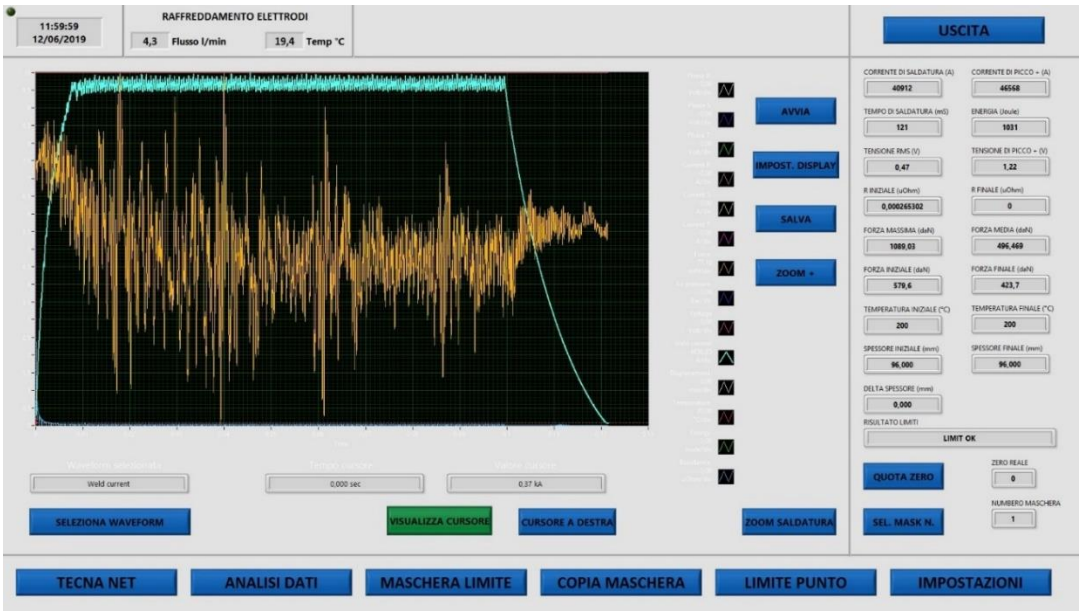

Figure 4.12 *Resistance welding machine screen*

Sample 1, 1st half, second polishing

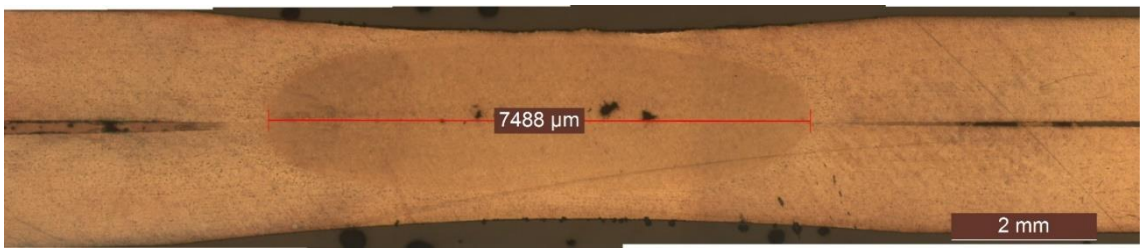

Figure 4.13 *25x Nugget*

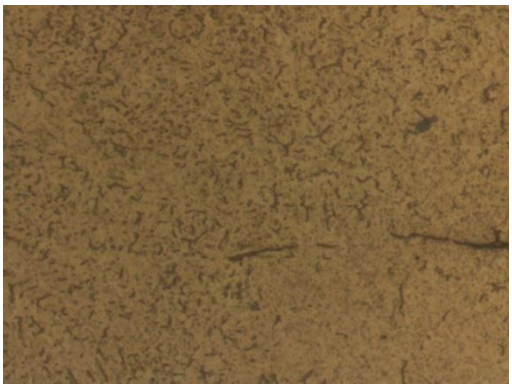

Figure 4.14 *1000x zone B nugget right center line Keller 20s + Weck 4s*

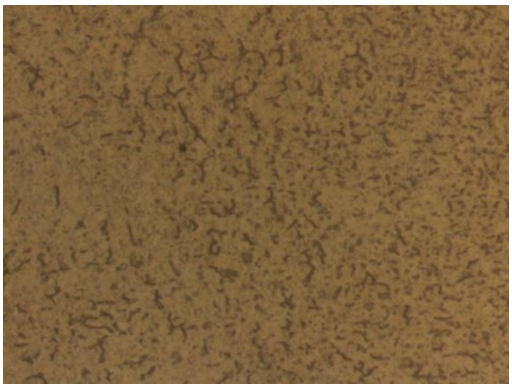

Figure 4.15 *1000x zona B nugget left center line Keller 20s + Weck 4s*

4.4 Laser Welding

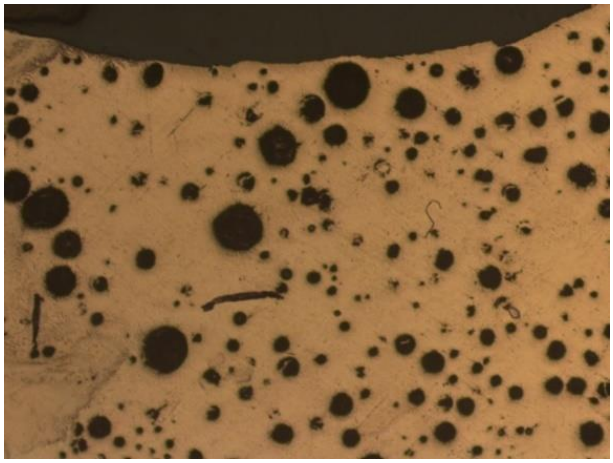

Figure 4.16 *Porosity on laser welding sample*

Laser welding can be used effectively with the aid of a filler chosen according to the alloy to be welded, and in any case with an Nd-Yag source, whereas we could only use a CO2 source.

It is also very difficult to weld without auxiliary filler because of the tolerances required in this configuration.

Characteristic parameters :

Sample	Power [kW]	Speed [m/min]	Focus [mm]	Gas
1	1.5	2	0	Helium
2	2	2	- 2.5	Helium
3	2.5	1.5	- 3.5	Helium
4	2	1.5	- 2.5	Helium
5	2	1.5	- 2.5	Helium

As already stated, this source is not suitable for welding aluminum, and has been replaced for virtually every application by Nd-Yag; but if reuse of this technology were to be considered, it would probably be necessary to decrease the power and increase the speed of the process.

Varying the focus allows the area of interest on the specimen to be enlarged at the expense of the depth at which material can be melted.

In most laser welding applications, the position of the focus is usually set at about 1/4 of the required penetration depth below the surface of the workpiece, we have increased this value to affect as little as possible the base material of the specimen underneath as can be seen from the micrographs.

Lately, the use of combined TIG and laser has been tested for various applications to achieve a better result.

4.5 Capacitor Discharge Welding

Figure 4.17 *Capacitor discharge welding setting*

Characteristic parameters:

Electrode diameter : 15 mm

Sample	Pressure [Mpa]	Voltage [V]	Current [kA]
1	83	2000+2000+2800	104,4+108,2+137,9
2	83	2000+2000+2800	105,8+109,2+139,1
3	83	2000+2000+2800	107,5+109,8+139,8
4	83	2000+2000+2800	107,3+109,4+140,1

The standard operations of the equipment involve two discharges at a given voltage and a third discharge at a higher voltage by the actuation of a second switch.

The following graphs are taken directly from the machine and related to sample 2, as well as the following micrographs.

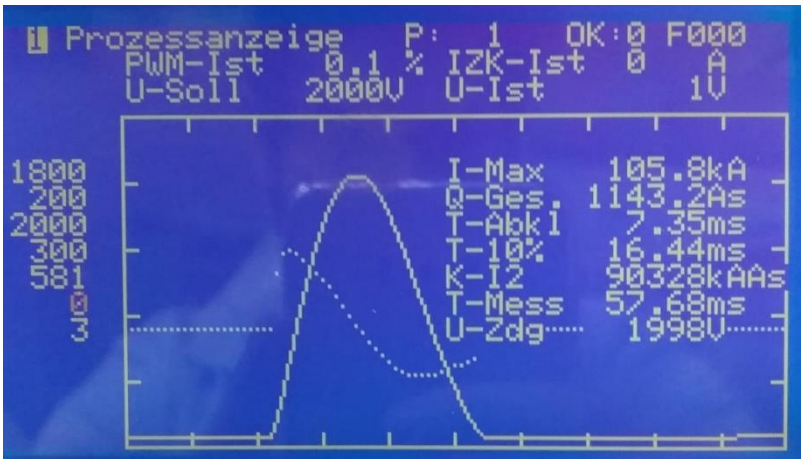

Figure 4.18 *First discharge*

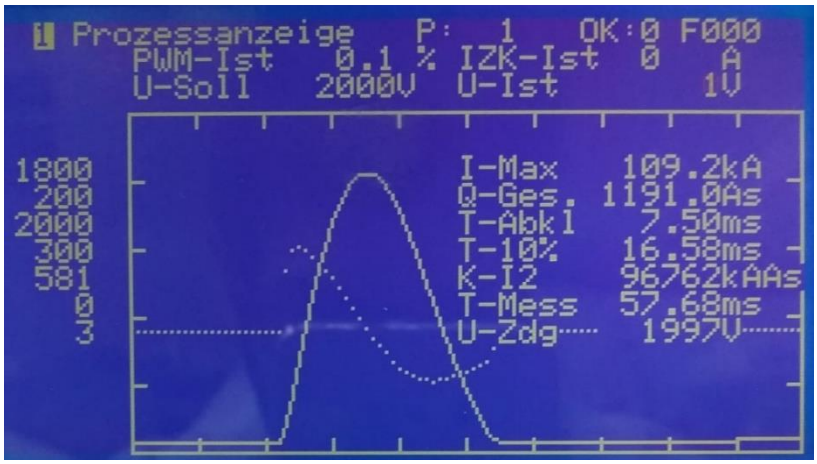

Figure 4.19 *Second discharge*

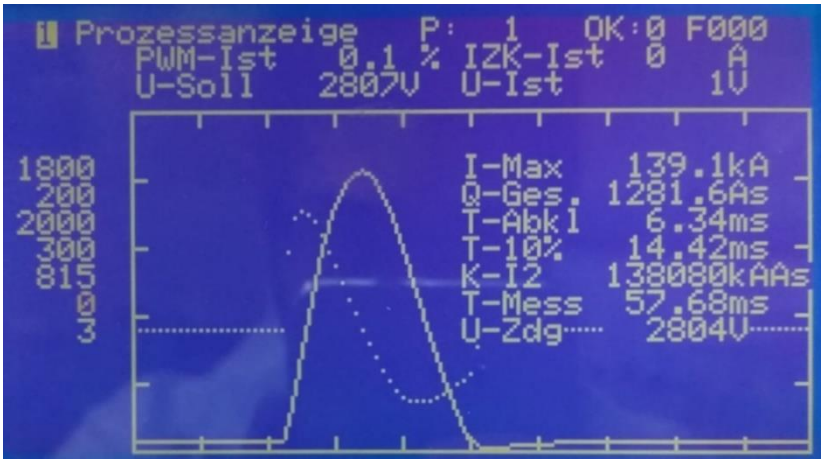

Figure 4.20 *Third discharge*

Sample 2, 1st half, first polishing

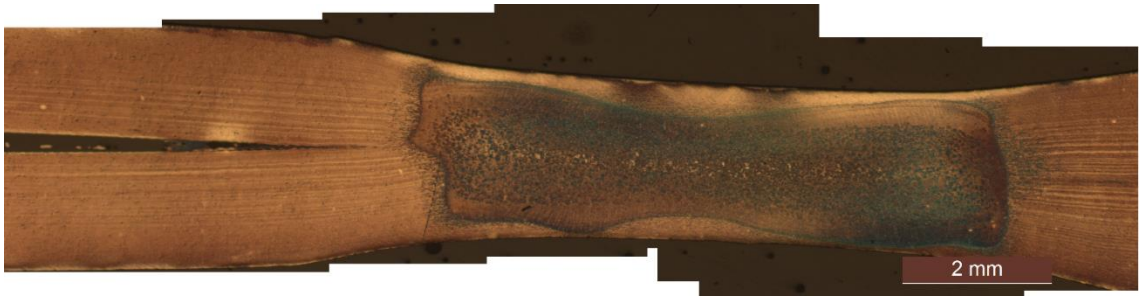

Figure 4.21 *25x Weck 20s + Keller 2s*

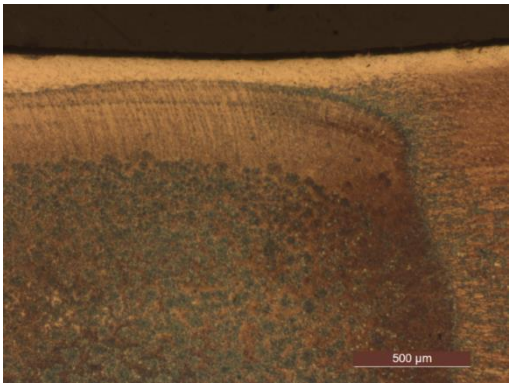

Figure 4.22 *50x Weck 20s + Keller 2s, transition to the right*

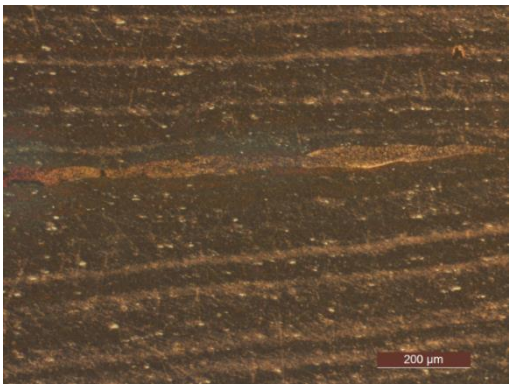

Figure 4.23 *100x Weck 20s, center line on the left*

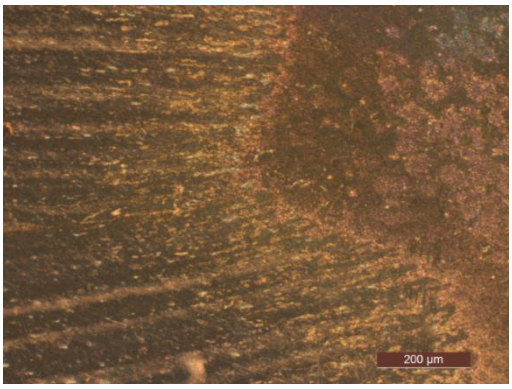

Figure 4.24 *100x Weck 20s center line, transition to the left of the nugget*

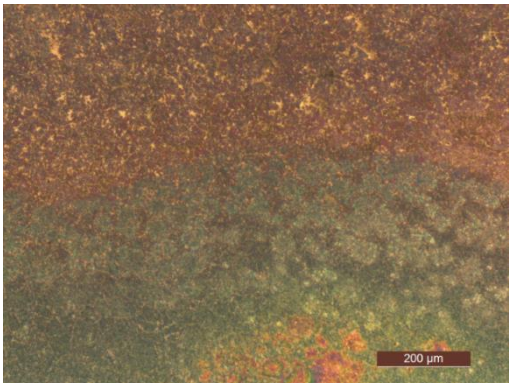

Figure 4.25 *100x Weck 20s, transition to the bottom left of the nugget*

The brownish zone results from a process of liquefaction and re-solidification. The re-solidified phase is mostly composed of aluminium and the surrounding light-coloured zone is richer in binding elements; it is more difficult to attack chemically and consequently appears lighter.

The green phase, on the other hand, is to be regarded as a transitional phase in which the material has initially undergone recrystallisation despite a lower temperature than in the brownish zone, but still sufficient to recrystallise.

Around the green zones we can see other equally clear zones indicating the presence of intermetallic phases, but in which the melting has only occurred in the eutectic zone while the green phase itself has not changed and comes from the previous recrystallisation phase.

When approaching the unaltered zone of the base material, the following changes in the microstructure occur:

- Increment of green phase
- Reduction of the proportion of eutectic that is fused
- Reduction of lighter areas

From a morphological point of view, the area inside the nugget is characterised by solidification rosettes while the green area is characterised by islands of unmelted material.

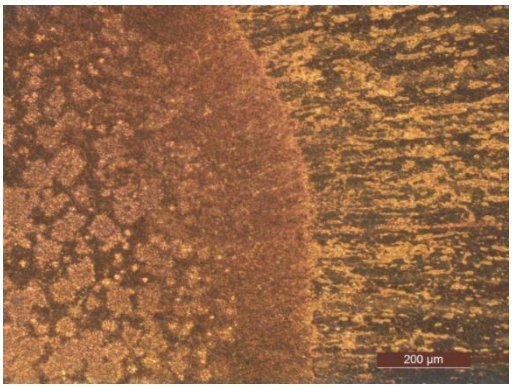

Figure 4.26 *100x Weck 20s, transition to the right of the nugget*

The rosettes are an indicator of resolidification where the central points of the rosettes indicate that rapid equiaxial nucleation and solidification (equal solidification pushing force in all directions) has taken place in that area, thus not influenced by any gradient.

It is expected to see this behaviour within the nugget, but it is not common in other areas.

The absence of a gradient is due to the excellent thermal conductivity of aluminium, which is able to conduct heat optimally in every direction even during a phase change.

If we had used a steel alloy we would not have seen rosettes but columnar structures, mainly in the areas in contact with the base material, because the latter would have dictated the direction of the gradient.

The dark areas are more related to the unaltered eutectic, in fact there can be no eutectic after resolidification.

This material when melted and re-solidified forms rosettes for the reasons explained above; but any eutectic if it is melted subsequently becomes a white phase, whereas if it is not melted it is attacked more by chemical reagents and appears dark in the micrograph.

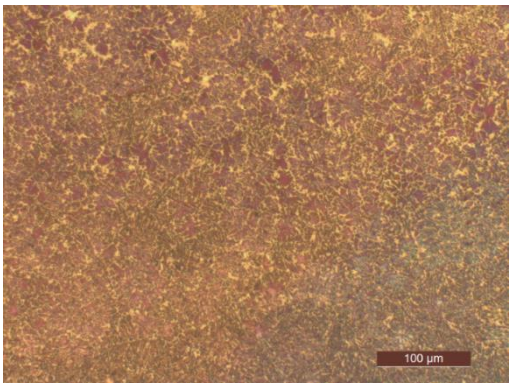

Figure 4.27 *200x Weck 20s, center line, towards the lower part of the nugget*

We can see larger and increasing white areas because we are in the molten zone, this was previously the liquid zone so its enlargement indicates a slight increase in temperature.

The liquid zone, which is richer in binding elements, expands at the expense of the brownish zone.

There are some areas that are a bit elongated, so we cannot say that there is a perfect isotropy, but they are probably part of the rosettes.

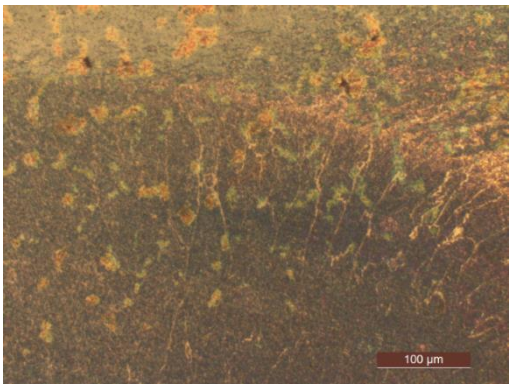

Figure 4.28 *200x Weck 20s, transition to the top right part of the nugget*

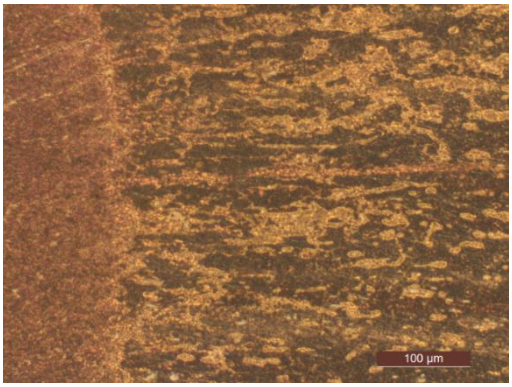

Figure 4.29 *200x Weck 20s, transition to the right part of the nugget*

We can appreciate an interesting microstructure because we can see a recrystallized zone at the interface between the unaltered zone of the base material and the HAZ; in some areas at the interface recrystallisation has taken place between the lamellae, in fact those lighter areas are recrystallized grains.

We can define the dark zones as unaltered eutectic and the light zones as recrystallized zones.

The grains probably remained more resistant to chemical attack because they did not melt, so the binding elements remained within the matrix, which is another indication of recrystallisation in the solid state, as we would expect from CDW process.

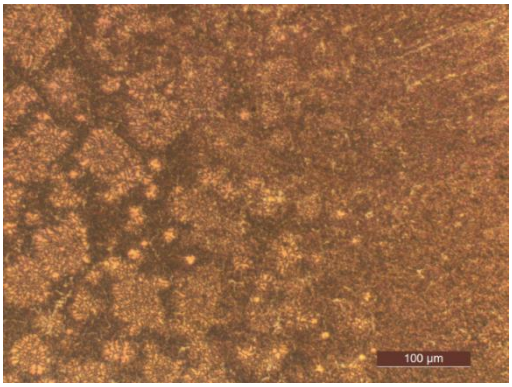

Figure 4.30 *200x Weck 20s, transition to the right part of the nugget*

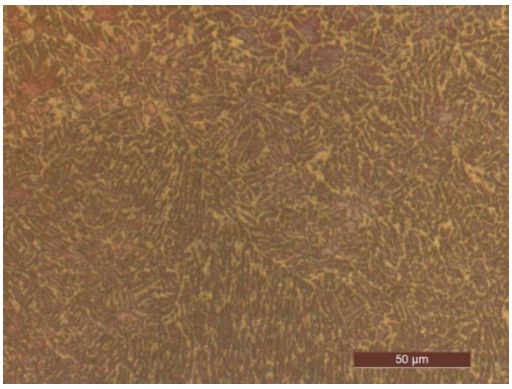

Figure 4.31 *500x Weck 20s, center line, towards the lower part of the nugget*

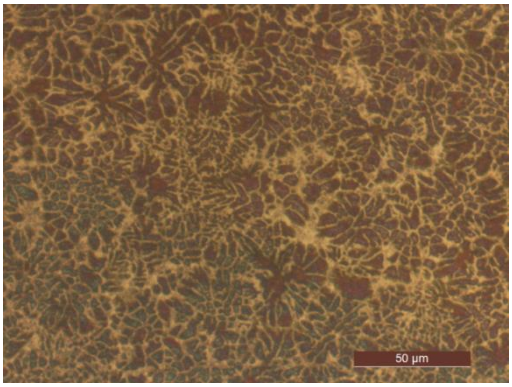

Figure 4.32 *500x Weck 20s, center line, transition to the left of the nugget*

Slight green coloring so we can deduce more affinity with the base material, while above on the left it is more similar to the core, in fact it becomes brownish where it is related to the core (totally melted and totally re-solidified area) while the green area is partially melted and partially re-solidified.

The light areas are the melted and re-solidified ones, the green areas are the unmelted ones, with the parameters used we have caused the melting in the core, actually not because of the high temperature but more because of the eutectic presence and because the material was hardened.

In fact, the parameters used are similar to those previously used on an aluminum-lithium alloy which was, however, rolled and strengthened by precipitation.

This 5754 alloy was not aged, but severely work-hardened, which lowered the recrystallisation temperature and some eutectic zones melted earlier because they were packed between the lamellae.

In a non-laminated material, the eutectic is a region that can be considered equiaxial, and when the temperature of the eutectic is reached it melts; in this alloy, however, the eutectic had been crushed between the various rolling fibres (not to be confused with the lamellae of the eutectic)

When a temperature close to the melting temperature of the eutectic is reached, both eutectic and matrix will start to stabilise, but with different phenomena: the severely work-hardened rolled fibre recrystallises at a lower temperature than we would normally observe, while the eutectic by definition melts when it reaches its eutectic temperature (lower than the melting temperature of the alloy).

This is why we can observe a mixture of the two phenomena in many micrographs.

The green zone is an area where the lamellae are not completely recrystallised

The area between the green lamellae is part of the pre-existing eutectic that has melted, a modest amount however and also evenly distributed.

During recrystallisation the lamination orientation is lost, in fact the broken fibre alignment results in a rather disordered lay-up.

There are brownish areas that are probably liquefied and re-solidified structures, and the green structures indicate that binding agents are present in those areas.

It would be worth assessing which binding agent Weck reacts most strongly with.

Since it is not possible for the binding elements to remain in the resolidifying phase during resolidification, it is very likely that these are pre-existing areas and therefore have not melted.

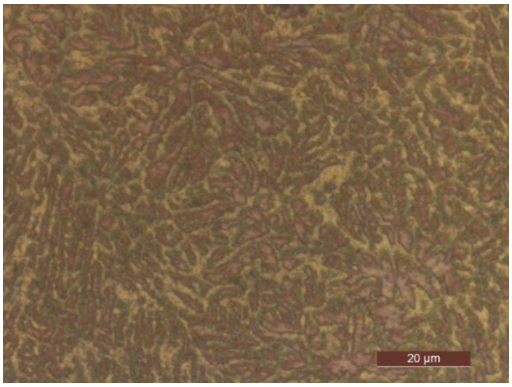

Figure 4.33 *1000x Weck 20s, center line, towards the lower part of the nugget*

It seems to be an unaffected zone, even in its heterogeneity it seems isotropic, we can note a slight prevalence of brownish areas towards the top of the micrograph

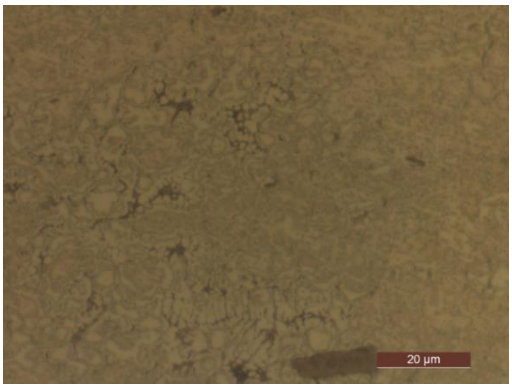

Figure 4.34 *1000x Weck 20s + Keller 2s, transition to the right part of the nugget*

The black areas appear to be micropores, but it is rare to find micropores in the transition zone and around the grains, so it could be a shrinkage porosity (it cannot be gas because otherwise it would tend to be spherical), probably these porosities between the grains have formed as the grains have shrunk at different rates leaving cavities.

Sample 2, 2nd half

Figure 4.35 *25x*

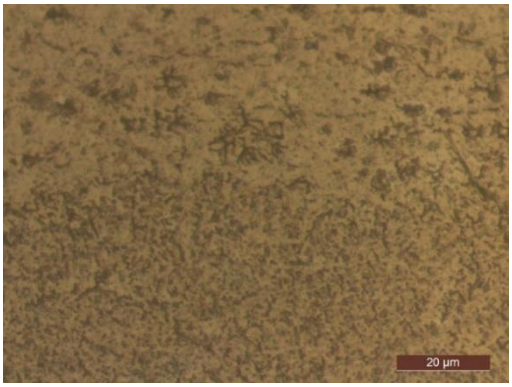

Figure 4.36 *1000x Keller 20s + Weck 4s, top central area of the nugget*

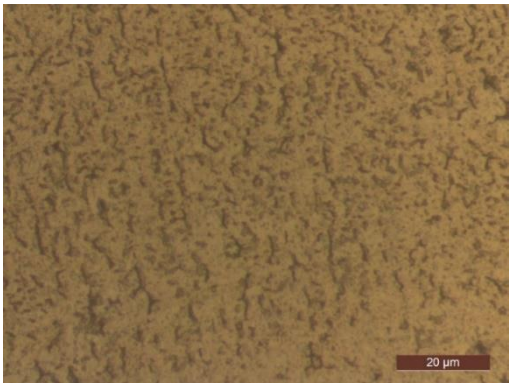

Figure 4.37 *1000x Keller 20s + Weck 4s, center line, transition to the right part of the nugget*

On the second half of the sample 2, we decided to use the Weck reagent for a shorter time in order to avoid possible artefacts under the microscope and to obtain a sharper image. The Weck reagent was used for 20 seconds on the previous sample and only 4 seconds on this one.

Even in these micrographs we can see how capacitive discharge technology helps to create a fine microstructure because the process allows for rapid cooling, aluminum and its alloys usually create problems precisely because they conduct heat very well.

Resistance technology encounters difficulties with aluminum alloys because the energy released per unit of time is quite low; the advantage of capacitive discharge is the possibility to give a large amount of energy in a very small time interval.

Capacitive discharge welding can be seen as an evolution of resistance welding because it works better on alloys that are difficult to weld with resistance technology, but allows spot welding only.

4.6 Instrumented Indentation Testing

Many of the mechanical properties of materials are studied by means of tensile testing. This requires specimens with a specific shape and minimum thickness which are often not compatible with production specifications.

Alternatively, non-conventional, non-destructive tests have recently been proposed for the estimation of tensile properties from simple, small specimens. In particular, the instrumented indentation test (IIT) is one of the most promising unconventional mechanical tests.

By continuously recording the forces and displacements during the execution of an indentation cycle, so-called indentation curves (ICs) are obtained.

Accordingly to ISO 14577, the discharge curve provides sufficient information to extrapolate the modulus and indentation hardness.

IIT is currently widespread and widely used in the field of nano- and micro-hardness. The localized nature of these tests allows the mechanical properties of real components or very small samples to be mapped. On the other hand, they have the disadvantage that they are not always representative of the mechanical behavior of the material. It is precisely for this reason that macro-indentation becomes even more important, as it is considered the most suitable for characterizing the elastic and plastic behavior of structural materials and establishing a possible correlation between indentation and tensile properties.

In an instrumented indentation test, the loading and displacement of the indenter during a controlled indentation cycle consisting of loading, holding and unloading is recorded using appropriate sensors. The quantities measured at the same time are thus the applied force F and the indentation depth h. From these two parameters, the indentation curves (ICs) are obtained, which have the typical pattern shown in Figure 4.38

Figure 4.38 *Indenter*

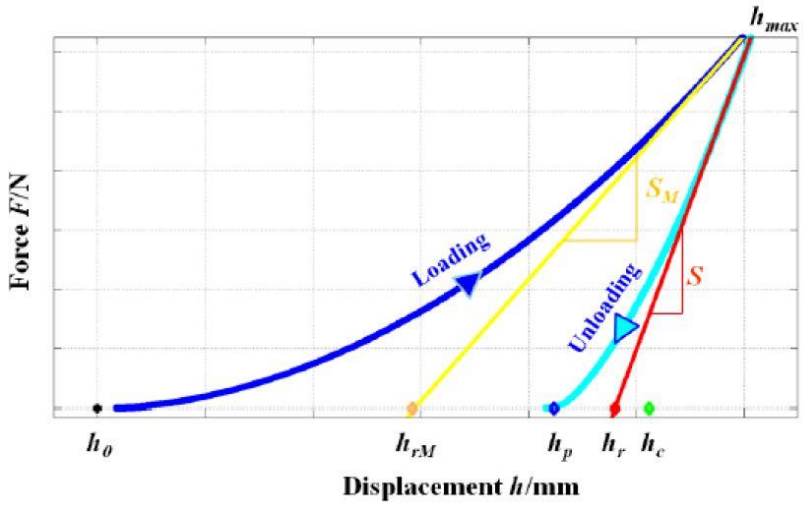

Figure 4.39 *Typical trend of indentation curves*

Indentation curves allow some important indentation parameters to be extracted:

- h_0 : point zero, the first contact point;

- h_{max} : the maximum depth of penetration of the indenter tip into the specimen;

- F_{max} : the maximum applied force;

- S_M : the tangent to the load curve at the point hmax;

- h_{rM} : the intercept of the tangent to the load curve at the point hmax;

- S : the tangent to the discharge curve at the point hmax;

- h_r : the intercept to the tangent to the discharge curve at point hmax;

- h_c : the contact depth;

- h_p : the plastic depth, i.e. the last point of contact corresponding to the result of the plastic deformation of the indentation when the elastic deformation has been fully recovered.

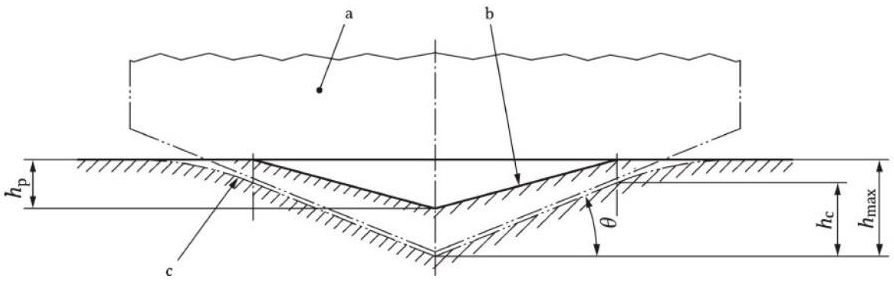

Figure 4.40 *Schematic representation of the cross-section of an indentation*

Where :

a : indenter

b : residual plastic surface related to an indentation performed on a body having a perfectly plastic response

c : surface of the tested specimen at maximum indentation depth with maximum applied load

θ : maximum angle between the surface of the tested specimen and the indenter

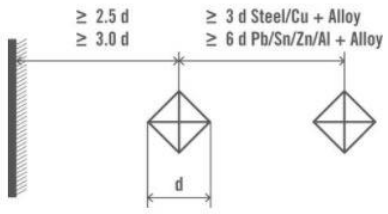

Figure 4.41 *Minimum distance between test points and to the specimen edge*

It is very common for indentations to give an indentation modulus that is not very close to Young's modulus, so the first criterion for understanding whether an indentation is valid or not is to find the indentation modulus that is close to Young's modulus, if this coincidence is found then even few macro indentations may be sufficient.

Subsequently, microindentations can be carried out in order to find a correlation between micro and macro, which is already a research topic that is not yet fully understood.

It is interesting to evaluate the modulus of indentation near a defect; the presence of a pore should reduce the mechanical resistance and should also be visible in the test results.

The potentially most interesting indentations are therefore the three in the nugget due to the presence of pores.

The indentation parameters make it possible to assess, without the need for any microscope or operator dependence, the Ac contact area involved in defining hardness in the case of instrumented indentation tests.

Furthermore it is possible to note how the indentation curves make it possible to identify, from the area subtended by the loading and unloading curves, the presence of elastic and plastic work.

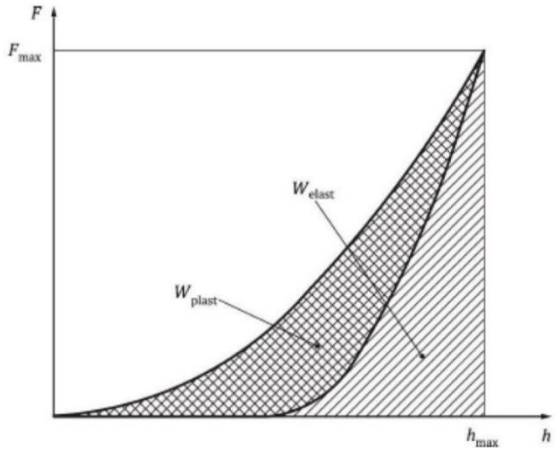

Figure 4.42 *Elastic and plastic part of indentation work*

We decided to indent the resistance welded specimen, because it could have been interesting to evaluate the indentation test on a specimen with cracks and porosity, but not as many as on the laser welded one.

A sample such as the one obtained with laser technology might be interesting to evaluate the limits and strengths of the indentation test, but the aim of this thesis was mainly to observe the differences between three specific technologies for welding aluminum.

Advantages of instrumented indentation testing

- Can be performed on any materials
- Automation possibilities
- Possible use in production control
- Determination of hardness value from elastic and plastic deformation
- Hardness value independent of test load for indentation depth ≥ 10 µm

Disadvantages of instrumented indentation testing

- Decreasing the degree of indentation places greater demands on the surface quality of the specimen (indentation depth ≥ 20 - average surface roughness)
- Vibration sensitivity, especially in the indentation depth range h < 15 µm
- Possibility of error due to elastic and permanent displacement of the specimen and components in the force flow during the test cycle
- Sensitivity to deviations in the shape of the indenter, particularly the tip

Micro indentation report

Point of load application : 5 N

Speed load application : 0,25 N/s

Load removal speed : 0,25 N/s

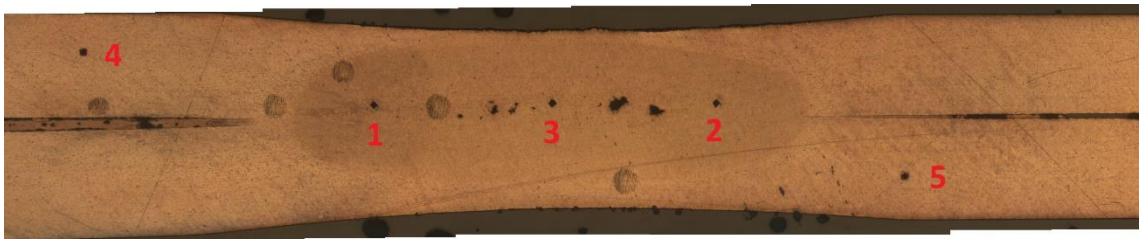

Figure 4.43 *Microindentation*

	h_{max} [µm]	HIT_i [N/mm²]	EIT_i [N/mm²]	m(hi) [kN/mm]	Ap_i [mm²]	h-correct [µm]
1	17,700	791,41	26566,08	2,60	0,01	1,228
2	16,562	805,28	67500,01	6,31	0,01	0,713
3	18,112	689,77	43112,39	4,43	0,01	1,147
4	13,926	1150,48	87080,90	6,73	0,00	0,788
5	14,622	1058,66	64626,00	5,28	0,00	0,621

	$Fmax_i$ [N]	W loading [Nmm]	W holding [Nmm]	W unloading [Nmm]	W plastic [Nmm]	W TOT [Nmm]
1	5,10	0,03	0,0002	0,004	0,03	0,03
2	5,03	0,03	0,0003	0,002	0,03	0,03
3	5,03	0,03	0,0003	0,003	0,03	0,03
4	5,03	0,02	0,0002	0,002	0,02	0,02
5	5,02	0,03	0,0003	0,002	0,03	0,02

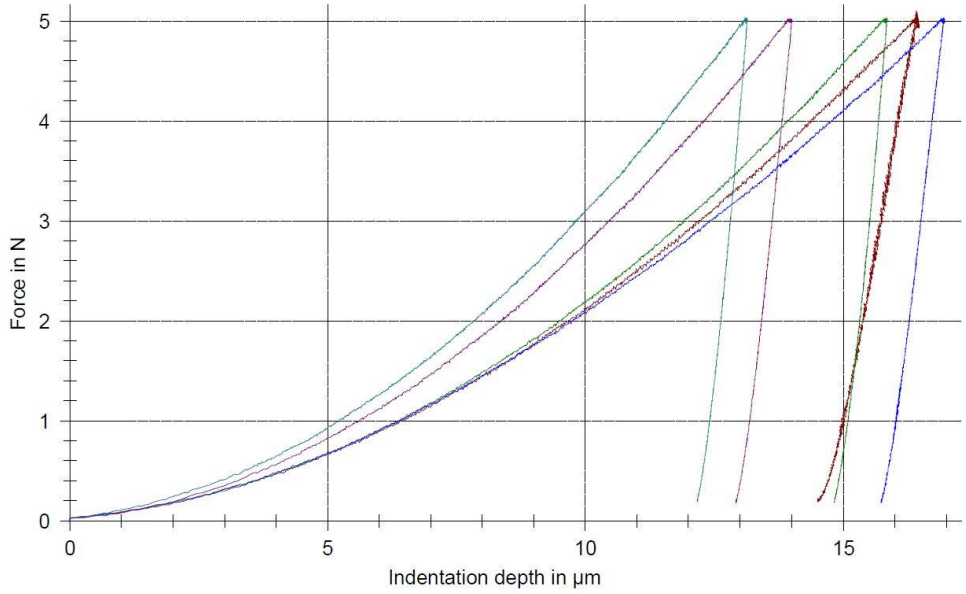

Macro indentation report

Point of load application : 100 N

Speed load application : 5 N/s

Load removal speed : 5 N/s

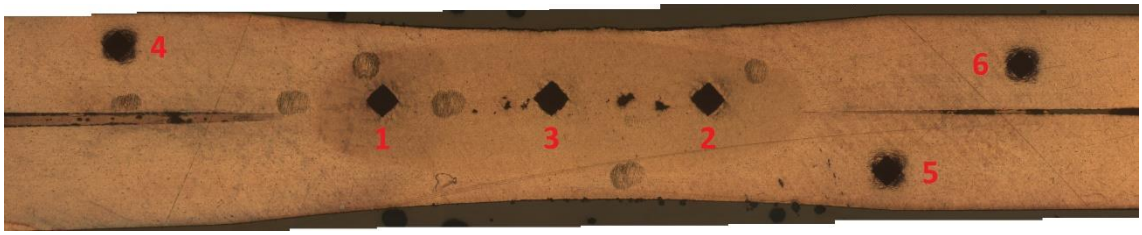

Figure 4.44 *Macroindentation*

For both micro and macro indentation the maximum force was reached in 20 s

	h_{max} [µm]	HIT_i [N/mm²]	EIT_i [N/mm²]	m(hi) [kN/mm]	Ap_i [mm²]	h-correct [µm]
1	83,166	695,69	25088,78	11,60	0,14	0,507
2	77,165	732,11	68735,35	30,04	0,14	0,569
3	81,660	660,19	53064,54	24,69	0,15	0,530
4	115,239	2114,05	3761,03	1,01	0,05	1,383
5	70,634	903,71	55091,54	21,88	0,11	0,673
6	67,849	1019,13	43557,89	16,42	0,10	0,551

	$Fmax_i$ [N]	W loading [Nmm]	W holding [Nmm]	W unloading [Nmm]	W plastic [Nmm]	W TOT [Nmm]
1	100,19	2,84	0,0256	0,590	2,87	2,28
2	100,03	2,54	0,0255	0,207	2,57	2,36
3	100,04	2,75	0,0223	0,278	2,77	2,49
4	100,04	5,90	0,3228	3,489	6,22	2,73
5	100,04	2,45	0,0264	0,273	2,47	2,20
6	100,04	2,34	0,0293	0,350	2,37	2,02

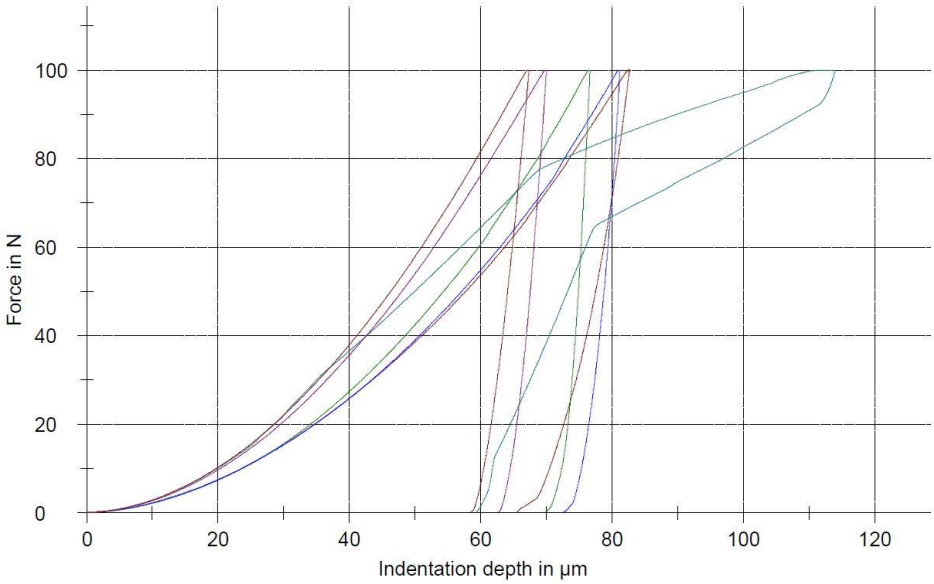

For AA5754 Young's modulus E is equal to 70 GPa.

We can notice that in the case of both the macro and the micro indentation in point 2 , the indentation modulus is very close to the desired correct value.

The indentation modulus can be slightly different from the Young's modulus because it is a weighted average of the elastic properties in a certain sample volume and the Young's modulus is directional.

5 Conclusions

As can be seen in the graph of the macroindentations, one more indentation was carried out with respect to the microindentations, the reason being the unreliability of the values of indentation number 4, probably due to a porosity present at a greater depth than that attainable with the microindentation.

This particular lap joint configuration with tapered specimens was chosen for possible further tensile testing, thus avoiding bending moment components during traction; in addition, to use less energy by having 2 thicknesses of 1.6 mm instead of 3.2 mm (given the considerable thermal and electrical conductivity, this reduction in thickness allows considerable energy savings).

With regard to the technologies used, some considerations are necessary; the resistance welding machine used is a medium-frequency machine and therefore allows the molten zone to be heated more evenly than other resistance technologies.

Capacitive discharge technology allows a very short welding cycle and less distortion of the materials due to the rapid release of energy, but it is still an under-researched technology, although promising for particular materials such as aluminum alloys or high carbon steels.

The source used for laser welding is CO2. The results obtained are further confirmation of the inadequacy of this source for welding a reflective material such as aluminum; the excessive porosity of the samples obtained makes them unusable for any structural application.

It might be interesting for future experiments to decrease the pressure value, the resistance welded sample shows more cracks than the one welded by capacitive discharge mainly for two reasons: the lower curvature of the electrodes used on the resistance machine, but probably the most important factor affecting the result obtained is the longer duration of the process, as the material has had time to modify more.

The metallographic analysis describes the morphological change of the material during the welding process, as for instance the recrystallization occurred at the welding line.

The instrumented indentation test allows the mechanical properties of weld joints to be characterized in restricted regions, while allowing correlation with properties of the conventional tensile test.

6 Bibliography

(n.d.). Retrieved from http://www.2c2m.it/Argomenti/saldature/Saldatura_resistenza.htm

(n.d.). Retrieved from www.metasald.com

2c2m Studio di progettazione. (n.d.). Retrieved from http://www.2c2m.it/Argomenti/saldature/Saldatura_resistenza.htm

(2015). *Aluminum Automotive Manual.*

Anna Maloveczky, A. K. (2018). The replacement of Resistance WElding with Laser Beam Welding. *Acta Materialia Transylvanica*, 101-104.

Association, E. A. (2015). *EAA Aluminium Automotive Manual – Joining.*

Dulal Chandra Saha, Y. -D. (2011). A Review on Al-Al/Al-SteelResistance Spot Welding Technologies for Light WEight Vehicles. *Journal of KWJS*, 397-402.

H. Zhang, J. S. (2002). Suppressing Cracking in Resistance Welding AA5754 by Mechanical Means. *Journal of Manufacturing Science and Engineering*, 79-85.

J. Kang, Y. C. (2015). Fatigue Behavior of Dissimilar Aluminum Alloy Spot Welds. *Procedia Engineering*, 149 – 156.

L. Han, M. T. (n.d.). Effect of aluminum sheet surface conditions on feasibility and quality of resistance spot welding.

Mazur W, K. A. (2016). Use of modified electrode caps for surface quality welds in resistance spot welding. *Journal of Manufacturing Processes*, 60-73.

metasald. (n.d.). Retrieved from www.metasald.com

metasald. (n.d.). Retrieved from www.metasald.com

S. HU, A. S. (2020). Comparison of the Resistance Spot Weldability of AA5754 and AA6022 Aluminum to Steels. *Welding Journal*, 224-237.

Tihomir Doksanovic, I. D. (2017). Variability of structural aluminum alloys mechanical properties. *Structural Safety*, 11-26.

X. Long, S. K. (2005). Residual stresses in spot welded new generation aluminium alloys Part B - Finite element simulation of residual stresses in a spot weld in 5754 Aluminum Alloy. *Science and Technology of Welding and Joining*, 88-93.

Yanjun Wang, W. T. (2019). A Method for Improving Joint Strenght of Resistance Spot Welds of AA 5182 - O Aluminum Alloy. *Journal of Manifacturing Processes*, 661-669.

Zhang Hongyan, S. J. (2011). *Resistance Welding - Fundamentals and Applications.* CRC Press.

Behulova M., B. E. (2017). Design of Laser Welding Parameters for Joining Ti Grade 2 and AW 5754 Aluminium Alloys Using Numerical Simulation. *Advances in Materials Science and Engineering*, 1-15.

Daftardar, S. (2009). Laser assisted friction stir welding: finite volume method and metaheuristic optimization. *Engineering*.

Ebindustries. (s.d.). Tratto da https://ebindustries.com/laser-welding-aluminum/

Forsman, T. (2000). *Laser Welding of Aluminum Alloys.* Lulea Tekniska Universitet.

Garavaglia M., D. A. (2020). Fiber laser welding of AA 5754 in the double lap-joint configuration: process development, mechanical characterization, and monitoring. *The International Journal of Advanced Manufacturing Technology*, 1643-1657.

Kose, C. (2016). Weldability of 5754 aluminum alloy using a pulsed Nd:YAG micro scale laser. *Materials Testing*, 963-968.

Leo P., P. P. (2016). Microstruttura e difettosità in giunti laser AA5754/Ti-6Al-4V. *La metallurgia italiana*, 13-22.

Peyre P., B. L. (2014). Generation and characterization of T40/A5754 interfaces with lasers. *Journal of Materials Pricessing Technologies* , 1946-1953.

ResearchGate. (s.d.). Tratto da https://www.researchgate.net/figure/Principles-of-the-butt-joint-and-the-formation-of-the-melt-pool-within-the-heat-affected_fig1_296664190

Tomashchuk I., S. P. (2014). Direct keyhole laser welding of aluminum alloy AA5754 to titanium alloy Ti6Al4V. *Journal of Materials Processing Technology*, 96-104.

Williams, A. (s.d.). *Health Science Journals*. Tratto da https://healthjournals.wordpress.com/2016/08/19/investigation-on-transient-thermal-responses/

Davis, D. (2018). Capacitor discharge resistance welding emerges as important projection welding option. *The fabricator*.

Dziho M.E., P. S. (s.d.). Contact force influence on welded joint properties at capacity discharge welding of small diameters wires.

Gould J. E., L. S. (2016). Development of an Open Architecture Capacitive Discahrge Welding System. *Ingproceedings*.

Ketzel M., H. M. (2019). Heat development of the contact area during capacitor discharge welding. *Weld World*, 1195–1203.

Koal J., B. M. (2020). Performing an Indirect Coupled Numerical Simulation for Capacitor DischargeWelding of Aluminium Components. *Processes*.

Kolarikova M., V. P. (2018). Joining of thin sheets from al alloy en aw 6016 by capacity discharge welding. *Metal*.

Maizza G., P. R. (2020). Correlation Between the Indentation Properties and Microstructure of Dissimilar Capacitor Discharge Welded WC-Co/High-Speed Steel Joints. *Materials* .

Meiners M., R. T. (2020). Current Distribution Monitoring in Capacitor Discharge Welding. *25th IEEE International Conference on Emerging Technologies and Factory Automation (ETFA)*, 447-453.

Panella F.W., D. V. (2019). CDW aluminium joints welding and optimisation with NDT/mechanical testing. *The International Journal of Advanced Manufacturing Technology*, 3689-3698.

Power Stream. (2006). Tratto da www.powerstream.com

Tuchtfeld M., H. S. (2019). Comparing the effect of electrode geometry on resistance spot welding of aluminum alloys between experimental results and numerical simulation. *Weld. World*, 527–540.

Zhou Y., D. S. (2001). Weldability of Thin Sheet Metals by Small-Scale Resistance Spot Welding using High-Frequency Inverter and Capacitor-Discharge Power Supplies. *Journal of Electronic Materials*, 1012-1020.

UNI EN ISO 14577-1:2002. Metallic materials - Instrumented indentation test for hardness and materials parameters - Part 1: Test method